Republic of Iraq
Ministry of Higher Education
and Scientific Research
University of Babylon
College of Materials Engineering
Department of Polymer Engineering and
Petrochemical Industries

Preparation and Characterization of Functionally Graded Polymeric Composite Material

A Thesis

Submitted to College of Materials Engineering/ University of Babylon as a Partial Fulfillment of the Requirements for the Degree Doctor of Philosophy in Materials Engineering/ Polymer

By:

Adwaa Mohammed Abdulmajeed Hamaad

Supervised by:

Prof. Dr. Ahmed Fadhil Hamzah

2022 A.D 1444 A.H

قال اللّٰهِ تعالى:

﴿يُؤْتِي الْحِكْمَةَ مَنْ يَشَاءُ وَمَنْ يُؤْتَ الْحِكْمَةَ فَقَدْ أُوتِيَ خَيْرًا كَثِيرًا وَمَا يَذَّكَّرُ إِلَّا أُولُو الْأَلْبَابِ﴾

صَدَقَ ٱللّٰهِ العَلِيُ العَظِيم

(البقرة: 269)

Acknowledgment

*First of all, I would like to confirm that this work will never be finished without the help of **GOD**, the greater of all creations and the Merciful **Prophet Mohammad** his viticulturist **Ahl-Albait** (Allah peace upon them).*

*I express my sincere gratitude to my supervisor **Prof. Dr. Ahmed Fadhil Hamzah**, for his patience, guidance and encouragement throughout this work.*

*My gratitude also goes to the **Materials engineering college in Babylon University**. Sincere thanks are also expressed to the staff of the material engineering college.*

*Great thanks to the **Mechanical Engineering College** at University Technology staff for their help and great efforts during the experimental work.*

*Special thanks to **Dr. Mahdi Mahmood Shaker, Dr. Ola Abdul Hussain Kadhum, and Eng. Hussam Raad Al Ibraheme** for their extensive support and efforts in solving the difficulties I faced during this work.*

I also wish to convey my utmost appreciation and thanks to my Family especially to my husband, my mother, brothers and sisters for their love, help, supports and extraordinary patience during the years of my study.

Adwaa Mohammed ***2022***

Dedication

I Would Like to Dedicate This Thesis to All for

Their Support and Encouragement

Whom I Love Most in All My Life

My Kindest Mother and Father

My lovely husband and children

To My Dear Brothers and Sisters

And to All People I Love.

Adwaa

CHAPTER ONE

INTRODUCTION

CHAPTER TWO

THEORETICAL PART

CHAPTER Three

EXPERIMENTAL WORK

CHAPTER Four

RESULTS AND DISCUSSION

CHAPTER Five

CONCLUSIONS AND RECOMMENDATIONS

REFERENCES

ABSTRACT

To avoid interphase problems such as stress concentration, poor adhesion between the reinforcing materials and the matrix materials, and other undesirable reflections caused by the composite materials. Functionally graded materials (FGMs) have been used, which are advanced composite materials with properties, which varying with the position. This study involves three parts. The first part includes manufacturing a centrifuge apparatus. This apparatus manufactured in a new way that differs from the centrifugation methods in previous research in the terms of the shape of the sample and the direction of the gradient by using acrylic dies.

The second parts involve synthesis FGMs by using manufacturing centrifuge apparatus at different parameter condition. The first parameter involves: different volume fractions of alumina (0.5, 1, 1.5 and 2% V_f), the second parameter include varying centrifugation speeds (600, 800, 1000 and 1200 r.p.m) and the third parameter include various centrifugation times (1, 2, 4 and 6 min). as well as manufacturing non-FGM to compare between results.

The third parts include studying the structural, physical, mechanical and tribological properties to compare between the FGM, non-FGM nanocomposites and pure epoxy.

The investigated mechanical properties included flexural resistance (Three-point bending), impact and hardness. Also, the tribological have been conducted to study the specific wear rate and coefficient of friction. The load has been exerted for all types of FGM at both sides, one side of homogenous nanocomposite and on the one side of pure epoxy.

The particle size analyzer results show that the ultimate size of the nanoparticles of Al_2O_3 is 520.1nm. The XRD show that the alumina nano-particles contained only the α-nano-Al_2O_3 phase

Also, the results indicated that the nanoparticles improve the mechanical and sliding wear resistance of non-FGM and FGM nano-

composites'. The maximum flexural strength and flexural modulus of FGM were enhanced by (43.69%) and (52.82%), respectively, if it was loaded from the nano-alumina side, whereas when (FGM) was loaded from the side of neat epoxy, the decrease in flexural strength was (122.42%) while the improvement of the flexural modulus was (81.215%) compared to the neat epoxy when the concentration of Al_2O_3 (2%V_f), rotational speed (N=1200 r.p.m.) and centrifugation time (t= 6 min.).

The results manifested that the impact strength for the materials loaded from the composite side was higher than that of the samples burdened from the pure epoxy side for all types of (FGM); in general, the maximum difference in the impact strength occurred when the FGM loaded from the nano-alumina rich side where the maximum value was 168% than the neat epoxy at time 4 min of rotational time 1200 (r.p.m) centrifugation speed, and 2% V_f.

The hardness of the samples was measured from the alumina-rich side to the epoxy-rich side (divided by five region) where the hardness differs in each region, which ensure the correct distribution of nanoparticles through the thickness of FGM which indicated that the hardness test considered an excellent test for the gradation of material properties through the thickness. as well as the hardness results showed the maximum increment in the hardness of around (16.8%) for the specimen N = 1200 (r.p.m), t = 6 min, and V_f = 2%) of FGM nanocomposite loaded from alumina rich side.

Also, results showed that the FGMs had superior sliding wear resistance compared to homogenous composites. FGM have a lower Coeff. friction was around (51.7 %) when samples loaded from the alumina rich side N = 1200 (r.p.m), t = 6min and V_f = 2%) compared with the pure epoxy specimen.

The impacted samples' fracture surfaces have been studied using scanning electron microscopy (SEM) at the max. and min. of centrifugation conditions and concentration of nano alumina after break to check the dispersion quality.

LIST OF CONTENTS

LIST OF SYMBOLS

- **English Symbols**

Symbol	*Description*	*Unit*
A	Cross-sectional area of specimen	m^2 or mm^2
ρ_m	Density of matrix	g / cm^3
ρ_p	Density of nanoparticles	
ρ_p	Density of particles	g / cm^3
ρ_e	Density of the epoxy matrix	g / cm^3
l	Distance between the pendulum's rotation axis and the pendulum's gravity center	mm
W_2	Energy of the pendulum hammer after breaking the specimen.	J
W_1	Energy of the pendulum hammer before breaking the specimen.	J
δl	Extension	mm
F	Applied Force	N
H	Hardness	--
h	Height	mm
U_c	Impact energy	J
G_c	Impact strength of material	J/m^2
r	Inside radius of the mold	m
K	Dimensionless constant	—
g	Local acceleration owing to the gravity	$m.s^{-2}$
m	Mass	kg
m_p	Mass of particles	g
m_c	Mass of the composite specimen	g
m_m	Mass of the matrix	g
V_m	Matrix volume fraction	
E	Modulus of Elasticity or Young's Modulus	GPa

G	Modulus of rigidity	GPa
h_2	Pendulum hammer's height after the impact	mm
h_1	Pendulum hammer's height before the impact	mm
n	Rotational speed	r.p.m
H_a	The Shore (A) hardness	--
H_d	The Shore (D) hardness	--
A_r	The total real area of contact	mm^2
V	Volume Fraction	%
V_p	Volume fraction of nanoparticles	%
V_e	Volume fraction of the epoxy matrix	%
V	Wear volume	mm^3
v_p	Volume of particles	cm^3
v_c	Volume of the composite specimen	cm^3
v_m	Volume of the matrix	cm^3
W_a	Weight of object at air	g
W_w	Weight of the object at water	g
b	Width of the Specimen	mm

- **Greek Symbols**

Symbol	*Description*	*Unit*
$\Delta\sigma$	Constant stress range	MPa
δ	Deflection	mm
ρ_f	Density of Fluid	g/cm^3
ρ_o	Density of object	g/cm^3
σ_{max}	Maximum stress	MPa
σ_m	Mean stress	MPa
σ_{min}	Minimum stress	MPa
υ	Poisson's ratio	--
σ_{fB}	Flexural stress at the break	MPa
σ_{fM}	Maximum flexural stress	MPa
λ	Wave length	A^o

LIST OF ABBREVIATIONS

Symbol	*Description*
ASTM	American Society for Testing and Materials Specifications
CF	Carbon Fiber
CNT	Carbon Nano Tubes
CFRP	Carbon-Fiber Reinforced Polymer
CCT	Centrifugal Casting Technique
CMC	Ceramic Matrix Composite
CVD	Chemical Vapor Deposition
CSM	Chopped Strand Mat
DSC	Differential Scanning Calorimetry
EP	Epoxy
FCP	Fatigue Crack Propagation
FRP	Fiber Reinforced Polymer
FEA	Finite-Element Analysis
FEM	Finite-Element Method
FGM	Function graded material
G-F	Glass Fiber
GFRP	Glass Fiber Reinforced Plastic
GnPs	Graphene nanoplatelets
T_g	Glass Transition Temperature
HC	Hybrid Composite
MMC	Metal Matrix Composite
PVD	Physical Vapor Deposition
PEEK	Poly Ether Ether Ketone
PEI	Poly Etherimide
PPS	Poly phenylene sulfide
PA	Polyamide
PC	Polycarbonate

PES	Polyether Sulphone
PE	Polyethylene
PET	Polyethylene terephthalate
PMC	Polymer Matrix Composite
PP	Polypropylene
PS	Polystyrene
PVC	Polyvinyl chloride
RT	Room Temperature
SEM	Scanning Electron Microscope
SHS	Self-propagating High-temperature Synthesis
S-N	Stress-number of cycles
UTS	Ultimate Tensile Stress
XRD	X-Ray Diffraction

CHAPTER ONE
INTRODUCTION

1.1 General Introduction

Many structural components encounter severe conditions and, hence, require material performance that varies with the location within the part. For example, the gear body has to be tough. In contrast, its surface must be stiff and wear-resistant, and the turbine blade body should be strong, tough and has a resistant to creep, whereas its external shell has to be refractory and has a resistant to oxidation. Many of the most demanding current applications of materials fall under this category [1 and 2].

Composite materials exhibit abrupt property transitions at the interface, resulting in component failure (via delamination) under extreme operating conditions. This disadvantage of conventional composites has been overcome by a new type of composite known as functionally gradient materials (FGMs) [3].

FGM is a revolutionary material belonging to a class of advance materials whose composition varies according to the location to optimize the structure's performance. Thermal stresses, residual stresses, and stress concentration factors are reduced due to the material's gradation in properties. The gradient in a material's properties is caused by chemical composition, microstructure, volume fraction, porosity and so on [4], as shown in Figure (1.1).

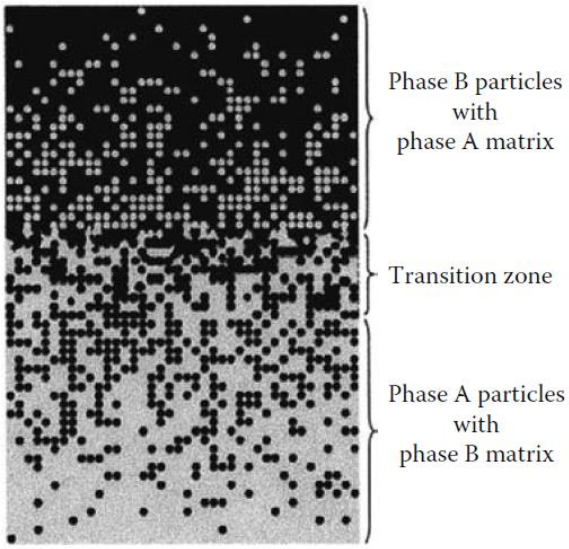

Figure (1.1): Variation of the volume fractions of constituent phases graded in one (vertical) direction in FGM [5]

FGM removes the sharp interfaces that exist in the composite, where the failure is started. It substitutes such sharp interface with a gradient interface that creates a smooth transition from any material to the following. The single characteristic of FGM is the capability for bonding the material for particular applications [6].

The result is a change in the material's properties, such as mechanical, tribological, or biocompatibility. Grading mechanical properties enable structure optimization and high performance and material efficiency. Simultaneously, this optimization can result in many mechanical issues, including estimating the final structure's effective properties and crack propagation behaviors [4].

FGM is a two-components composite material described via a compositional gradient between the two components. By contrast, conventional composites are homogeneous mixtures, implying a compromise between the desired properties of the component materials, as shown in Figure (1.2) [1].

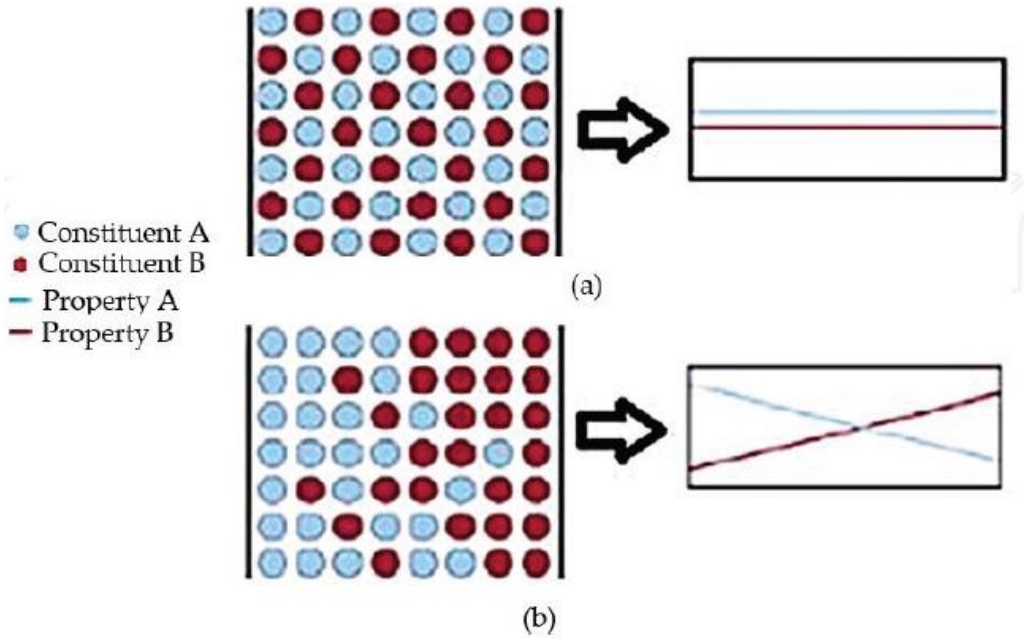

Figure (1.2): The difference between a) traditional composite and b) functionally graded materials [1]

In general, materials exhibit uniform function and property. However, in FGMs, one side's property is distinct from the others. Thus, the material may have multiple processes; for instance, a single side may possess a high mechanical strength, while the other side may have a high thermal resistance; therefore, there're "two requirements" in single material [7].

A significant field of FGM investigation is the development of the polymeric FGM, which has developed rapidly due to the desire for an optimal combination of constituent properties, such as low cost, erosion resistance, lightweight, hardness of surface, resistance to wear, resistance to impact, and high durability [8].

Recently, nano filler-reinforced FGM has gained increased interest as a source of new properties and functions. Because of their large surface areas, nano scale fillers give distinctive characteristics to the high-performance materials that are not present in micro fillers. Lately, the FGM idea has been implemented to the nano composites to optimize the reinforcing nano filler consumption and create nano composites with different properties for multi-functional applications [8].

1.2 Origin and History of FGM

Structures of FGM can be found in nature, in the animals and plants bio-tissues, as well as in the body of humans, such as in the bones and teeth. For example, a tooth and more specific dental crowns are excellent examples of the functionally graded materials. It needs a high resistance to wear external (Enamel) as well as a ductile interior structure.

Plants examples include bamboos, shells, and coconut leaves. Shells and bamboos are extremely strong close the external surface as well as extremely soft and tough on the inner. Additionally, bamboo possesses highly superior features. It's flexible, lightweight and strong, all of which result from the hollow's nodes, which create a hierarchy and stepwise structure as in Figure (1.3) [9].

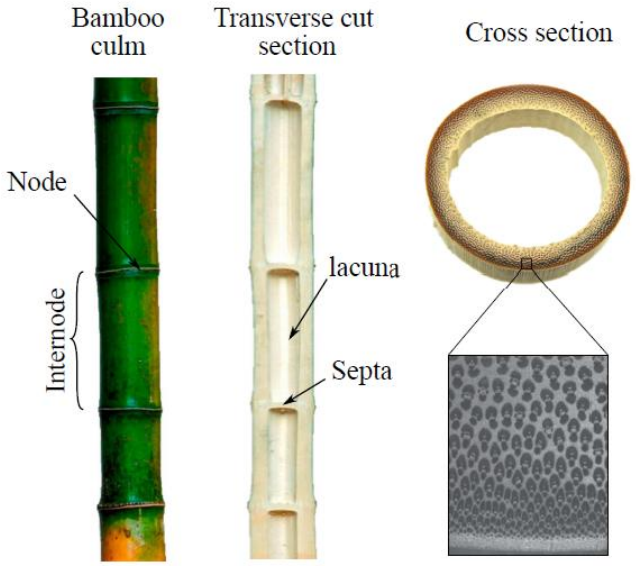

Figure (1.3): Bamboo tree cross-section showing the stepwise structure through the thickness [10]

The idea of the "functionally graded materials" was initially presented in 1984 via the Japanese materials scientists' group [11]. They were discussing their space plane fantasies in an old university building's room. A space plane's outer body is exposed to a very high-temperature environment (approximately 1700 degrees Celsius) and hence it must have high resistant to severe conditions caused by the difference of temperature (around 1000

degrees Celsius) between the inner and the outer. No material is impervious to such a condition. The researchers developed the so-called FGM concept, which entails gradually changing (grading) the composition of a space plane body's material for achieving the increased mechanical properties as well as the thermal resistance. They were designed with a ceramic outer surface exposed to a high-temperature environment and a thermally conductive inner surface [12].

1.3 Applications of the Functionally Graded Materials

The initial statement of the functionally graded material was connected to their prospective use in the thermal problems. Such materials being regarded in Japan for the thermal barrier coatings to protect the planes that go to the space from the elevated surface temperature as well as holding an elevated thermal gradient throughout the thickness [13].

There are numerous other successful uses of the functionally graded material idea, like the structural walls that serve the dual objectives of thermal barrier as well as the sound insulation while maintaining a high specific strength due to composition and porosity grading. Additionally, separating graded varnish particles, such as TiO_2/mica, may create attractive interference colors for automobiles. Gradients of flexibility or elasticity combined with the rigidity may enhance the sports devices performance, such as tennis rackets, skis and golf clubs [14]. Nowadays, the functionally graded material has a wide use in numerous fields that include the followings:

1. The structural thermal barrier materials.
2. The aerospace, such as the body of space plane, the constituents of rocket engine, and so on.
3. The chemical plants, such as reaction vessels, slurry pumps, heat pipes, heat exchangers, and so on.

4. The nuclear energy, such as fuel pellets, the initial fusion reactor's initial wall, the component of nuclear reactor, and so on.
5. The optic uses, such as lens, optical fibers, and so on.
6. The electronic uses, such as sensor cells, graded band semi-conductor substrates, and so on.
7. The biomaterial, such as the delivery systems of drug, artificial skin, implants, and so on.
8. The commodities use, such as cutting tools, glass of windows, bodies of car, sports goods, materials of building, and so on. [14]. Figure (1.4) shows the potentially applicable fields for FGMs.

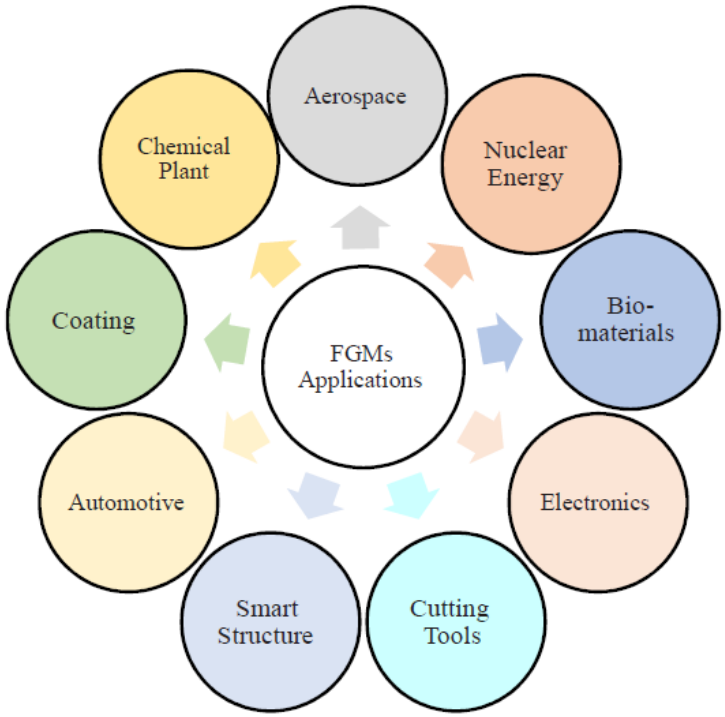

Figure (1.4): Potentially applicable fields for FGMs [15]

1.3.1 Gear's Application:

Gears are basically used to transmit power and motion from one shaft to others. It gives better transmission as compared to other drive such as belt, rope and chain drives [16]. FGM is useful in applications where high wear resistance and high bulk toughness are a necessity. Therefore, special processing is required to produce these materials in order to exhibit

characteristics that are not achievable by monolithic or homogeneous materials.

By using FGM in the gear structure promises better performances in term of wear resistance and ability to stand high thermal loads [17]. Centrifugal casting technique is used to manufacture FGM based thermoplastic gears. FGM gear can provide an attractive alternative over monolithic or homogeneous composites gear. The schematic view of fiber reinforced homogeneous (commercially available) gear and FGM gear is shown in Figure (1.5).

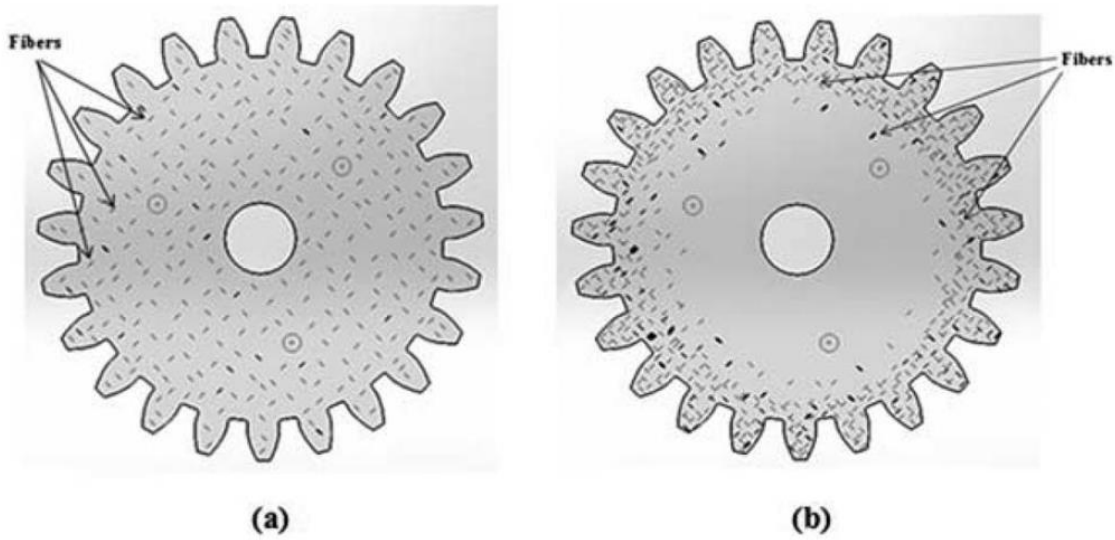

Figure (1.5): Schematic view of fiber reinforced gears (a) Homogeneous gear. (b) FGM gear [17].

In FGM gears, the high concentration of fibers in polymer gear tooth and base circle region helps to increase the hardness and thermal conductivity of the gear tooth. The thermal conductivity of fiber is high as compared to thermoplastic materials. This phenomenon results in decrease of surface temperature, as well as surface wear of the gear tooth [17].

1.4 FGMs manufacturing by means of centrifugal casting technique (CCT)

The CCT in FGM manufacturing involves the uniform mixing of particles with material matrix and pouring the resultant mixture into a spinning mold forming a compositional gradient and allowing it to solidify. The centrifugal casting method is exciting due to the possibility of gradient control using process parameters. The centrifugal casting process is developing rapidly and has the potential to dominate the field of FGM production. However, it is still in the development stage due to inadequate knowledge of particle distribution and control [18].

The grading determines the functionality and can be regulated and enhanced by certain processing parameters, such as particle size and volume, centrifugal rotation speed, mold temperature, molten metal alloying temperature and cast geometry. The size and concentration of the ceramic particle in a matrix has a correlation with hardness and wear [18].

1.5 The Problem

The main reasons for failure in polymer composite gears are mechanical and wear. To overcome this problem FGM gear are used that must have a very hard surface to resist wear, and a tough core to resist the high impact that occurs during the operation.

Gears are made of polymer and its composite are now used to replace the metallic gears which can be used in low load condition. It provides the low cost, light weight, self-lubricity, high damping resistance and low noise.

1.6 The Aim

The design of a novel fabrication method for producing continuous FGM which used in various application. The principal objective of the present investigation is to determine whether an FGM possesses good wear and mechanical properties than the non-FGM material, and the subsequent steps conduct this work:

1. Manufacturing a centrifugal apparatus in a new way that differs from the centrifugation methods in previous research in the terms of the shape of the sample and the direction of the gradient by using acrylic dies.
2. Using a centrifugal apparatus to produce continuous graded and fabricate equivalent non FGM with two components (Epoxy and Nano Alumina) over the cross-section of the rectangular sample in addition to neat epoxy for comparison purposes.
3. Studying the effect of adding alumina nanoparticles as reinforced materials with different samples of FGMs and comparing them with the epoxy and homogenous nanocomposites using mechanical tests, such as three-point bending, hardness and impact strength.
4. Studying the tribological properties of the FGM to calculate specific wear rate and coefficient of friction then the results are compared with equivalent non FGM samples and pure epoxy resin experiments.
5. Studying the dispersion of nanoparticles of the fractured specimens after impact loading by scanning electron microscope (SEM).

1.7 Thesis Layout

This thesis includes five chapters, as follows:

1- Chapter one includes a brief introduction to the functionally graded materials, their applications, and fundamental principles for understanding the subjects in the succeeding chapters.

2- Chapter two includes the theoretical considerations and a brief review of the previous works, including the mechanical and tribological properties of the functionally graded material reinforced with different nanoparticles and non-FGM with alumina nanoparticles.
3- Chapter three comprises the experimental outline and description of the specimen geometry, equipment, and the experimental procedure.
4- Chapter four illustrates the results, analysis, and discussion of the experimental data. These analyses are presented in the form of graphs and tables.
5- Chapter five lists the conclusions of the work and gives some recommendations for future work and research in the field of wear of the functionally graded material.

CHAPTER TWO
THEORETICAL PART

2-1 Introduction

Functionally graded materials are spatial composites which display discrete or continuously varying compositions over definable geometrical length. The gradients can be continuous on a microscopic level or layers comprised of metals, ceramics and polymers. The material gradients induced by spatial variations of properties make FGMs behave differently from common homogeneous materials and traditional composites [14].

The use of FGMs avoids the problems associated with the presence of an interface in a material, poor adhesion, unwanted reflections, etc. They can provide an optimum response to an external field in functional applications [19].

The utilization of nano-filler in polymeric composites helps to improve mechanical, tribological characteristics and thermal stability and other properties. The final selection of nano-filler ultimately depends up on the requirements of end user. Polymer composites are mostly used in Tribological applications due to the possibility of changing their properties with addition of fillers and fibers [20 and 21].

The idea to induce continuous gradation intrinsically in a material so as to have an outer surface with improved wear resistance has always appealed to material scientists and engineers. There are more than 40 techniques available for the synthesis of FGM; however, the emphasis is always to opt for that technique which has low cost, good reproducibility, and takes less time to produce FGM [22].

Centrifugal casting is one of the promising methods for the production of FGM. The components produced by centrifugal castings have good micro structural properties and less porosity compared with conventional casting techniques and provides excellent mechanical properties [23].

2.2 Types of Functionally Graded Materials

Functionally graded materials can be classified into several ways [24 and 25]:

1. Based on the initial area of application
2. Based on processing method.
3. Based upon the nature of gradient.

2.2.1 Classification based on the initial area of application:

There are different types of areas, in which FGMs are now being used that are different from the initial area of application. The different types of FGMs include porosity gradient structured FGMs, chemical gradient-structured FGMs, and microstructural gradient-structured FGMs [26].

2.2.1.1 Chemical composition gradient FGM:

This is the type of FGM, where the chemical composition is gradually varied, according to the spatial position in the material. This could be in the form of a single phase, or in a multiphase material. A single-phase FGM is produced when the composite is produced from a single phase, as a result of the solubility of the chemical elements of one phase in the other phase. This usually occurs during the sintering process [27].

The most commonly designed and most commonly used **FGM** are the ones with a multiphase chemical composition. The phases and chemical composition are made to vary across the bulk volume of the material. As the composition of material is varied from one material into the other, it will result in different phases with different chemical compositions that would help to achieve the intended application, for which the FGM has been designed.

2.2.1.2 Porosity gradient FGM

In this type the porosity in the material is made to change with the change in the spatial position in the bulk material. The schematic diagram of

a typical porosity gradient functionally graded material is shown in Figure (2.1) [28 and 29].

This type of FGM is very important for the biomedical applications, Porosity gradient materials are produced by the deposition of powder. Porosity gradient materials could be porosity density gradation or pore size gradation. The porosity density is produced with the amount of porosity changing with respect to the spatial position across the volume of the material. The pore size gradient of the FGM, on the other hand, is produced by varying the pore sizes or the pore shape, or both. The pore size gradation can be achieved by varying the powder particle sizes that are used at different locations in the bulk material during the gradation process [30, 31, and 32].

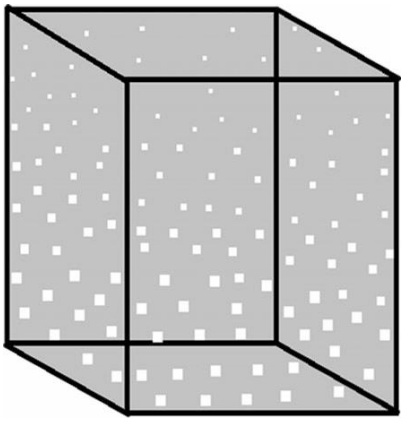

Figure (2.1): Schematic diagram of porosity-graded FGM [28]

2.2.1. 3 Microstructure gradient FGM

In this type the microstructure is tailored so that different microstructures are produced in the material, which is made to change gradually, so as to achieve the required properties from the material.

Microstructural gradation can be achieved during the solidification process, such that the surface of the material is quenched, for example, when producing a very hard surface property of the material. The core of the same material is allowed to cool down slowly, which would help to produce different microstructures from those on the surface of the material to the innermost part. A schematic diagram of a typically graded microstructure is shown in Figure (2.2) [25 and 28].

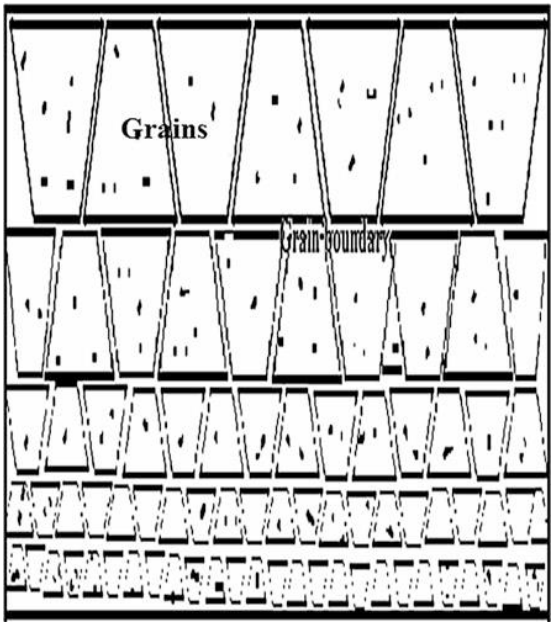

Figure (2.2): Schematic diagram microstructure gradient FGM [28]

Classification Based on processing method

FGM can be divided into two broad groups namely thin FGM and bulk FGM [33 and 30].

2.2.1.1 Thin FGM

It consists of relatively thin sections or thin surface coating, produced by:

- Physical or chemical vapor deposition (PVD/CVD)
- Plasma spraying
- Self-propagating high temperature synthesis (SHS)
- Ion beam assisted deposition ….. etc.

2.2.2.2. Bulk FGM

It consists of volume of materials which require more labor-intensive processes. Bulk FGMs are produced using:

- Powder metallurgy technique
- Centrifugal casting method
- Solid freeform technology …… etc.

2.2.3. Classification based upon the nature of gradient

Depending upon the nature of gradient, FGMs (composites) may be grouped in to the following types:

1. Fraction gradient type as shown in Figure (2.3 a).
2. Shape gradient type as shown in Figure (2.3b).
3. Orientation gradient type as shown in Figure (2.3c).
4. Size of material gradient type as shown in Figure (2.3d).

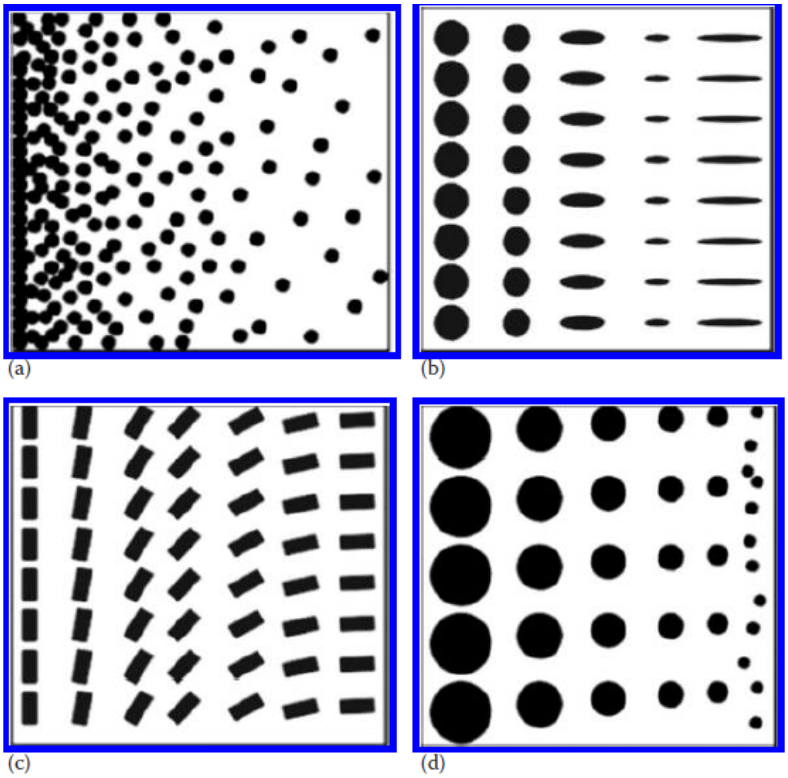

Figure (2.3): Based on nature of gradient, different types of FGMs may be (a) fraction gradient type, (b) shape gradient type, (c) orientation gradient type and (d) size gradient type [19]

2.3 FGM Design

Several FGMs are manufactured by two phases of materials with different properties. Since the volume fraction of each phase gradually varies in the gradation direction, the effective properties of FGMs change along this direction. Therefore, there are two possible approaches to model FGMs [33].

2.3.1. Continuous-graded structures (homogenous graded)

This type is an incessant formation, whereby compositional change seems invisible with no distinct discrete gradation of layers as shown in Figurer (2.4a), and can be achieved by using centrifugal casting technique.

2.3.2 Stepwise-graded structures (inhomogeneous graded)

This type is achieved by stacking layers with near-composition as a fractional material's composition dominates while the other declines with position as shown in Figurer (2.4b). Stepwise gradation, which occurs in powder metallurgy technique, sprays casting [33].

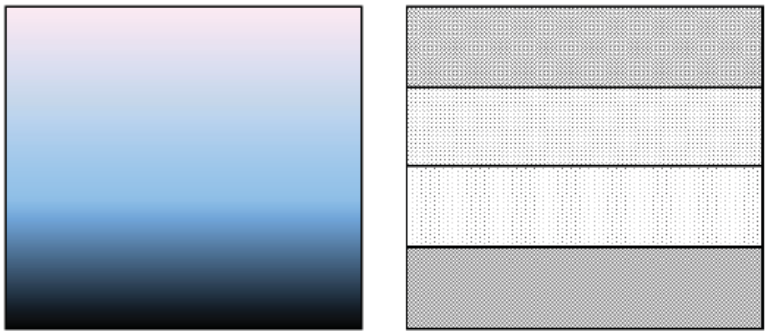

Figure (2.4): Type of FGM structure: (a) continuous and (b) stepwise graded [34 and 30].

2.4 Fabrication processes of the FGMs

Although the performance of FGMs has been theoretically documented since the 1970s, the findings impact has remained restricted for several years owing to a shortage of the appropriate synthesis approaches for the functionally graded materials.

Japan took another 15 years to conduct systematic research upon the production procedures for the FGMs as part of a national research program upon the FGM. Then, a significant portion of FGMs research has been devoted for fabricate these materials using various developed manufacturing methods. As the synthesis procedure is enhanced, the powder cost and the entire process being minimized, enabling the FGM use to be expanded [35]. However, FGM fabrication processes can be classified in the following chart in Figure (2.5).

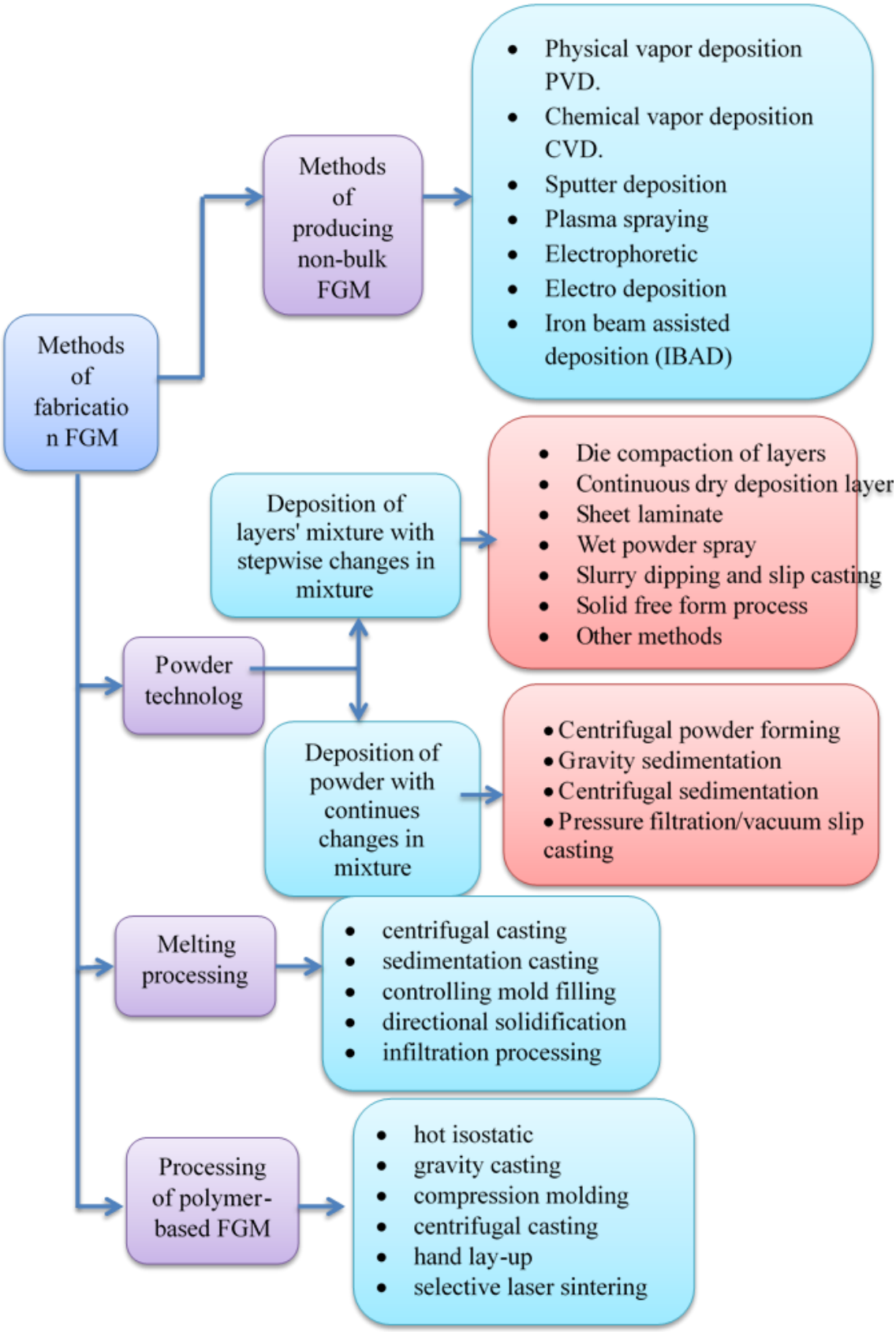

Figure (2.5): Classification of the FGM fabrication methods [36].

2.4.1 Centrifugal casting

The centrifugal casting is a casting method in which the force of gravity when pouring the molten into the mold is increased by rotating or spinning the mold assembly. Centrifugal casting consists of producing castings by causing molten to solidify in rotating molds. The speed of rotation and melt pouring rate vary with the alloy and size and shape being cast [37].

Centrifugal casting offers greater potential for graded structure manufacture than gravity. The main reason for this is the higher pressure in the melt, which facilitates infiltration in a graded preform. Another reason is that usually the centrifugal force exceeds essentially the gravitational force, and because of this particle in composite slurry move faster than in the case of gravity casting. Moreover, by management of rotation speed, one can control the magnitude of the centrifugal force, which means to control particle velocity in liquid composite during solidification. The latter is impossible in gravity casting and gives an important advantage of centrifugal casting for production of a variety of graded structures [38].

Due to the application of centrifugal force, the castings are completely free from any porosity defect, denseness and strength are high [39].

The principle behind centrifugal casting technique is the usefulness of forces generated from centripetal acceleration obtained during the rotation of the centrifugal mold to distribute the constituent elements present in the liquid metal. The centrifugal forces play significant role during the pouring and solidification which results in higher density elements at the outer periphery of the cast component and the nonmetallic slag inclusions in the liquid melt and the gas bubbles which are less dense comparatively forced to the inner surface as depicts by Figure (2.6) [40].

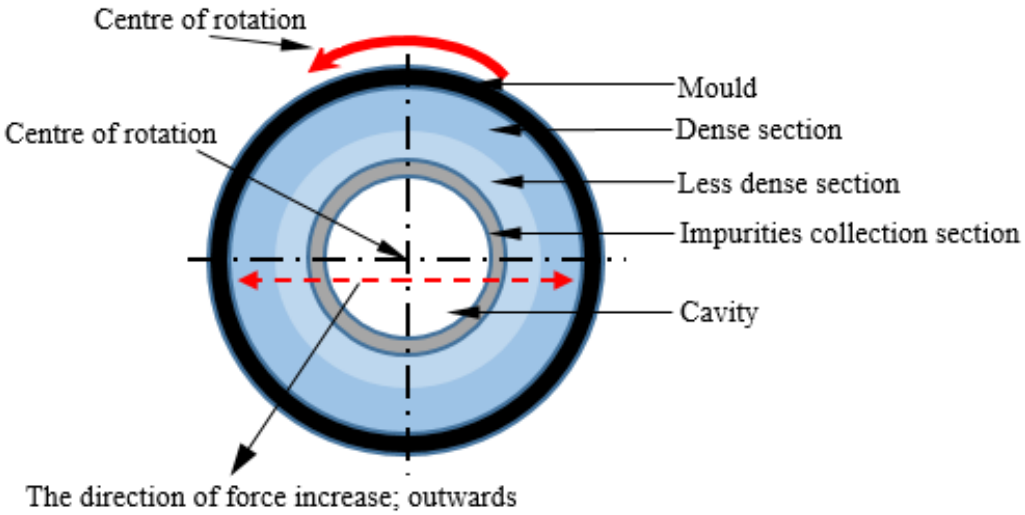

Figure (2.6): A schematic of a centrifugal casting system [41]

When particles containing liquid/slurry is subjected to centrifugal casting with the aid of centrifugal force, two distinct zones are normally attained at the two ends of the component - particle enriched region and depleted region. The extent of particle segregation and relative locations of enriched and depleted particles zones within the casting are mainly depends on the processing parameters, such as the metal viscosity, melt temperature, solidification direction, cooling rate, the densities of the reinforcement particles and the constituent elements present in the matrix liquid, particle size and the rotational speed of the mold during the casting process [26].

2.4.1.1 Classification of centrifugal casting

Centrifugal casting is mainly classified as:

1. True centrifugal casting,
2. Semi-centrifugal casting and,
3. Centrifuged casting.

1. True centrifugal casting

In this process, while the mold rotates about its axis, which may be horizontal, vertical or inclined at any suitable angle, the molten is poured in, so that the internal shape is formed by centrifugal action. The molten solidifies, forming a hollow casting without the use of a central core. The

method is ideal for hollow cylindrical castings, such as bushings, gun barrels, pipes, and hollow propeller shafts [39].

Figure (2.7) illustrated horizontal centrifugal casting. The molten is poured into a horizontal rotating mold at one end. In some operations, mold rotation commences after pouring has occurred rather than beforehand. The high-speed rotation results in centrifugal forces that cause the molten to take the shape of the mold cavity. Thus, the outside shape of the casting can be rounding, octagonal, hexagonal, and so on. However, the inside shape of the casting is (theoretically) perfectly round, due to the radially symmetric forces at work. Centrifugal force is defined by equation (2.1): [42]

$$F_C = \frac{mv^2}{r} \tag{2.1}$$

Where F: force (N); m: mass (kg); v: velocity (m/s); and r: inside radius of the mold (m).

Velocity (v) can be expressed as:

$$V = \frac{2\pi nr}{60} = \frac{\pi nr}{30} \tag{2.2}$$

Where n: rotational speed (rev/min.).

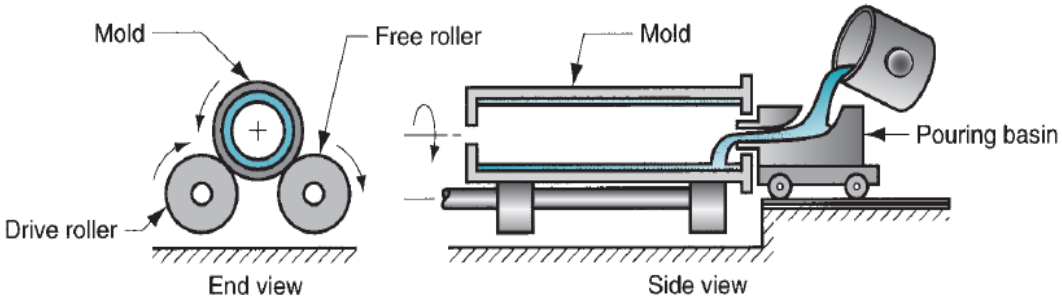

Figure (2.7)**:** Setup for true centrifugal casting [42]

In the vertical centrifugal casting, the axis of rotation is usually horizontal but can be vertical for short work pieces. The outside shape of the casting can be round or of a simple symmetrical shape. However, the inside shape of the casting is always round. During cooling, lower density impurities will tend to rise toward the center of rotation. Consequently, the properties of the casting can vary throughout its thickness. The effect of

gravity acting on the liquid metal causes the casting wall to be thicker at the base than at the top. The inside profile of the casting wall takes on a parabolic shape [39 and 42].

2. Semi-centrifugal casting:

This method is employed for making large-sized castings which are symmetrical about their own axis, for example, pulleys, spooked or disked wheels, gears and propellers. While the mold rotates about a vertical axis in a properly balanced state, the metal is poured into a central sprue from where it first enters the hub and then is forced outwards to the rim by centrifugal force [43, 44]. In general, the rotational speed is lower than that used in true centrifugal casting. The mold is designed with risers in the center to supply the feed metal as shown in Figure (2.8) [45].

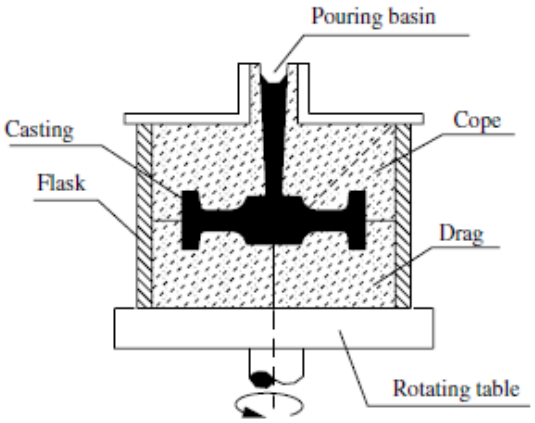

Figure (2.8): Semi-centrifugal casting [45]

3. Centrifuging casting

This process is used for smaller, intricate parts, and radial symmetry of the part is not a requirement as it is for the other two. Centrifugal force provides the pressure that ensures complete filling of the mold cavities. Molds are located radially about a central sprue or riser, which acts as the axis of rotation. Rotation can be about a vertical or horizontal axis and is at a relatively low rotational speed. Molds may be stacked as shown in Figure (2.9). Small caps and brackets, and dental inlays are among the components cast. The vertical and inclined axis is generally more convenient to use since

the metal can be poured more easily and the castings can also be removed with less difficulty [44].

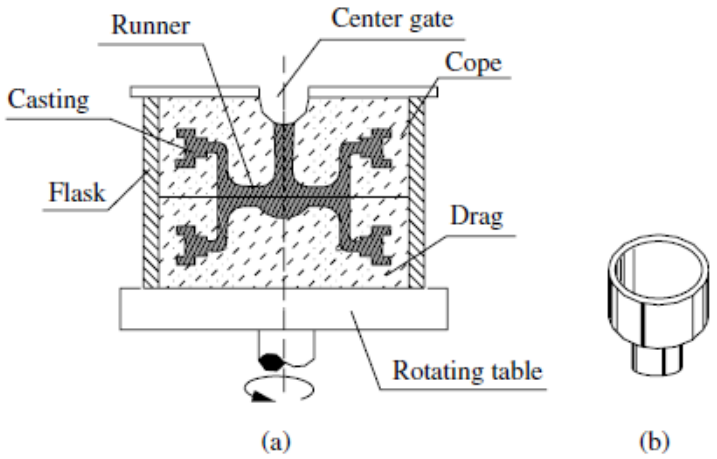

Figure (2.9): Centrifuging casting: a) mold for eight castings, b) the casting [45]

2.4.2 Advantages of centrifugal casting [26 and 45]

- ❖ Centrifugal casting does not need a gating system for elements to direct the flow of metals, so it is a time saving process.
- ❖ Good quality castings can be produced in terms of surface finish, accuracy in the dimensions, and reduced porosity such as gas porosities.
- ❖ A faster solidification can be achieved with a high quality of metallurgical properties due to the centrifugal force.
- ❖ The centrifugal force generated is about 150 times as compared with to gravitational force.
- ❖ True centrifugal casting is characterized by better mechanical properties of the cast than is true in conventional static casting: nonmetallic impurities that segregate toward the bore can be machined off؛ the casting is relatively free from defects; there is less loss of metal compared to that in conventional sand casting; production rate is high; there are no parting lines.
- ❖ The centrifugal force improves homogeneity, finishing and accuracy of the final cast product.

2.5 Material used in this Study

2.5.1 Epoxy Resin

The term epoxy, epoxy resin, or epoxide (Europe) refers to a broad group of reactive compounds that are characterized by the presence of an oxirane or epoxy ring, shown in Figure (2.10). This is represented by a three-member ring containing an oxygen atom that is bonded with two carbon atoms already united in some other way [46].

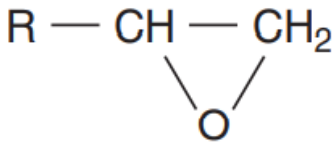

Figure 2.10: The epoxy or oxirane ring structure [46]

A general formula for an epoxy resin can be represented by a linear polyether with terminal epoxy groups and secondary hydroxyl groups occurring at regular intervals along the length of the chain. The epoxy resin structure and properties influenced by the various chemical groups are illustrated in Figure (2.11) [47].

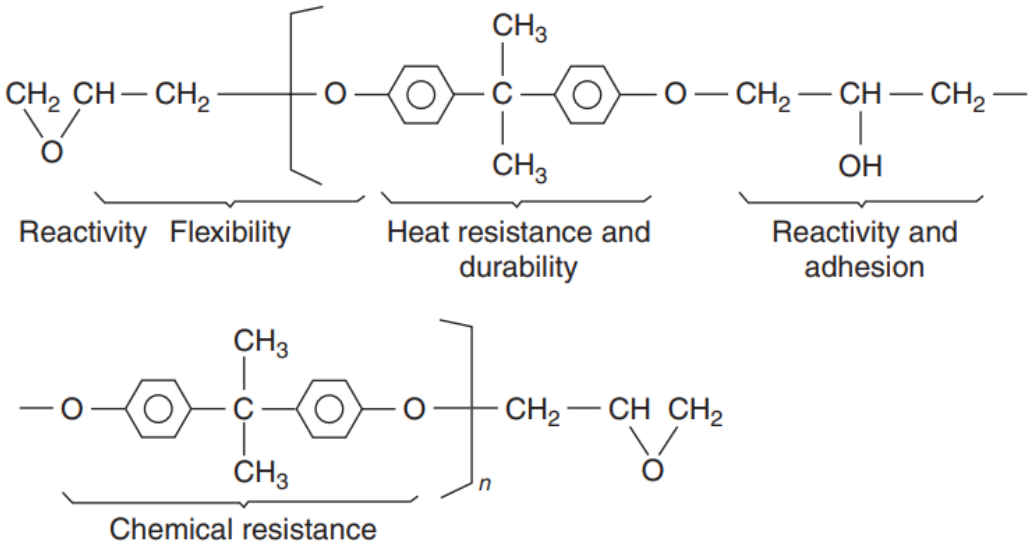

Figure 2.11: The structure and properties of an epoxy resin [46]

Several important statements can be made relative to the structure of the epoxy molecule [46]:

• The epoxy groups at both terminals of the molecule and the hydroxyl groups at the midpoint of the molecule.

- The large part of the epoxy resin backbone contains aromatic rings, which provide a high degree of heat and chemical resistance.
- The aliphatic sequences between ether linkages confer chemical resistance and flexibility.
- The epoxy molecule can be of different molecular weight and chemistry. Resins can be low-viscosity liquids or hard solids. Low viscosity can be obtained at 100 percent solids, which results in good penetration and wetting.
- A large variety of polymeric structures can be obtained depending on the polymerization reaction and the curing agents involved. This can lead to versatile resins that can cure slowly or very quickly at room or at elevated temperatures.
- No small molecules such as water are liberated during the curing process. Thus, epoxies exhibit low shrinkage, and they can be cured under very low pressure. This provides an adhesive joint with a very low degree of internal stress when cured.

Thermoset epoxy resins are defined by their superior mechanical, electrical, and chemical resistance and low moisture absorption. Due to their highly cross-linked structure, their applications are severely limited [48].

Epoxy resins have low fracture toughness, low impact strength, and a low resistance to wear. Mixing nanoparticles such as nano-alumina, carbon nanotubes, and graphene improves the strength and modulus of epoxy resin [49].

The epoxies are monomers or pre-polymers reacting with the curing agents for forming thermosetting plastics with high performance. Epoxy

resin markets have historically been motivated via the request made in various applications, including protective coatings for consumer durables printed circuit boards, electrical insulation, building and civil construction, and adhesives [50].

Crosslinking agents must convert the epoxy resins into hard, non-fusible thermoset grids. These cross-linkers are also known as hardeners or curing agents, aiding in curing or crosslinking the epoxy resins [51].

2.5.2 Reinforcements (Nano-Al_2O_3)

In general, nano-materials are characterized by at least one dimension in the nanometer (1 nm = 10^{-9}m) range [52]. Some materials exhibit additional characteristics or properties compared to the same coarser material in the nano range order. These materials are significantly used in innovative technological applications and products [53].

Several types of nano-materials are classified according to their composition and shape. A practical way for their classification is according to the structural features of their elementary units and the number of dimensions, which are outside the nano-scale. Thus, they can be (0-D) (zero-dimensional), like nanoparticles (silica, alumina, titanium, etc.), 1-D (one-dimensional) like nano-rods and fibrous materials such as carbon nanotube, and 2-D (two-dimensional) like nano-layers such as graphene nano-plate [54].

The reinforcing materials are discontinuous and have more strength than the matrix material in nano-composite [53]. Nano-composites and micro composites have relatively dense micro-additives that require a high weight ratio for developing the mechanical properties of the matrix; therefore, the weight of the composite rises. Nevertheless, a nano-composite can significantly enhance matrix tribological and mechanical properties with a low content of nano additive, resulting in a lightweight composite [56, 57].

Additionally, nano-filler can be a problem if it withstands dispersal and forms agglomeration. It has a weak filler-matrix interface bonding, reducing the transfer of stress. It increases the resin's viscosity as the content of nanoparticles increases, limiting its process ability. These flaws impair the polymer's properties [8].

The Aluminum oxide has long been utilized as filler due to its elevated hardness; in the Nano metric sizes, alumina verifies its high hardness and thus its ability to enhance the nano composites' mechanical properties. The nano-Al_2O_3 is widely obtainable upon the market in multiple purities and particle sizes at a reasonable price [58].

Nanosized alumina is characterized by high surface area, excellent stability at high temperature, high conductivity and good mechanical properties. Chemically it is inert to most alkalis and acids, has a good adsorption capacity ……, etc. due to these properties' nano-alumina is increasingly used to produce various mechanical compound, insulator, or in parts that are subjected to extensive abrasion. Nano-alumina has also used in composite based on epoxy resin or Portland cements with the main objective to enhance the mechanical properties [59].

Alumina nano-particles are oxide and exist in nature in various forms, most commonly as bauxite. Bauxite is an impure form of hexagonal gibbsite and can be extracted from clay or coal fly ash. Carbon Nanotubes and Carbon Nanofibers in Concrete—Advantages and Potential [59].

Alumina occurs in two forms: transition or metastable phases. α-Al_2O_3 is the stable phase of alumina, whereas the metastable phases, i.e., chi (χ), eta (η), kappa (κ), theta (θ), delta (δ), and gamma (γ), depend on the synthesis temperature. The conventional methods for producing α-Al_2O_3 incorporate solid-state, thermally-influenced transformations from the hydrates of aluminum oxide. The amount of and total transformation to the corundum structure depends on the time and temperature of the thermal treatment [60].

The crystal structure of α-Al_2O_3, which is called corundum structure, ideally consists of close packed planes (A and B planes) as shown in Figure (2.12).

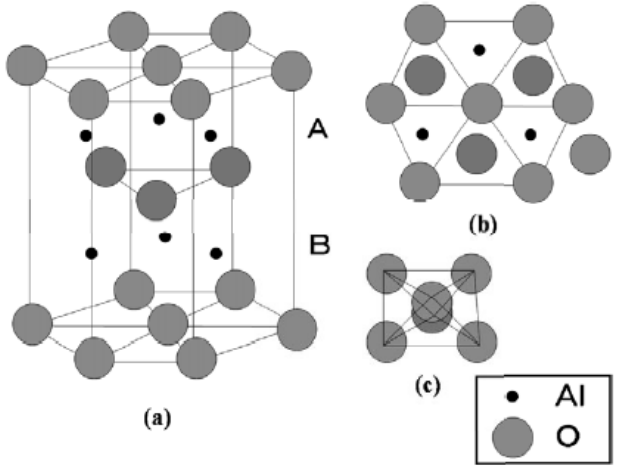

Figure 2.12: (a) Structure in α-Al_2O_3, (b) top view of the corundum structure, and (c) octahedral structure of α- Al_2O_3 **[61]**.

2.6 Mechanical Test

Polymers have a wide range of mechanical properties due to their atomic structure and bond strength. Numerous properties of polymers are quantified and recorded similarly to those of metallic materials. The terms stress-strain, modulus of elasticity, strength, impact, and hardness refer to polymers as they do to metals [62].

2.6.1 Three-Point Bending Test

Flexural properties give an indication of the response of a material under bending load. Flexural stress-strain characteristics are derived by monitoring both the force required to flex a material and the displacement that the material undergoes as a result of the applied force at a constant deformation rate. The mode of loading can take one of three forms:

• Three points

• Four points

• Simple cantilever

By far the most common is three-point loading. As the name implies, this mode of loading is achieved by applying the force to the specimen at three points, as shown in Figure (2.13). The central loading point being equidistant from the outer two supporting points [63].

In practice the specimen usually sits on the two outer supporting rods and the force is applied through the central loading rod, which will have both a force transducer and some form of displacement measuring device attached [64, 65].

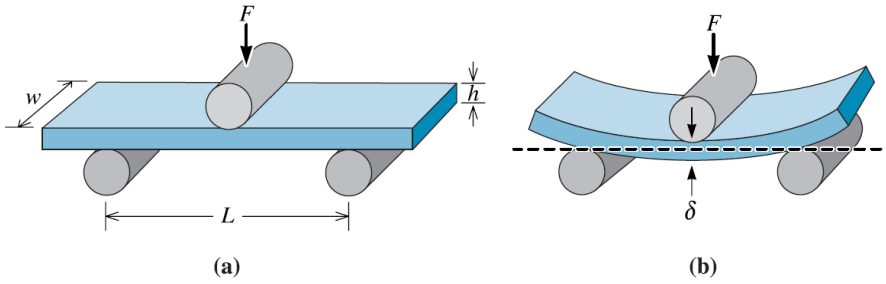

Figure (2.13): (a) Three-point bend test, and (b) The deflection (δ) determined via bending [64].

Unlike the tensile test, the flexural test allows easy sample preparation and does not involve clamping of the sample [65]. In general; three test parameters are reported from a flexural test: flexural strength, flexural strain and flexural modulus. Flexural strength is the ability of a material to withstand bending force applied perpendicular to its longitudinal axis. Flexural strain reflects the flexibility of a material. Figure (2.14) shows typical flexural stress–strain diagrams of various polymers. Diagram (a) in this figure shows the brittle fracture behavior of materials [66].

According to Figure (2.14), the material parameters explained in the following can be determined for various plastic materials. Flexural *strength* σ_{fM}*:* the maximum flexural stress tolerated by the specimen during the experiment. In the case of material behavior as shown in diagram (a), this value is identical to σ_{fB}. *Flexural stress at break* σ_{fB}*:* this value is determined if specimen break occurs during the experiment [66] .

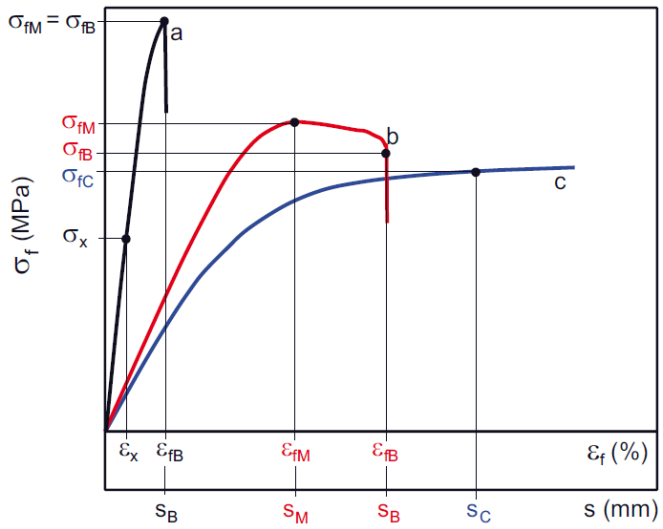

Figure (2.14)**:** Typical flexural stress–strain diagrams of polymers in the bend test [66].

2.6.2 Hardness test

The hardness test is among the most often applied methods in mechanical material testing. That is because it can be performed comparatively simply, quickly and, from an equipment point of view, efficiently. Since slight damage to a component surface in the form of one or more relatively small indentations usually has little effect on its function, the hardness test is mentioned among the nearly non-destructive test methods. That makes it possible to test very small components and thin layers that can hardly provide information on the profiles of other properties.

The term hardness is usually taken to mean a measure the resistance of the material to indentation but has also been applied to scratch resistance and resilience. The result depends on the indentor geometry and degree of indentation as well as the time of indentation after which the measurement is made.

The type of deformation under load can be observed on the indentations, ranging from rubber-elastic (elastomers), (thermoplastics) and (thermosets) as in Figure (2.15).

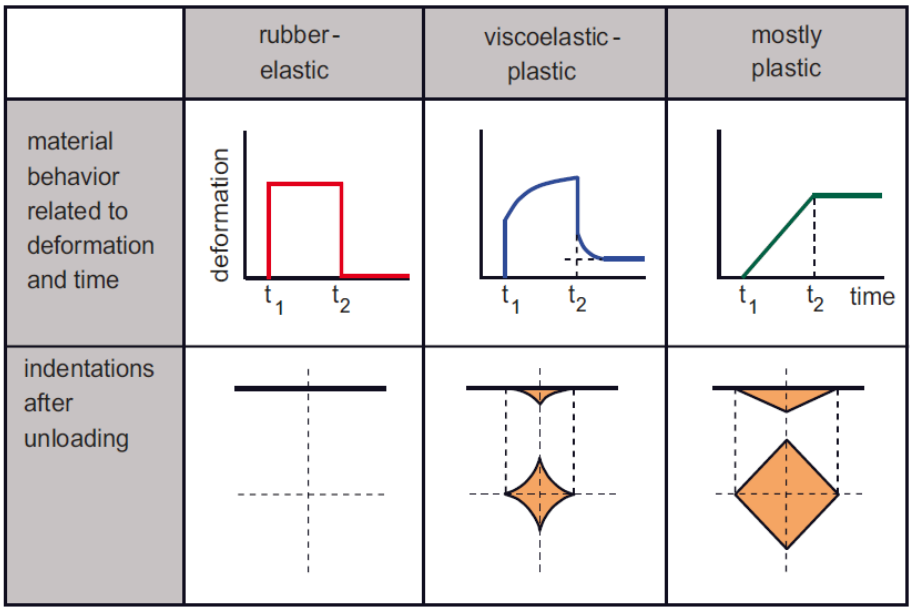

Figure (2.15): Relationship between material behavior and indentation shape [66].

The most widely used scale is probably the Shore durometer hardness scale, available in two major variants: Shore A and Shore D, as illustrated in Figure (2.16). Shore scales are typically utilized to determine the hardness of polymers (rubbers and plastics). The Shore (A) scale is employed to obtain the elastomeric properties of the soft elastomers (rubbers) and soft polymers. The Shore (D) scale is utilized for determining the hardness of the rigid elastomers as well as most different polymer materials (Thermoplastics and Thermosets) [67].

These durometers are small, hand-held instruments with indentors of given geometry that is pressed into the surface of the material to be measured under a spring of given stiffness. Although originally designed to be hand held, they are often used on a stand. The amount of penetration of the indentor is measured by a suitable scale marked directly in hardness degrees. Traditionally the scale was a dial gauge but modern instruments can have digital read out [68].

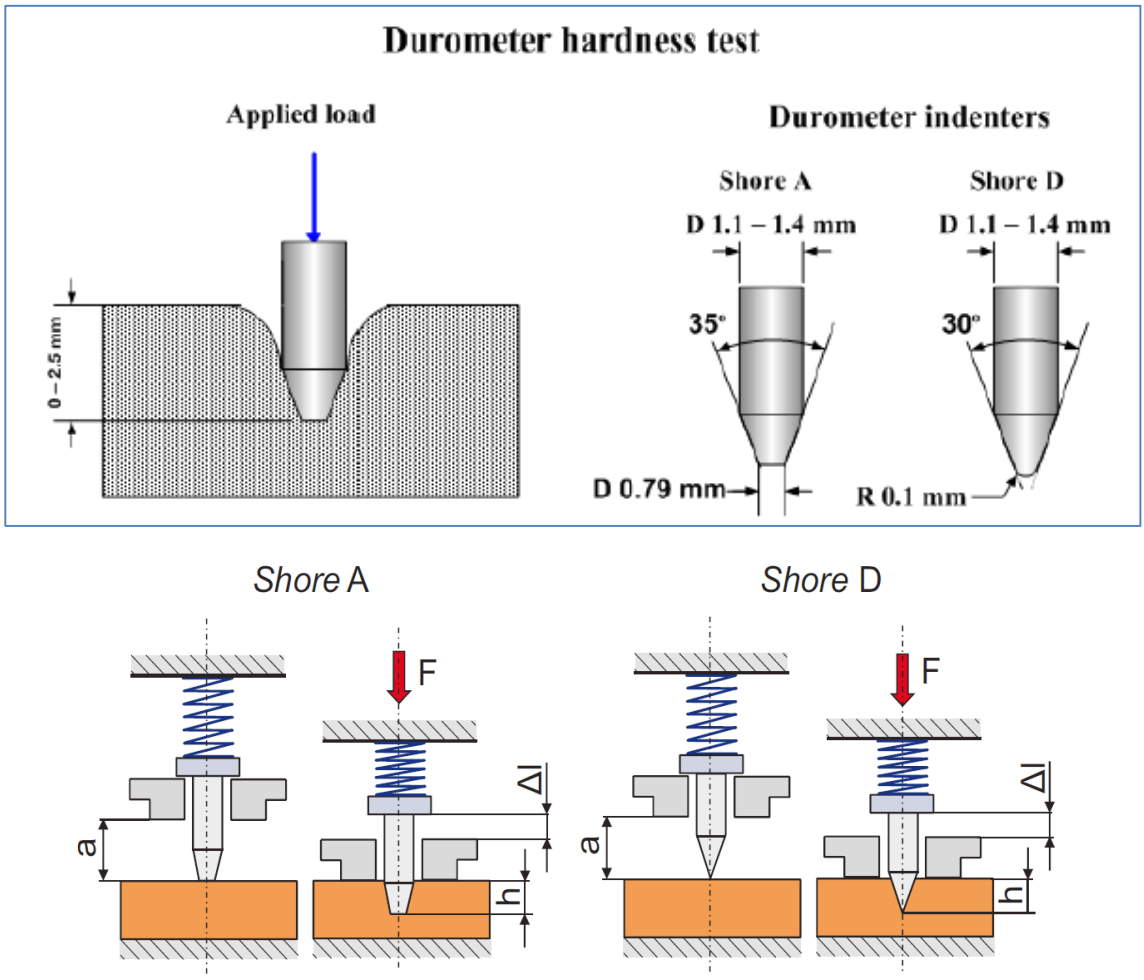

Figure (2.16): Shore Durometer [69].

In this procedure, a truncated cone (Shore A) with an included angle of 35° and a diameter at the flat of 0.79 mm, this operates under a spring pressure determined by [70]:

$$F = 550 + 75\ H_a \qquad (2.3)$$

Where F is the applied force in (N) and H_a is the Shore A hardness.

The Shore D scale is appropriate for most common harder plastics, which has a truncated cone with a spherical cap with a 30° included angle and a slightly rounded (0.1 mm radius) tip and is operated by a spring [69]:

$$F = 445\ H_d \qquad (2.4)$$

Where H_d is the Shore D hardness.

2.6.3 Impact test

Impact tests involve striking a suitable specimen with a controlled blow and determining the amount of energy absorbed by the sample as it bends or breaks. The energy value indicates the material's toughness. It differs from the other mechanical tests since it is fast for measuring the needed energy to break the specimen in bending mode. Impact tests can be divided into two classes: pendulum impact tests and drop-weight impact tests [66].

The pendulum impact test employs a pendulum type of hammer. It is carried out in two ways: Izod and Charpy. The apparatus used for the pendulum test consists of a heavy base with a vice for clamping the specimen and a pendulum hammer swinging at a sample. The machine base must be kept on a rigid platform to prevent vibrational energy losses [66].

These Izod/Charpy tests are widely applied in industry due to the ease of sample preparation, and it is possible to generate comparative data very quickly. In the Izod test the specimen is fixed as a cantilever with the help of a vice Figure (2.17). The Charpy test is also carried out in the same apparatus and specimen. The only difference is that in Charpy test the specimen is supported as a simple beam. The Charpy impact test is performed on notched and un-notched specimens with two-point support and serves to evaluate the toughness behavior of plastics under impact loading [66].

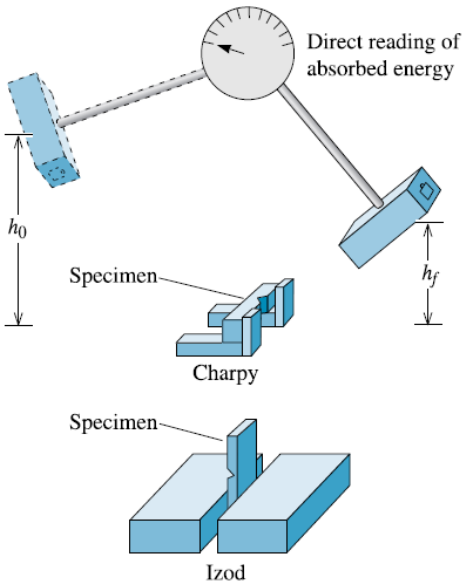

Figure (2.17): Impact loading in Charpy and Izod configurations [64].

In such a test, a heavy pendulum begins at the height of (h_o), swings throughout its arc, and strikes and breaks the specimen before reaching the final height (h_f) lower. One can calculate the difference in potential energy when one knows the pendulum's first and final heights. This distinction refers to the amount of impact energy absorbed via the specimen throughout the failure [69].

When the test is performed, the energy (W) absorbed by the specimen is calculated from the difference between the pendulum hammer height over specimen before and after impact and the mass (m) of the pendulum hammer [66].

$$W=W_1 - W_2 = m.g\ (h_1 - h_2) = m.g\ .\ l\ (\cos\beta - \cos\alpha) \qquad (2.5)$$

W_1: pendulum hammer energy before specimen breaking

W_2: pendulum hammer energy after specimen breaking

h_1: height of pendulum hammer before impact

h_2: height of pendulum hammer after impact

l: distance between the axis of rotation of the pendulum and the center of gravity of the pendulum

g: local acceleration due to gravity (g = 9.81 m/s^2)

β: starting angle

α: angle of rise

2.7 Tribology

Tribology is the field of science and technology dealing with contacting surfaces in relative motion –which means that it deals with phenomena related to friction, wear and lubrication. Tribology played a central role in early technological evolution, even in ancient times [70]. Actual surfaces, always exhibit some degree of roughness as shown in Figure (2.18) illustrates that the actual physical contact occurs at localized spots within the area. These points at which the actual contact occurs are referred to as junctions. The sum of the individual contact areas of these junctions is called the real area of contact. While the apparent or nominal area of contact represented the overall noticeable area of the body in contact with other body.

Assume that the real area of contact is composed of n circular junctions of diameter d. Further, assume that if the wear fragment is formed; it will be hemispherical shaped with a diameter d. The total real area of contact (A_r) is then [71]:

$$A_r = \frac{n\pi d^2}{4} \qquad (2.6)$$

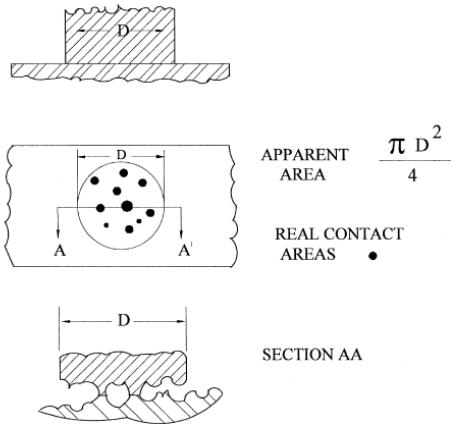

Figure (2.18): Apparent and real area of contact. Contact occurs are discrete locations, called junctions [71].

In modern industrialized societies there is a growing need to reduce or control friction and wear for several reasons, for example to extend the lifetime of machinery and bio-systems, to make engines and devices more efficient, to develop new advanced products, to conserve scarce material resources, to save energy, and to improve safety [70].

2.7.1 Specific wear rate

In general, wear may be defined as damage to a solid surface caused by the removal or displacement of material by the mechanical action of a contacting solid, liquid, or gas. Neither should the assumption that wear is entirely mechanical be accepted, because chemical corrosion may combine with other wear factors [72]. Wear plays an important role in determining life span of products or machine elements, and is one of the main causes of service, maintenance or finally replacement in every aspect of life [73, 74]. Wear volume loss can be calculated from equation below:

$$\text{Volume loss}(\text{mm}^3) = \frac{\text{mass loss(g)}}{\text{density}(\frac{\text{g}}{\text{cm}^3})} \times 1000 \qquad (2.7)$$

2.7.2. Wear form

Wear has been classified in various ways. One of the simplest classifications of wear is based on the presence or absence of effective lubricants namely lubricated or non-lubricated wear. Another possibility is to classify wear on the basis on the wear mechanisms the main classification includes adhesion, abrasion and surface fatigue, corrosive, erosive or fretting wears [75].

2.7.2.1 Adhesion Wear

During relative motion between the two bodies in contact, parts of the softer body can break and adhere to the harder body, thus creating pits and parallel furrows as shown in Figure (2.19) [76]. Adhesive wear depends upon the bond strength, which relates to the physical chemistry of the contact material and lubricant, on the load, and on the material hardness [77].

If one assumes that the wear particles are geometrically similar, the wear volume would be expected to be proportional to the real areas of contact at which adhesion occurs, and also to the distance of sliding [78,79]. The adhesive wear law:

$$V = K\frac{W}{H}L \qquad (2.8)$$

Where: V the wear volume, *K* is a dimensionless constant, *W* is the total normal load, *L*: is the distance of sliding, *H* is the hardness of the material.

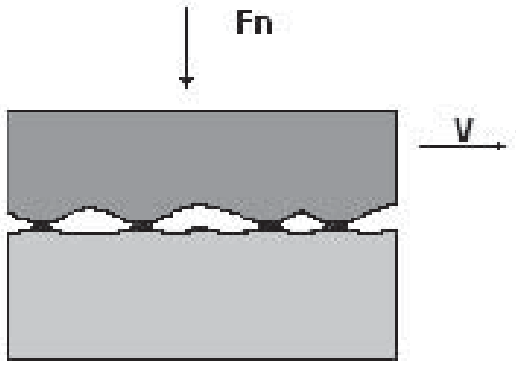

Figure (2.19): Adhesive wear [80]

2.7.2.2 Abrasive Wear

The abrasive wear is defined as surface material falling off caused by harder particles from outside or hard peaks on the coupling surfaces during friction [81]. Abrasion occurs between two surfaces in relative motion and can be split into two main categories as shown in Figure (2.20): (i) two body and (ii) three body. Two-body (or 'grooving') abrasion is caused by hard protuberances on the counter face, while in three-body (or 'rolling') abrasion, hard particles are free to roll and slide between two sliding surfaces [81].

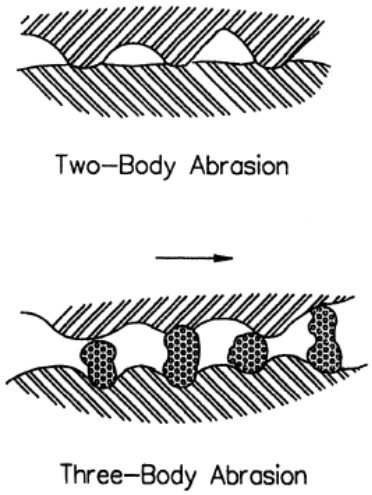

Figure (2.20): Abrasive wear situations [82]

2.7.2.3 Erosion Wear

The erosion is the progressive loss of material from a solid surface due to the mechanical interaction between the surface and some fluid, multicomponent fluid or liquid or solid impact particles as shown in Figure (2.21). The erosive wear occurs when the materials are carried not parallel to surface flow, but when they fall over the surface due to gravity or centrifugal forces. As a result, the material tends to be damaged, depending on its structural characteristics and associated properties [82].

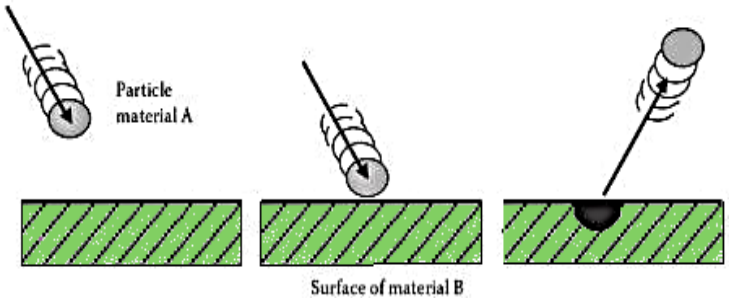

Figure (2.21): Erosive Wear [83]

2.7.2.4 Corrosive Wear

The removal of materials from the interacting surface by electrochemical reactions leads to corrosive wear. The localized electrochemical reactions can cause pitting, intergranular, or intragranular corrosion. Stress corrosion failure results from the combined effect of stress and corrosion. At elevated temperatures, reactions with oxygen, carbon,

nitrogen, sulfur, or flux result in the formation of an oxidized, carburized, nitride, sulfurized, or slag layer on the surface. Temperature and time are two important factors controlling the rate and severity of high-temperature corrosive attack [84].

2.7.2.5 Fatigue wear

Progressive loss of original material from one or more solid surfaces caused by repeated compressive stressing of the contacting solid surfaces by a rolling element as shown in Figure (2.22). The most important types of fatigue wear occur in tribosystems involving hertzian contacts, such as a sphere on a flat, a flat on a cylinder, a cylinder on a cylinder, crossed cylinders, etc.

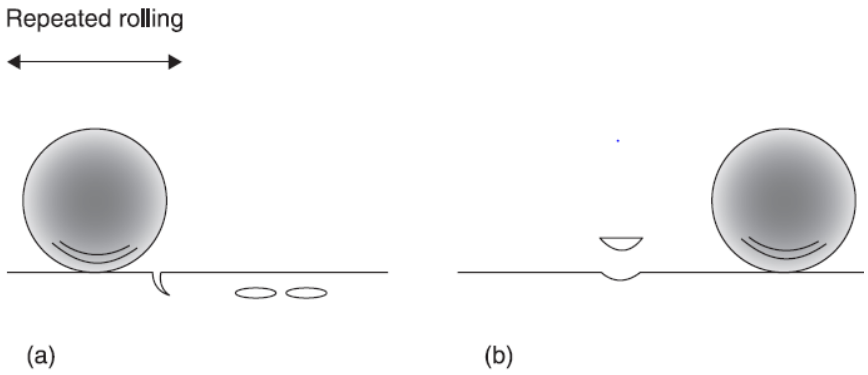

Figure (2.22**):** Schematic illustration of typical surface fatigue wear due to cyclic stress [85]

2.7.3 Wear Process Curve:

Figure (2.23) is a typical curve for the wear process. In this working condition, the wear process curve consists of three stages: running-in, stationary and severe, which indicates the relationship between the wear rate and time or sliding distance. A wear process curve is usually composed of three stages [86].

1. Running-in stage: At this stage, the wear rate gradually increases with increase of time. Figure (2.24) show the surface morphologies before and after running-in.

2. Steady wear stage: After running-in, the friction surface will be at a steady state. At this stage, the wear rate stays almost constant.

3. Severe wear stage: At this stage, the wear rate increases rapidly with time, such that the working conditions become drastically worse

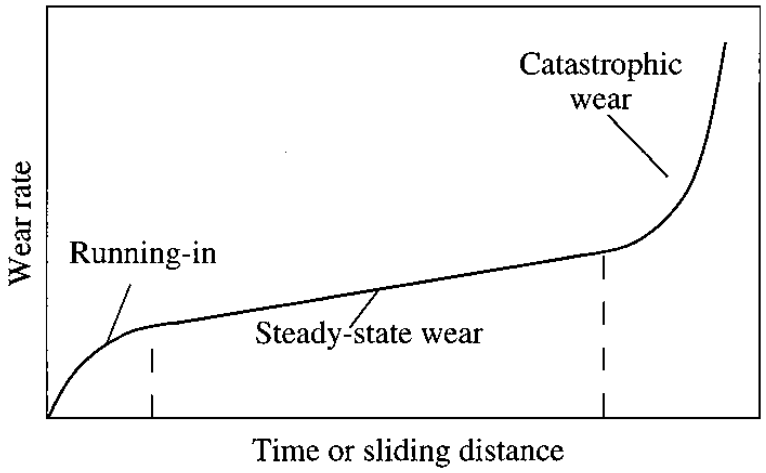

Figure (2.23): Typical wear stages appearing over longer service times in sliding contacts [86,87]

Figure (2.24): Surface morphologies before and after running-in [87].

2.7.4 Wear in Sliding and Rolling Contacts

Sliding wear tests may be performed with a large variety of geometrical configurations as in Figure (2.25). It is practical to distinguish between tests where the test bodies are symmetrically or asymmetrically arranged [86, 87].

1. **Symmetrical arrangements** are not often used in model tests; an example, however, are rings arranged as in Figure (2.25c) simulating the symmetrical and conformal contact of axial.

2. **Asymmetrical configurations**: Probably because of their simplicity and flexibility in terms of test conditions and specimen shape, rigs of the

asymmetrical pin-on-disk configuration in Figure (2.25 e) have become some of the most popular model tests for evaluating sliding wear. Pin-on-disk rigs with attached heat stages and cover boxes enabling tests in controlled atmospheres are commercially available. Also pin- or block-on-cylinder configurations in Figure (2.25 d) are frequently used [88].

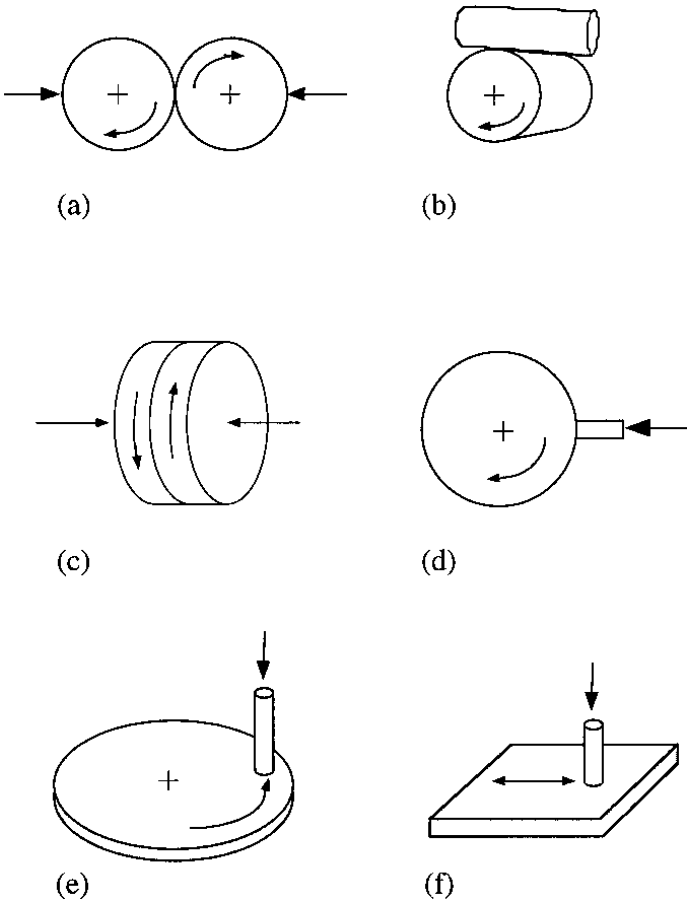

Figure (2.25): Illustrations of common sliding wear test configuration.
(a) Cylinder on cylinder (b)pin on cylinder (c) disk on disk
(d) Disk on plate (e) pin on disk (f) pin on plate [86, 87]

2.7.5 Friction:

Friction is a very common phenomenon in mechanical systems that may be increased or decreased depending on the sliding pairs and operating parameters. The discrepancy between metallic and polymeric friction is due to the differences in the elastic- plastic behavior of metals and the viso-elastic behavior of polymers [88].

The force known as friction may be defined as the resistance encountered by one body in moving over another. This broad definition embraces two important classes of relative motion: sliding and rolling. The distinction between sliding and rolling friction is useful, but the two are not mutually exclusive, and even apparently 'pure' rolling nearly always involves some sliding. In both ideal rolling and sliding, as illustrated in Figure (2.26), a tangential force F is needed to move the upper body over the stationary counter face [73].

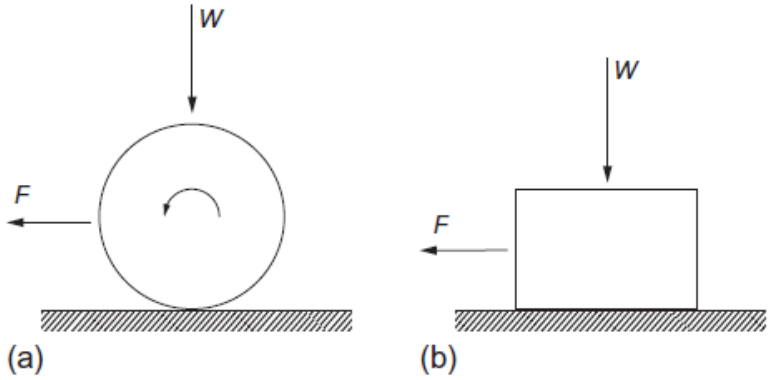

Figure (2.26): A force (F) is needed to overcome friction and cause motion by (a) rolling or (b) sliding [68].

2.7.6 Factors affecting friction and wear of polymers:

The various factors which influence the friction and wear rate of polymers and composites will be considered individually. They can be divided into "application" parameters such as applied load, sliding speed, roughness, and temperature and "environmental" factors like the presence of fluids, inert gases, or vacuum, etc. [89].

2.7.6.1 Sliding speed and time

Generally, the effect of speed and time are to increase the wear of polymers due to an increase in the contact surface temperature generated at the points of rubbing contact. However, these trends depend on the type of material [88].

2.7.6.2 Applied load and contact pressure:

The mechanism of friction and wear of polymers varies depending on the applied normal load. At high loads, thermal softening of the polymer and plastic deformation at the asperity interactions has a dominant role in determining the real area of contact [88].

2.7.6.3 Temperature:

The mechanical properties of all polymers and composites decrease as the temperature is increased so that their wear rates would be expected to increase with temperature. The actual variation of wear rate with temperature will also depend on the influence of fillers and the way in which they modify the counter face during sliding and on the formation of oxides or other films on the counter face [89].

2.7.6.4 Counter face roughness

Surface roughness has a complex effect on both friction and wear. At low surface roughness, both wear and friction are determined by adhesion of the smooth surfaces. Further increases in surface roughness will increase both friction and wear due to increased abrasive action of the surfaces. The roughness value at which the minimum occurs will depend on both the materials and methods used to manufacture the surface [90].

2.7.6.5 The influence of fillers

It has already been noted that the large majority of non-metallic commercially available bearing materials are composites in which one or more filler is combined with a polymer and that filler abrasiveness plays a significant role in determining the influence of counter face roughness on wear rate [91].

2.7.6.6 Effect of Environment

Polymeric materials exhibit a great deal of sensitivity to the environmental conditions (temperature, humidity, gases, liquids, etc.). Not only are friction and wear sensitive to the operating environment, they are

often more sensitive than bulk properties. Temperature affects friction of polymers in the same way as the complex modulus and other mechanical properties [92].

2.8 Literature Survey

The present section reviews the existing literature that being directly relevant to the thesis topic; it could be grouped into two categories:

1. Mechanical and tribological properties of graded and non-graded alumina nano-composites with epoxy matrix
2. Mechanical and tribological properties of FGMs manufacturing by using centrifugal casting method**.**

2.8.1 Mechanical and tribological properties of graded and non-graded -alumina nano-composites with epoxy matrix

Hussein and Ali [92], 2015 studied the mechanical (hardness, impact, and wear) properties of the epoxy nanocomposites containing varying amounts of SiO_2 and Al_2O_3 nanoparticles (0.5%, 1%, 1.5%, 2 %, 2.5%, and 3%). The nano-composites were manufactured using two distinct procedures (high shear mixing followed by ultrasonication). An enhancement in the whole measurement for all composites was observed, where (EP/ Al_2O_3, EP/ SiO_2) composites with 2.5%nano Al_2O_3 show better hardness and impact results. The addition of nanoparticles (especially nano Al_2O_3) decreased wear values, while the values of hardness and the energy of impact increased by almost 30% and 80% respectively.

Malia and Baraa [93], 2016 performed the effect of adding Nano Al_2O_3 particles with different concentrations (10, 15, 20, 25 and 30) % wt. on the mechanical properties of composite material based on epoxy resins and epoxy polysulfide blend matrix. For composite materials the mechanical properties were improved by adding the Al_2O_3 particle. In comparison to epoxy resin, the wear rate of the epoxy composite containing 30% Al_2O_3

under loads (5, 10 and 15) N decreased by 71.4 %, 47 %, and 54.9%, while the wear rate of the blended composite containing 30% Al_2O_3 decreased by even more, by 89 %, 79 %, and 76%, at the same loads. The optical microscope photos of epoxy Nano Al_2O_3 composite surfaces showed that the high effect and the wear were worse than the surface of the blend Nano Al_2O_3 composite.

Yousri et al. [94], 2017 studied the effect of alumina nanoparticles on composite performance in terms of mechanical and physical properties. This study uses an epoxy resin-coated alumina nanoparticle mixture with a weight percentage of (0.25, 0.5, 0.75, 1) %. These tests include those that measure bending stiffness, hardness and wear. Compared to pure epoxy, the composite material with (0.25% wt.) shows increment about 7% and 67 % in mechanical properties for bending strength and wear resistance, respectively.

Kumar et al. [95], 2018 prepared a layered functionally graded polymer nanocomposite (FGMPC) via distributing the Al_2O_3 nano particles in the matrix of epoxy. To achieve the gradation, the weight portion of Al_2O_3 nano particles was varied in the direction of thickness. The neat epoxy layers with the (0.25, 0.5, 0.75 and 1 wt.%) concentrations were consecutively cast in vertical acrylic molds for producing the sheet of graded composite with a (5 mm) thickness. In contrast, (FGPNC) flexural properties were evaluated using a 3-point bending test burdened from the pure as well as (1%) weight fractions side. The greatest increase in tensile characteristics was observed for nanocomposites containing (1%) nano particles. The tensile strength and modulus of elasticity were increased by (5%) and (14%), respectively, above the neat epoxy for nanocomposites containing (1%) nano particles. For the loading from the side of the pure epoxy, the FGPNC increased the flexural strength and the elasticity modulus by (10%) and (23%), correspondingly, above the pure epoxy specimens.

Bazrgari et al. [96], 2018 evaluated mechanical and tribological performance of epoxy-alumina nanocomposite. In order to achieve high quality dispersion of epoxy-alumina nanocomposite, ultrasonic mixing was employed. Results reveal that epoxy matrix properties have been affected by introduction of nanoparticles. Flexural strength, stiffness and impact strength of nanocomposite increased due to infusion of 1% V_f. of Al_2O_3 nanoparticles into epoxy matrix. Furthermore, wear rate and coefficient of friction of nanocomposite significantly decreased due to introduction of 1% V_f. of Al_2O_3 nanoparticles into the epoxy matrix. These improvements were not observed when 3% V_f. was introduced into epoxy matrix because probability of agglomeration of nanoparticles increases in this situation. Finally, high mechanical properties of epoxy-alumina nano-composite with good wear properties, allows the material to partially or fully replace fibers in conventional fiber-reinforced composites.

Raju et al. [97], 2018 carried out the abrasive wear behavior and mechanical behavior of glass fiber reinforced epoxy (G-E), Nano Silicon dioxide filled with G-E (SiO_2-G-E) and Nano Aluminum oxide filled with G-E (Al_2O_3-G-E) composites, Pin-on-disc test, Impact strength test and hardness test. Samples of G-E with (0%, 5%, 10% and 15) % wt. content of SiO_2 and Al_2O_3 were tested under different loads and abrading distances. Also, the wear volume and specific wear rate of the specimen are determinate, while the worn surface morphological features are exanimated by (SEM). Results showed varied responses under different abrading distance because of the inclusion of different wt. % of SiO_2 and Al_2O_3 filler loading. Further, the test results show that glass fabric reinforcement obviously improves the strength of epoxy and glass fabric- Al_2O_3 exhibits a synergistic effect on the wear resistance and reinforcing epoxy simultaneously. Further, it was also noticed that G-E composite wear is

reduced to a greater extent by addition of the Nano fillers of SiO_2 and further more by Al_2O_3.

Mishra et al. [98], 2020 synthesized functionally graded material (FGM) by dispersing the Al_2O_3 nanoparticles (rod and spherical form) in the epoxy. Gradients in the direction of thickness were conducted via changing the nano particle weight percentage. Layered FGM samples were produced via sequentially casting the layers of pure epoxy and nanocomposites containing (0.25, 0.5, 0.75 and 1%) nano particles in a vertical acrylic mold. Three-point bending was employed for determining the flexural characteristics of the FGM specimens. If the load was exerted from the side of nanocomposite, the FGM flexural modulus increased by 13%, while the flexural strength increased by (8% - 9%) above that for the neat layered epoxy for the two kinds of the nano particle.

Fouly and Alkalla [99] 2020 investigated how alumina nanoparticles with a low loading fraction by weight effect on the physicochemical and tribological characteristics of epoxy nanocomposites. The epoxy matrix is homogeneously dispersed with the nano particles of Al_2O_3 at loading portions of (0, 0.1, 0.2, 0.3 and 0.4 wt.%). The densities, modulus of elasticity, hardness, toughness, friction coefficient, and specific wear rate of the composites of epoxy were determined experimentally. Results indicate an enhancement in the mechanical and tribological properties of the epoxy nanocomposite.

Shareef et al. [100], 2021 used hand lay–up technique to fabricate functionally graded polymer nanocomposite (FGPNC) arranged via mixing the Alumina (Al_2O_3) nanoparticles with an epoxy matrix through five layers of 1.2 mm thickness for each layer. Different volume fractions were taken (0, 1, 2, 3 and 4) % of the used nanoparticles and were cast in molds made from acrylic for creating the graded composite sheet in the thickness direction. The results showed that the flexural strength and flexural modulus

of the functionally graded polymer nanocomposite enhanced by (51.7%) and (67%), respectively for the FGM loaded from the neat epoxy side.

2.8.2 Mechanical and Tribological Properties of Functionally Graded Composite Materials Using Centrifugal Casting Method

Siddhartha and Yadav [101], 2015 used red mud (an industrial waste) to investigate the mechanical and wear characteristics of red mud epoxy-based homogeneous and their functionally graded materials (FGMs) developed for potential application in tribological systems. Significant operational and material parameters are examined. According to this study, the sliding wear performance of FGMs is superior to that of homogeneous composites. The highest impact strength and tensile modulus of all synthesized composites are found in FGMs, indicating that centrifugation has improved the materials' crack arresting capability.

Singh et al. [102], 2015 investigated titanium dioxide (TiO_2) as a filler to fabricate polyester-based homogeneous composites and their functionally graded materials (FGMs), where the filler contents (0–20 wt. %). Simple mechanical stirring and vertical centrifugal casting technique is used for fabricating homogeneous composites and FGMs, respectively. Sliding wear tests are performed using a pin-on-disc machine. It is concluded that 20% wt. of TiO_2 filled polyester-based FGMs exhibits lowest specific wear rate among all the fabricated composites.

Singh et al. [103, 2015 presented mechanical and tribological properties of zinc oxide (ZnO)-filled polyester composites, fabricated by two different techniques. These two techniques are simple mechanical stirring and vertical centrifugal casting. Dry sliding wear tests are performed over a range of sliding velocity (1.57–3.66 m/s), normal load (10–30 N), filler content (0–20% wt.), and sliding distance (1000–3000 m) using a pin-on-disc apparatus. This study establishes that the FGMs exhibit superior

mechanical properties and wear resistance as compared with homogeneous composites. Among all the fabricated composites, FGMs filled with 20% wt. ZnO filler has maximum hardness and flexural strength i.e. 70 HRL and 39 MPa, respectively. Impact strength is maximum for 10% wt. ZnO filled FGMs with 1.3 J. FGM filled with 20% wt. of ZnO filler has minimum specific wear rate of 0.33×10^{-5} mm^3/Nm and neat polyester has a maximum of 0.97×10^{-5} mm^3/Nm.

Stabik and Chomiak [104], 2016 achieved the assumed gradation of the hard coal particle distributed in a matrix of epoxy using centrifugal casting technique. Two types of epoxy resins as a matrix and two types of hard coal with various granulations as filler were used. Samples were created by varying the volumetric content, the type of filler used, and the centrifugal casting parameters of samples. According to the detailed experimental program, the structure's microscopic show that the composites are characterized by continuous change of the filler particles content in radial direction, so they can be classified as graded materials. Results also show that gradation of particles content and thus gradation of properties may be planned and foreseen when mechanisms of gradation formation are known.

Singh and Vashishtha [105], 2016 investigated the influence of nano-TiO_2 filler with polyester on the mechanical and wear properties. Using mechanical stirring and vertical centrifugal casting techniques, uniform nanocomposites and FGMs are developed. To create homogeneous nanocomposites and FGMs, (5% and 10%) filler content is used. The sliding wear test is performed by using pin-on-disc tribometer, where nanocomposite pins and the hardened ground steel disc sliding on top of the pin. FGMs filled with nano-TiO_2 have superior mechanical and wear resistance properties. Nano-TiO_2-filled FGM has the lowest specific wear rate of any fabricated nanocomposites.

Prasad et al. [106], 2018 prepared the composite materials by centrifugal casting techniques. The functionally graded composite materials reinforced with natural fillers (aegle marmelos, terminalia chebula and soapnuts seeds, particle size 2 mm) were prepared on polyester. The influence of filler loading (3 to 12 %wt.) on physico-mechanical properties of hybrid composite materials were investigated as per the ASTM standards. It was found that the tensile strength of the hybrid composite material was increased by 34% as compared to that of pure polyester whereas the impact strength was increased 3.87 times of pure polyester with filler content of 12 %wt. aegle marmelos, 9% w.t terminalia chebula, 6 wt.% soap nut seed.

Singh and Siddhartha [107], 2018, manufactured the polymer gears by using conventional and horizontal centrifugal casting techniques. Gears are fabricated from PP material reinforced with 15% and 30% glass fibres. Gear made by the traditional method is known as homogeneous gear. Horizontal centrifugal casting produces functionally graded materials (FGMs) based on PP. The aim of this work is to investigate and compare the noise emission from homogeneous and FGMs gears during operation. The results show that the noise emission from the gears is increased with increase in the speed. PP FGM gear emits more noise as compared to PP homogeneous gear. Neat PP gear produces minimum noise among all the fabricated gears.

Gangil et al. [108], 2019 studied graded and homogeneous glass fibre, and marble dust reinforced vinyl-ester composites and their influence on the mechanical properties and wear effectiveness. In terms of mechanical properties, both graded and homogenous composites exhibit an increase in hardness and tensile strength, where graded composites having a greater impact than homogenous composites. The results also indicated that the graded composites have sufficient potential for tribological applications.

With an increase in marble content, the wear resistance of manufactured homogeneous and graded composites improves significantly.

Prasad et al. [109], 2019, used natural waste fillers like Terminalia chebula, soap nuts seeds, and Aegle marmelos to prepare polyester-based composite utilizing the method of centrifugal casting. The physical-mechanical behaviour of hybrid composites was studied about filler loading (3 %, 6 %, 9 %, and 12 %wt.). The results indicated that the hybrid composite with (12 wt% Aegle marmelos, 9 wt% Terminalia chebula, 6 wt% soap nuts seed) have been a maximum tensile strength of (47.83 MPa) and impact strength of (5.8 Joule) and hardness of (71VH). Compositions containing (12 wt.%) soap nuts seed and (3 wt.%) Aegle marmelos resulted in the lowest specific wear rate (0.00196 mm^3/Nm).

Farahnakian et al. [110], 2020, manufactured FGMs containing two kinds of filler materials with using polyester resin as a matrix. The dual filler functionally graded polymer materials (DF-FGPM) were created using the centrifugal technique. Copper-Silicon Carbide and Iron-Fused Alumina are used as two cases of dual filler materials. The method of image processing and the test of 3-point bending were used to estimate samples' flexural strength and microstructure respectively. The results of particle distribution showed the different behavior of particles which can enhance surface and volumetric properties, simultaneously. Due to the importance of the interfacial layer in the composite structure, developed FGM presented achievements of loading during the three-point bending test.

2.8 Scope and Concluding Remarks (Summery)

Many previous studies dealt with the improvement in mechanical and wear properties of composites due to different types of filler addition to the thermoset polymer. Some of these studies:

- It's obvious that the adequate investigations have been carried out upon the polymer-based FGM, but to the best of the author's knowledge, the nano Al_2O_3-packed epoxy-based functionally graded materials by centrifugal casting method haven't been synthesized up to now.
- The nano fillers addition can enhance the wear properties. Nevertheless, there's a shortage of investigation upon the wear behavior of epoxy resin packed with functionally graded nanocomposites reinforced by alumina nanoparticles under different concentration, centrifugation time and rotational speed of centrifugal casting.

In this work, FGNM were produced based on the centrifugal casting method where the graded of nano-alumina particles occurred through-thickness of of rectangular samples. The Al_2O_3 nanoparticles were added and dispersed in the epoxy matrix by ultrasonication.

The studied mechanical properties of the graded and non-graded nanocomposite were flexural resistance, impact, and hardness. Different types of the functionally graded materials under different (volume fraction, centrifugation time, and rotational speed), homogenous nanocomposite (0.5 %, 1 %, 1.5 %, and 2% Al_2O_3), and pristine epoxy were used for evaluating their mechanical and wear properties. The load was applied from the side of the pure and composite of all types of FGM. SEM for impact fracture was used to show the nano-alumina distribution and graded through-thickness.

CHAPTER THREE
EXPERIMENTAL WORK

3.1 Introduction

The experimental work deals with the practical procedure, which includes three parts.

- The first part involves manufacturing a centrifugeapparatus. This apparatus manufactured in a new way that differs from the centrifugation methods in previous research in the terms of the shape of the sample and the direction of the gradient by using acrylic dies
- The second part focuses on the volume fraction calculation and manufacturing of FGM with the basis of epoxy as a matrix and reinforced by nanofiller and manufacturing the equivalent homogenous nanocomposite.
- The third part includes testing the prepared samples under static loads to get the FGM properties. The structural tests involved, particle size analyzer to get particle size measurements of nano-alumina, XRD to show the phase structure analysis of alumina nanoparticles as well as the SEM to investigate the fracture surfaces of impacted samples at the maximum and minimum centrifugation conditions and concentration of nano-filler.

  The physical property was the density, while the mechanical tests included bending, impact, and hardness. And the tribological test include specific wear rate and coefficient of friction. The experimental work in this study is shown in Figure (3.1).

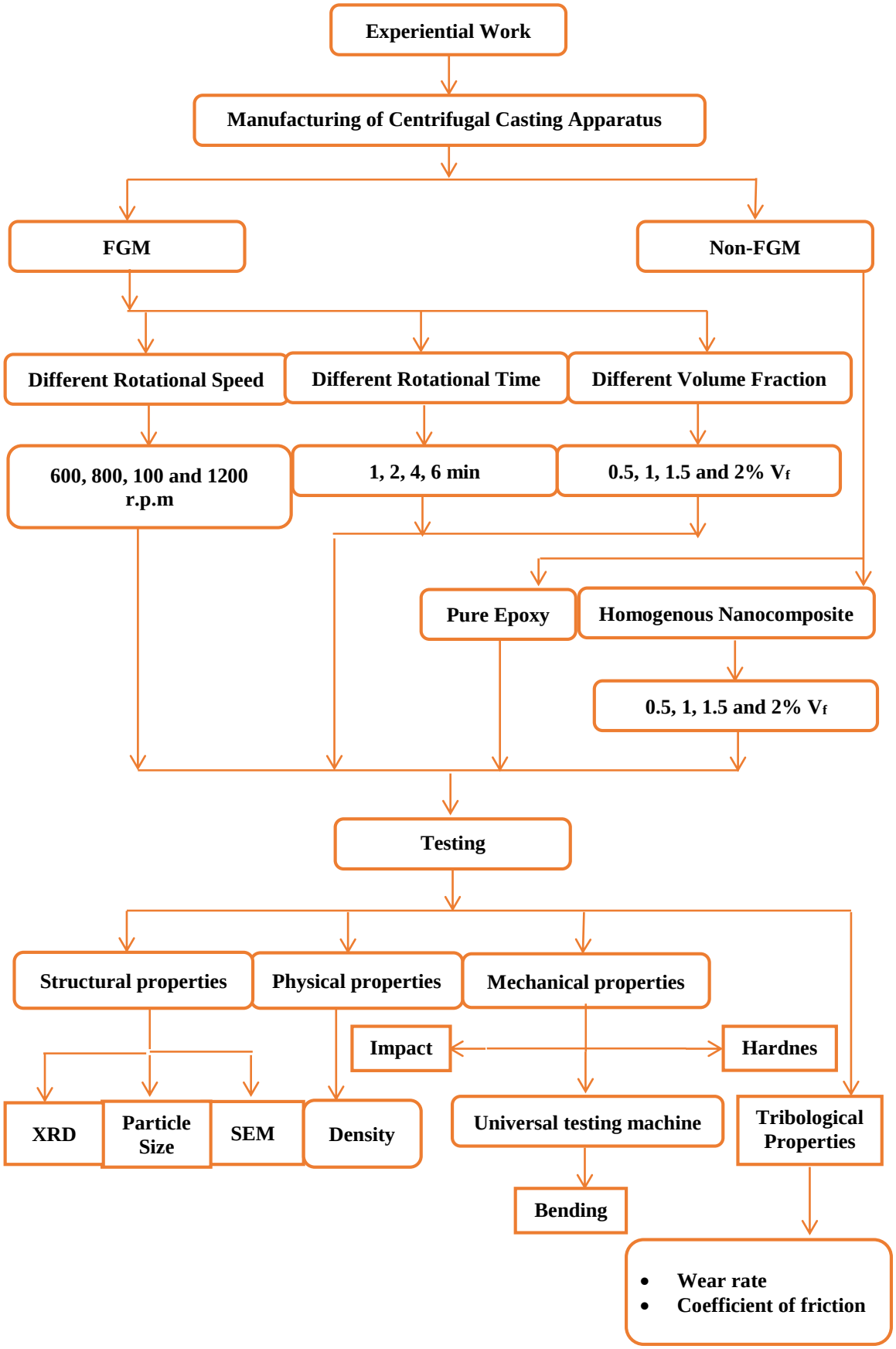

Figure (3.1): Schematic procedure of the experimental work

3.2 Material Used in This Work

3.2.1 Epoxy Resin

In this study, a trademark epoxy resin (Quickmast 105 base) produced via Don Construction Products (DCP) Company has been utilized as a matrix in the form of liquid; it has less viscosity than other thermosets. And, it has been converted into a solid state by adding a ratio of (4:1) of a hardener (Quickmast 105 hardener) from the supplied company. Table (3.1) lists the technical properties of (Quickmast 105) depending on the (DCP) company datasheet.

Table (3.1): The technical characteristics of Quick-mast 105 (from the supplier's datasheet)

Compressive strength	**Flexural strength**	**Tensile strength**	**Density**	**Viscosity**	**Poisson's ratio Ratio**	**Glass Temp. (Tg) °C**
70 MPa	50 MPa	25 MPa	1.1 g/cm^3	3-5 poise at 25°C 1-2 poise at 35°C	0.33	80

3.3 Nano-Alumina

Figure (3.2) depicts the alumina nanoparticles used in this investigation. The nanoparticle reinforcements utilized are the alumina (Al_2O_3) nanoparticle which made via Hongwu International Group Ltd. The characteristics of Al_2O_3 nanoparticle are detailed in Table (3.2).

Figure (3.2): The nano-Al_2O_3 powder

Table (3.2): The properties of alumina nanoparticles (from the supplier's datasheet)

Properties	**Values**
Purity (%)	99.9
Average Particle Size, nm	50 -100
Specific Surface Area, m^2/g	5 -10
Microstructure Shape	spherical
Poisson's Ratio	0.22
Young's Modulus, GPa	347

3.4 Calculation of Volume Fraction

The reinforcement's volume fraction (V_f) is defined as a ratio of the volume of reinforcement to the whole composite volume.

The fabrication process of a composite depends on the volume fraction (V_f) of the mixing materials, which can be calculated as follows [111, 61]:

$$m_c = m_p + m_m \tag{3.1}$$

$$\rho_p = \frac{m_p}{v_p} \tag{3.2}$$

$$\rho_m = \frac{m_m}{v_m} \tag{3.3}$$

Where:

m_c : Mass of the composite specimen (g),

m_p : Mass of particles (g),

m_m: Mass of the matrix (g),

ρ_p : Density of particles (g / cm^3),

ρ_m : Density of matrix (g / cm^3),

v_p : Volume of particles (cm^3), and

v_m : Volume of the matrix (cm^3).

And volume fractions are computed as follows:

$$V_p = \frac{v_p}{v_c} \tag{3.4}$$

$$V_m = \frac{v_m}{v_c} \quad (3.5)$$

$$V_p + V_m = 1 \quad (3.6)$$

Where:

v_c : Volume of the composite specimen (cm^3).

V_p : Particles volume fraction.

V_m : Matrix volume fraction.

By substituting Equations (3.4) & (3.5) into Equations. (3.2) & (3.3), to obtain the dependent equations in the evaluation of volume fraction in the experimental procedure as follow:

$$m_p = \rho_p \times v_c \times V_p \quad (3.7)$$

$$m_m = \rho_m \times v_c \times V_m \quad (3.8)$$

3.5 Dies Preparation

The acrylic dies of 6 mm thickness were used to prepare the samples. Each die consists of three layers. The middle layer contains grooves of the sample shape required for a test installed on the lower layer used as a base to prevent mixture leakage and the upper layer used as a cover for the middle layer, as shown in Figure (3.3). The die has been produced utilizing a Computer Numerically Control (CNC) machine and ground for giving the last product composite samples having dimensions of (220 × 10 × 6) mm^3 according to the international standard specimens.

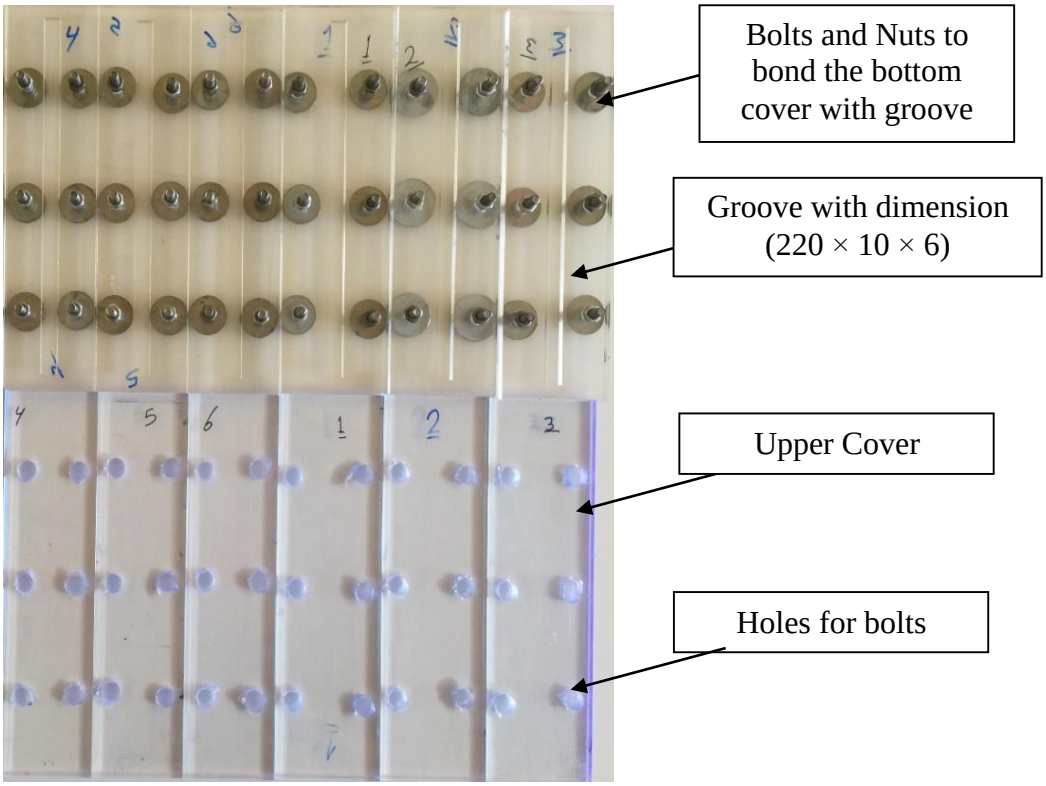

Figure (3.3): The acrylic dies for the homogenous composite and functionally graded materials (All dimensions are in mm)

3.6 Preparation of Nanocomposites

For preparing a consistent mixture, the whole reinforcement addition process to the resin was conducted in an appropriate solvent (thinner). To prepare the samples of neat epoxy for creating similar situations compared to the other models, an appropriate quantity of epoxy resin was placed into an adequate amount of thinner solvent. After blending for 15 min in a mechanical stirrer, the mixture was put into a vacuum vessel for 30 min. The solvent has to be evaporated totally beneath the state of the vacuum produced via a vacuum pump. After that, a hardener stoichiometry ratio, i.e., 4 (epoxy resin)/1 (hardener), was supplemented and blended consistently for 15 min and degassed via the vacuum pump to remove the air bubbles for 5 min. This mixture was then placed into an acrylic mould and closed by upper cover to be cured for two days at room temperature.

To prepare homogenous epoxy/nanoparticles, the desired amounts of reinforcements are (0.5, 1, 1.5, and 2) % V_f Al_2O_3 nanoparticles were dissolved into an adequate quantity of stated solvent. The obtained mixture was blended to make it uniform by using a magnetic stirrer for (15 min) and was sonicated at an amplitude of (75%) for (15 min), (50s ON and 10s OFF). The required quantity of epoxy was supplemented to such a mixture via a similar technique as stated earlier. It was mechanically mixed for 15 min and degassed using a vacuum pump for 30 min to remove the air bubbles and evaporate the thinner.

The stoichiometry ratio of the hardener was added and manually mixed gently at a very slow speed for 10 min and degassed using a vacuum pump for 5 min to remove the air bubbles. Finally, the homogenous mixture was put in the acrylic mold and closed by upper cover to cure for two days. This process is revealed in Figure (3.4).

Figure (3.4): Procedure pursued in the investigational work for fabricating a uniform and FGNC

3.7 Preparation of FGPNC

The fabrication process of the FGNCs synthesized via the centrifugal casting method has been separated into two steps:

The first step involves preparation of the completed mixture which form of (alumina nano-filler as reinforcement and epoxy resin as the matrix) via suitable distribution and mixing procedures as described in the preceding method for the homogenous nanocomposite, then pouring the liquid mixture into the acrylic dies and closing the upper cover for casting purpose.

In the second step, after closing these dies, put them in a centrifuge apparatus under certain time and speed. The centrifuge apparatus manufactured in a new way that differs from the centrifugation methods in previous research in the terms of the shape of the sample and the direction of the gradient by using acrylic dies. The centrifuge apparatus produces functionally graded composites manufactured under the same conditions during the die rotation process (in terms of vibration, temperature, rotation time, and die rotation speed). The centrifuge apparatus consists of several parts, as shown in the following points:

1. Disc: The centrifuge apparatus contains three separate dies, and they are installed between two discs' perpendicular to the axis of rotation. Where the angle between three facing dice are 120^{o}, as shown in Figure (3.5).

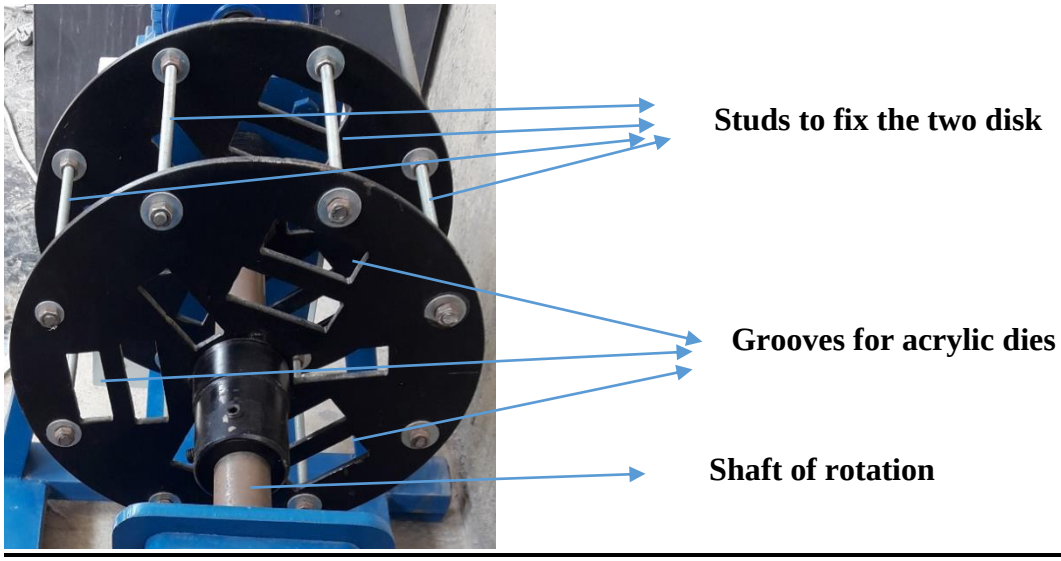

Figure (3.5): Two discs to support the dies

2. DC electric motor: The discs shown in Figure (3.5) are connected by a DC electric motor whose speed reaches to 2800 r.p.m, where the voltage regulator controls the speed of the device. The centrifugal plumbing system used in the research consists of a convertor from a three-phase approach to a single-phase system, the Universal Power Supply unit (UPS), and the speed Regulator suitable for the engine operation. These parts are shown in Figure (3.6).

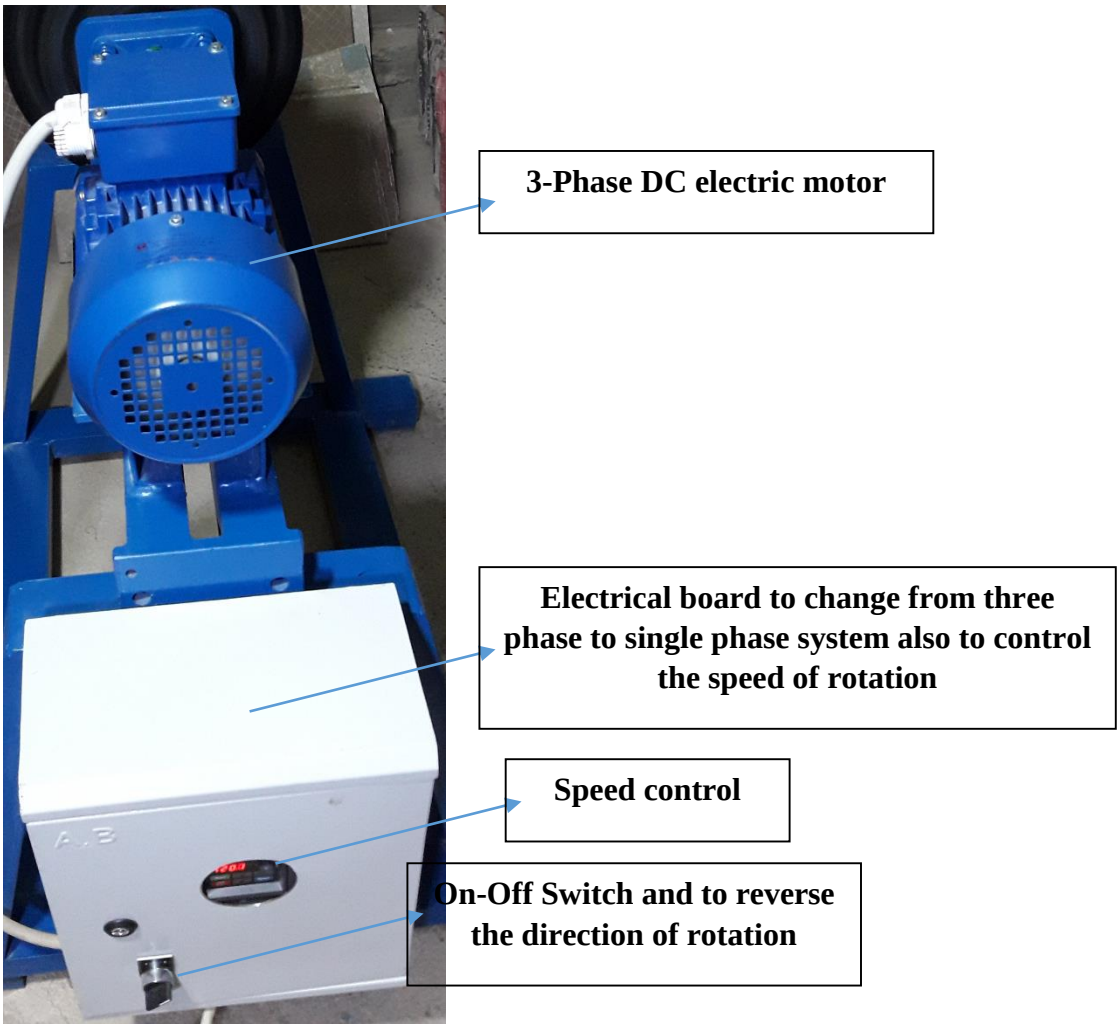

Figure (3.6): DC electric motor parts

3. Bearing: motor requires bearings to allow the spindle of rotation to tum while maintaining the correct state as shown in Figure (3.6). The advances in bearing geometry led to increase in speed capability and reduced the vibration.

4. Coupling: in the machine industry is interpreted as "a part that connects two shafts" and is generally called "coupling," "shaft coupling," or "joint". The advantages of the coupling were reduced the friction and vibration between the shaft and electric motor, as shown in Figure (3.7).
5. Slide: it's used to slide the right disk to open and close the acrylic die, as shown in Figure (3.7).

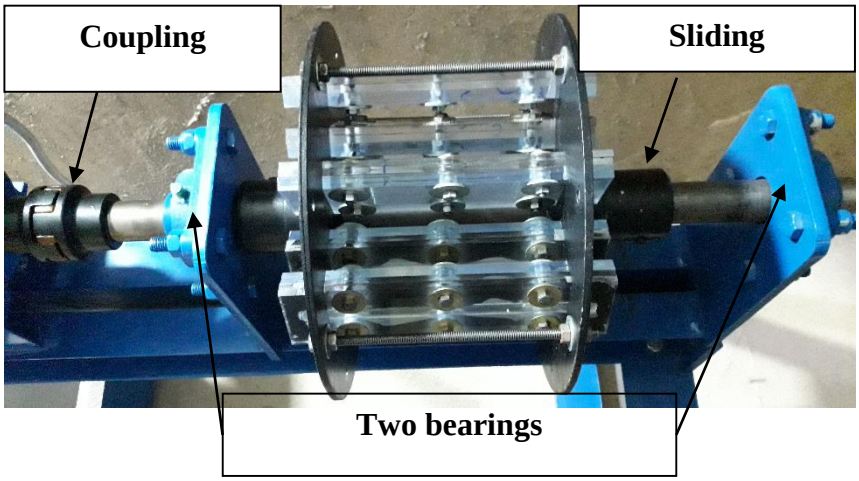

Figure (3.7): Some parts of the centrifugal apparatus

6. Rubber base: rubber is very good at absorbing vibration. The protective rubber base will absorb the impact and reduce the machine's noise significantly, as shown in Figure (3.8).
7. Steel frame: It is a base to carry centrifuge components, such as the electric motor, disks and the rotary shaft, as shown in Figure (3.8).

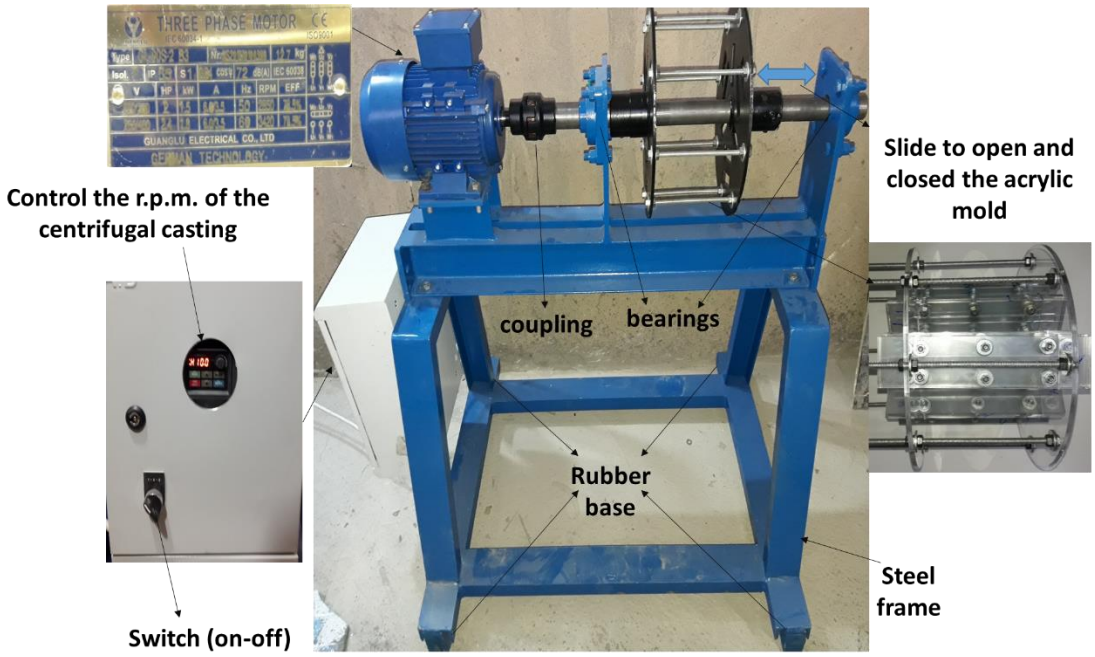

Figure (3.8): Centrifugal casting apparatus

The initial step of preparing specimens by utilizing centrifugal casting techniques was using the wax to cover the walls of the die to facilitate the sample's removal from the die after the solidification process. The synthesis procedure for FGNCs consisted of two distinct steps. The first step involved preparing a mixture of nanofiller and molten matrix using the same dispersing and blending techniques described above for the homogenous nanocomposite. In the second step, the dies were mounted in the centrifuge apparatus at a certain speed and time, as shown in Figure (3.8). Note that the high mixing speed leads to the entry of air bubbles into the mixture. Air bubbles play a significant part in determining the mechanical characteristics of the manufactured model, so it became necessary to get rid of them as much as possible by using a vacuum. In this work, three main factors in the centrifugal process were studied. The first factor was studding the effect of different time of rotation (t=1, 2, 4, 6 min) with constant volume fraction 2% nano-Al_2O_3 and constant rotational speed (N=1200 r.p.m.), the second factor was studding the effect of various rotational speeds (N= 600, 800, 1000, 1200 r.p.m) with constant volume fraction 2% nano-Al_2O_3 and constant time of rotation (6 min) and the third factor was studding the effect of different

volume fraction of nano-alumina filler (0.5, 1, 1.5, 2%) with constant rotational speed(1200 r.p.m) and constant rotational time (6min).

3.8 Testing

The utilized tests in the present work are detailed in this section, and the all tests were conducted at room temperature.

3.8.1 Nano particle size analyzer

The particle size of the alumina nano-filler has been statistically measured by employing (Brookhaven 90plus, Nanoparticle size analyzer) available in the Nano Technology Center at University of Technology, as depicted in Figure (3.9). The sample was initially properly spread and sonicated into the deionized water for 10 minutes.

Figure (3.9): laser particle size analyzer device.

3.8.2 X-Ray Diffraction (XRD) Test:

The phase structure analysis of alumina nanoparticles was identified with XRD- system (XRD-6000 SHIMADZU, Department of ceramics and building materials/ College of Materials engineering/ University of Babylon), using a scanning speed of 6º/min as shown in Figure (3.10). The

diffraction occurs when the incident ray satisfies Bragg's law given in equation (3.9) [112].

$$n\lambda = 2d \sin\theta \qquad (3.9)$$

Where (n) is a positive integer, (λ) is the wavelength of incident ray (λ=1.5406 A^0), (θ) is the angle between the incident ray and the sample surface, and (d) is the inter-planar distance (A˚). The diffracted ray is received by the detector which is rotates at a speed. Finally, the diffraction data (values of diffraction angels and the intensity of the diffracted ray) is obtained using computerized system over 2θ range of (20-70°). The d-spacing values of the tested powder were calculated using equation (3.9); the result was compared with the standard data of d-spacing for ceramic materials given by the Joint Committee on Powder Diffraction Standard (JCPDS).

Figure (3.10)**:** XRD Instrument

3.8.2 Scanning Electron Microscopy (SEM)

The microstructure of the fracture surface was examined via utilizing this device. The mechanism of this instrument was scanning the sample's surface with an electron beam. Then, the re-directed or back-scattered beam is collected and scanned on a cathode ray tube. The apparent image at the screen depicts the materials surface. This surface might be first polished and then etched, and must be conductive. If material's surface is not conductive, a thin layer of gold or another conductive material must be applied. SEMs have a very large depth of focus. Also, their useful magnification ranges from (100X) to (20,000X).

SEM device has been utilized to display the surface of fractured impact test samples. Depending upon the synthetic crystal's technology, a device type (TESCAN-Company, Model Mira3) has been used in such a test, as illustrated in Figure (3.11). TESCAN detectors offer quick and effective solutions to improve imaging quality. The samples that subjected to the test have rectangular shape with a dimension (5 x 10 x 6) mm^3 .at beginning the fractured surface of impact's sample test was machining. Then a thin gold layer was then sputter-coated to avoid charging using a sputter-coating instrument (EM Technologies Ltd., made in the United Kingdom). At the physics faculty on North Kargar Street (North Amirabad), samples were measured in Tehran (Iran).

Figure (3.11): SEM Instrument (TESCAN –company, model Mira3).

3.8.3 Density

In the current study, there are two parts of density measurements have been performed; one part has been to compute the density of the nanoparticle via dividing the nanoparticles mass by the nanoparticles volume in a cylinder beaker which containing a solvent liquid (thinner), as depicted in the Figure (3.12). The other part involves calculation the theoretical and practical density of nanocomposite and FGM samples. The rule of mixture (ROM) was used to calculate the theoretical density (ρ_{th}) of composite as [111]:

$$\rho_{th} = V_p \rho_p + V_e \rho_e \qquad (3.10)$$

Where: V_p and ρ_p are the volume fraction and density of nanoparticles.

While: V_e and ρ_e are the volume fraction and density of the epoxy matrix.

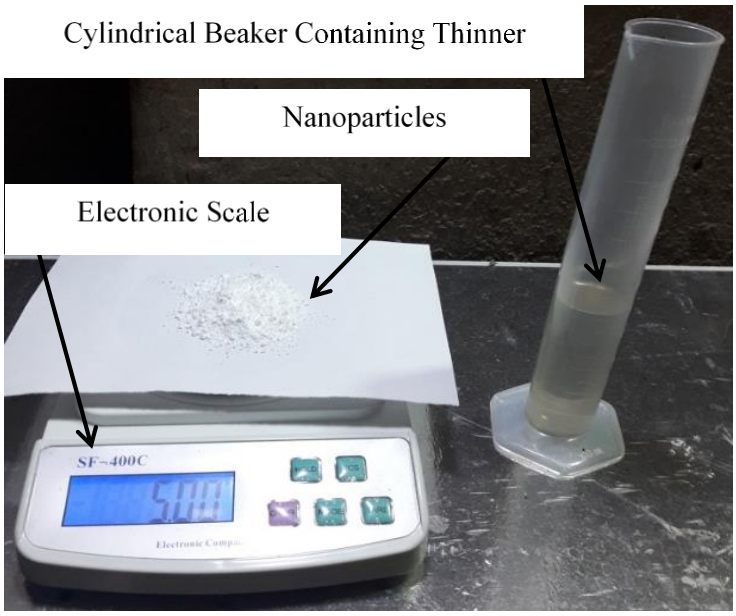

Figure (3.12): The measurement procedure of nanoparticles density

By utilizing Archimedes' principle, the samples' density of functionally graded polymer nanocomposite (FGPNC) and epoxy was experimentally determined. At first, it must measure the weight of each sample in the air. After that, the specimen was placed in a crucible containing deionized water for two minutes to eliminate air bubbles. Following that, the weight was determined using distilled water. Archimedes' principle explains the disparity between the two measurements as a weight loss in water.

A density test has been carried out employing the Matsu Haku High precision density tester GP-120S analyser as shown in Figure (3.12). The density instrument available in the Polymer and Petrochemical Industries Department at the Materials Engineering College /University of Babylon Then, the density is calculated based on the following equation [113] and the law of Archimedes:

$$\rho_c = \frac{W_a \, \rho_w}{(W_a - W_w)} \tag{3.11}$$

Where:

ρ_c: Composite density

ρ_w: Water density

W_a: Weight of the object in the air

W_w: Weight of the object in the water

Figure (3.12): The density tester

The following formula calculates the samples' void content percentage [107].

$$void\ content(\%) = \left(\frac{\rho_t - \rho_e}{\rho_t}\right) * 100 \quad (3.12)$$

Where:

ρ_t: Theoretical density, g/cm^3.

ρ_e: Experimental density, g/cm^3.

3.8.3 Mechanical tests

A. Three-Point Bending Test

Within the FGPNC samples, gradation is provided in the thickness direction, indicating the variation of stiffness property toward the thickness. This test was utilized to determine the flexural properties of pure epoxy, various FGM models, and equivalent homogenous nanocomposite. The samples were loaded onto the universal testing machine from both sides for all types of FGM and from one side for homogenous and pure epoxy. By

using ASTM D790, the length (L), width (w), and thickness (h) of the flexural test sample are 60 mm, 10 mm, and 6 mm, as shown in Figure (3.13).

As depicted in Figure (3.13), the 3-point bending tests have been performed upon a (50 kN), Tinius Olsen H50KT Universal Testing Machine which available in the Laboratory of Strength of Materials at the Department of Mechanical Engineering Department/University of Technology. During bending tests, the crosshead velocity was 1 mm/min. Through the loading process, the outcomes of tests have been unceasingly displayed upon a Digital Computer in terms of force (N) against the specimen's deformation (mm). Each test was performed on (5) samples, and the mean result was calculated.

As in tensile and compression testing cases, the force and displacement must be transformed into Stress - Strain features for rectangular bars by using the following equations [65].

$$\text{Flexural stress } \sigma_f = \frac{3\text{FL}}{2wh^2} \quad (3.13)$$

$$\text{Flexural strain } \epsilon_f = \frac{6\delta h}{L^2} \quad (3.14)$$

Where:

L: The support span, i.e. the beam spacing between the centers of the (2) external supporting rods in mm.

h: Beam thickness in mm.

w: Beam width in mm.

F: Force in N.

δ: Specimen deflection at the mid of the span in mm.

σ_f: The flexural stress in N/mm^2.

ε_f: The flexural strain.

Via such equations, the flexural modulus can be determined by [65]:

$$\text{Flexural modulus } = \frac{m\text{L}^3}{4wh^3} \quad (3.15)$$

Where*: m* is the slope of the Force-Deflection curve between the reference strains.

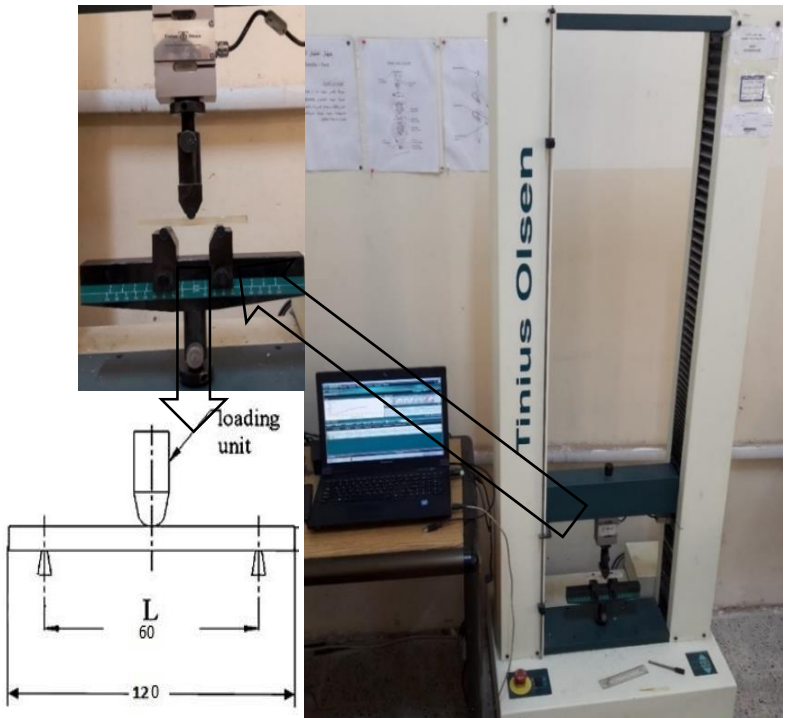

For 3-point bending (ASTM D790)

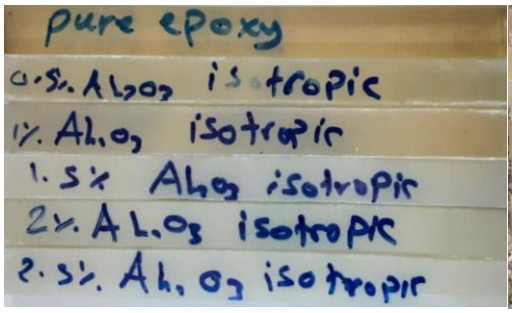

Homogenous at different volume fractions

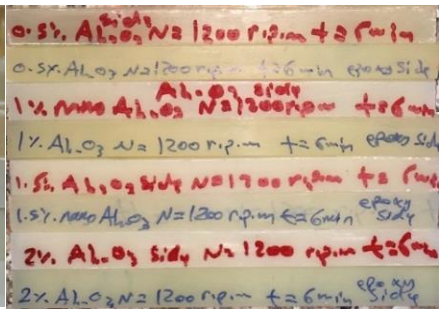

FGM at different volume fractions

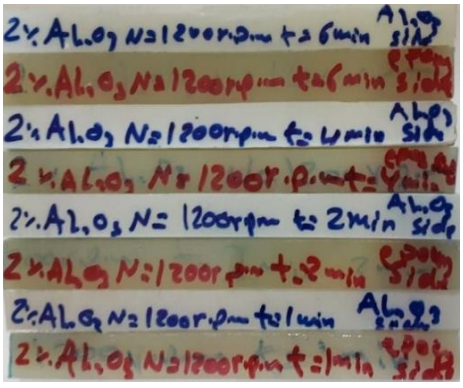

FGM at different time of rotation

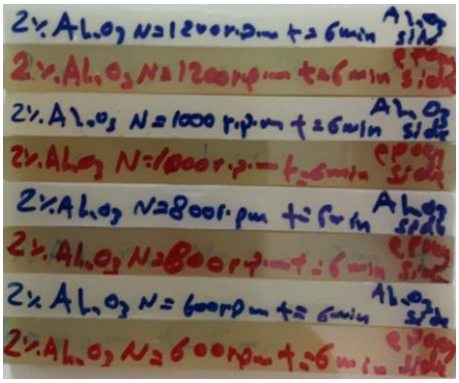

FGM at different speed of rotation

Figure (3.13): Universal testing machine and samples used

B. Impact test

As shown in Figure (3.14), the impact tests have been carried out employing the impact device (Type GUNT Hamburg), which available in the Polymer and Petrochemical Industries Department at the Materials Engineering College/ University of Babylon.

The impact test has been conducted employing an un-notched Charpy-Impact testing device following the standard (ASTM D256), using a rectangular specimen having dimensions (55 x 10 x 6) mm^3 as in Figure (3.15). In this test each value of the energy represents the average of five samples.

This instrument is consisting from an energy gauge and a pendulum. The Charpy's impact test comprises a standard specimen that can be broken with a single blow from a swinging hammer. The procedure for examining in this instrument involves raising the pendulum to its maximum height and maintaining its rigid position.

In this test the specimen is fixed in a horizontal position. Then the energy gauge is reset to zero, and the pendulum was released, whereas its potential energy is converted to kinetic energy, and a portion of this kinetic energy is utilized for fracturing the specimen, while the energy gauge measures the tested model's fracture energy.

For determining the Charpy impact strength of an un-notched sample, the energy absorbed via the model's breaking is dividing to its original cross-sectional area [92]:

$$G = W / A \qquad (3.16)$$

Where:

G: The material's impact strength (J/m^2)

W: The absorbed energy (J)

A: The sample's cross-sectional area (m^2)

Figure (3.14): The impact testing device

Figure (3. 15): Experimental impact test samples.

C. Hardness test

In this study, the hardness of the sample was measured by utilizing a hardness test digital device (Type TIME®5431), as depicted in Figure (3.16). This device was available in the Polymer and Petrochemical Industries Department in the Materials Engineering College at the University of Babylon. The hardness test was done for pure epoxy samples, homogenies composites (epoxy + nano-Al_2O_3), and both sides of all the functionally graded material models. The test was performed via maintaining the

penetration of the tool of Shore D instrument which fixed upon the surface of the sample. At last, the hardness number is appearing upon the Electronic Display device.

The Shore D test has been used to measure the hardness of the surface, with the hardness device indenter connected to a Digital Scale that gradually increasing within (0-100 unit), capacity of (5±0.5) kg and a dwell time (10 sec) per standard ASTM D2240 [92]. In shore D tests, the indenter is forced into the material's surface to be tested for a specified time. The hardness results were recorded directly by digital scale, and each measurement requires only a few seconds. The hardness test results are the average of (5) readings from different samples. For examining the gradation properties through thickness, a hardness test was performed; where the hardness property for each layer was determined by utilizing grinding and polishing machine type (Mopao-160E) to prepare the samples for hardness tests through remove layers via layers. The concept is to obtain the hardness profile through the model and compare the hardness of layers and the intermediate graded layers.

Figure (3.16): The testing hardness (Shore D) device

3.8.4 Specific wear rate Test

Wear tests were done by using pin-on-disc friction on a wear monitoring test bench (Model MT/60/NI/HT/L), as shown in Figure (3.17), to see how well these homogenous compounds and FGM worked in dry slip conditions. These tests were done according to ASTM G 99. In the pin-on-disc experiment, different samples of homogeneous and graded nanocomposite with different filler content, centrifugation time, and rotation speed were employed as a (10×10×6) millimeters the dimension of cubic sample used in the pin-to-disc studies. The counter surface is a hard carbide pin with a (Ra) value of 0.1 μm, a hardness of 57HRc, and a diameter of 7 mm.

This gadget allows for the continuous recording of simultaneous friction force and coefficient of friction readings during testing. A sequence of tests was carried out at a 400 r.p.m. sliding rotational speed, and with a standard load of 30 N. The sliding distance was determined as a function of the 20-minute test duration. Then the specific wear rate (mm^3/N.m) based on "volume loss" is expressed as [113].

$$W_s = \frac{\Delta m}{\rho.t.V_s.F_n} = \frac{\Delta V}{D.F_n} \quad (3.17)$$

Where:

Δm: The loss of mass throughout the test (in gm.)

ρ: Density of composite in (in gm./cm^3)

t: Duration of the test (in a sec)

V_s: The velocity of sliding (in m/sec)

F_n: Average normal load (in N).

The specific wear rate is defined as the volume loss of the specimen per unit of sliding distance per unit of moderately applied sliding resistance,

ΔV: Volume loss in mm^3.

D: Abrading length in mm.

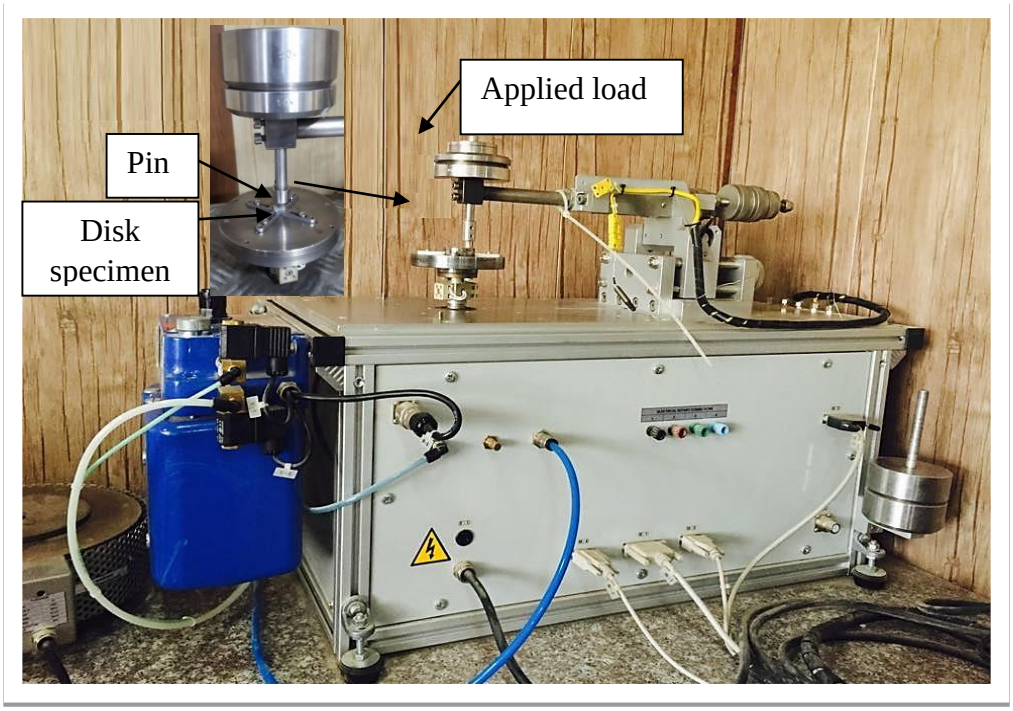

Figure (3.17): Pin-On-Disc Sliding Machine

Before testing, the surfaces of both the sample and the pin were washed with acetone and thoroughly dried. The sample set was initially weighed with an electronic balance to an accuracy of ± 0.0001 gm. Slip wear loss is measured by the beginning and ultimate weight difference. Each set of utilized test standards was applied to three samples. The findings presented are the average of three measurements.

CHAPTER FOUR
RESULTS AND DISCUSSION

4.1 Introduction

In this chapter, the results of the experimental work are presented and discussed in details. these results include the structural, physical, mechanical and tribological properties for homogenous composite and FGM.

Structural test includes particle size analyzer, (XRD), and (SEM). Where particle size analyzer provides the size of alumina nano-particles while, XRD results show the chemical structure and phase of alumina nano particles, and SEM results show the internal structure and fracture region of the samples that are subjected to impact test after failure.

Also, the present chapter has discussed the mechanical test results. The mechanical tests involve the 3-PB properties which include (Young's modulus, ultimate flexural strength, and elongation at break), the impact and hardness results of a homogenous nano-composite and FGMs with various centrifugation conditions. At the same time, the tribological properties of this nano-composite to get specific wear rate and coefficient of friction.

4.2 Particle Size Analyzer Result:

The particle size measurements for nano Al_2O_3 are shown in Figure (4.1). In this Figure, the ultimate size of the nanoparticles of Al_2O_3 is (520.1 nm); this depicts the wide agglomerated area and the lousy dispersion into the water. The device treats the agglomerated or the gathered structures as a single molecule and measures its full size, which agrees with [114].

Elapsed Time	00:01:30
Median Diam.	482.7 nm
Mean Diam.	520.1 nm
Polydispersity	0.161
GSD	1.472

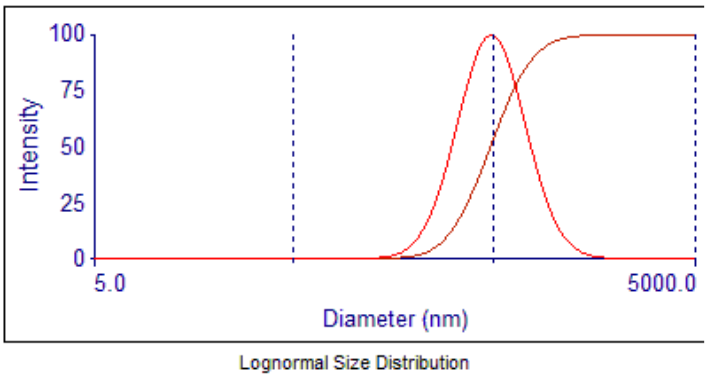

d(nm)	G(d)	C(d)	d(nm)	G(d)	C(d)	d(nm)	G(d)	C(d)
255.6	26	5	437.7	97	40	626.3	80	75
294.1	44	10	459.7	99	45	668.3	70	80
323.4	58	15	482.7	100	50	720.3	58	85
348.6	70	20	506.7	99	55	792.1	44	90
372.0	80	25	532.2	97	60	911.4	26	95
394.2	87	30	560.1	93	65			
416.0	93	35	591.0	87	70			

Figure (4.1): Particle size of Al_2O_3 nanoparticles

4.3 X-ray diffraction Result

Figure (4.2) shows the XRD diffraction peaks of the Al_2O_3 nanoparticles used in the present study, revealing that the alumina powder contained only the α-nano-Al_2O_3 phase where the reference code 00-011-0661. These Al_2O_3 peaks match those in a previous study conducted with [58]. The XRD image in Figure (4.2) confirms the peak value (X axis) shows nano-powder as α-Al_2O_3 Joint Committee on Powder Diffraction Standard (JCPDS) [93, 95].

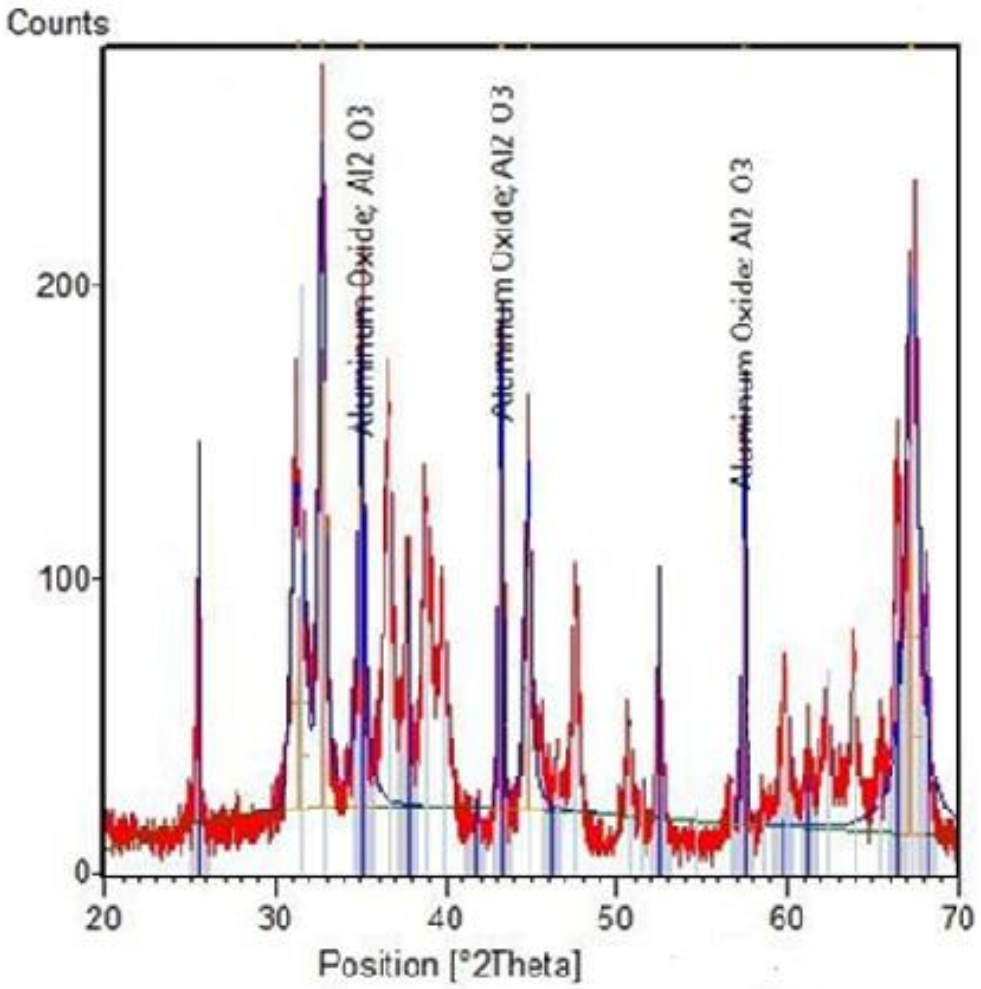

Figure (4.2): XRD pattern of pure α-alumina

4.4 Density Results

During manufacturing composite materials either the air or the volatiles might be trapped between filler and matrix and they will form as voids. The existence of voids effects on several of the composites' mechanical properties and performance. These voids act as a stress concentration within the material, and these cause failure mechanisms (such as crack initiation and propagation) and resulting in catastrophic part failure. The amount of void in composite materials can be determined via the comparison of their theoretical density with their experimental density. The theoretical density of the composites was first calculated by using the rule of mixtures and verified experimentally through Archimedes' technique.

Figure (4.3) depicts the effect of alumina nanoparticle addition on the density of epoxy composites at various volume fractions. The addition of alumina nanoparticles increased the density of the epoxy matrix material and this is achieving an improvement of the bonding between the particle and matrix, confirming the benefit of fillers as a particulate reinforcement. The main reason for the increase in the density of the composite material is the higher density of alumina nanoparticles (3.97g/cm3) compared to the density of pure epoxy (1.1 g/cm^3). The density suggested that the particle breakage had little effect on the composites.

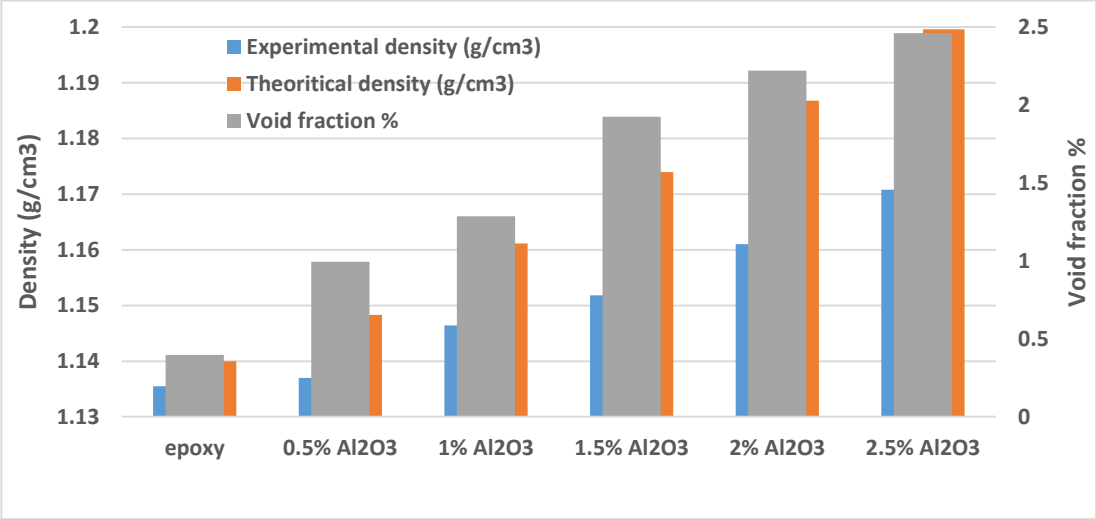

Figure (4.3): The theoretical, experimental densities and the corresponding content of void of the neat epoxy and alumina composite at different volume fractions

From Figures (4.3) and (4.4) it is clearly observed that the homogeneous composites have more void-fraction as compared to graded composites; this may attribute to fabrication technique adopted for preparation of the composites. The presence of alumina particle has different effects on density of homogeneous composites as well as FGMs. Where FGMs is found to be more than their homogeneous counterparts; also, FGMs exhibit less void fraction as compared to homogeneous composites. The

reason behind this is agglomerates were well removed due to centrifugation force applied to them during synthesis that ultimately resulted in improved dispensability and lesser void fraction.

Therefore, one can state that for a certain sample size, the gradation in the volume fraction (V_f %) of particles can lower the FGPC weight in comparison with that of the monolithic composites. In centrifugal casting the samples are rotated at a speed of 1200 r/min for 6 min. Therefore, the voids/bubbles (if any) are thrown towards the center due to centrifugal action where they collapsed rapidly; hence automatically the void fraction reduces. In case of fabrication of homogeneous composites manual stir casting or gravity method is used; therefore, chances of inherent voids are more. Thus, centrifugal technique is more efficient than the gravity method in minimizing the void content. In both cases, void fraction increases with particle loading and this may be attributed to poor interaction/ adhesion between alumina particle and epoxy matrix materials. This agreement with [115].

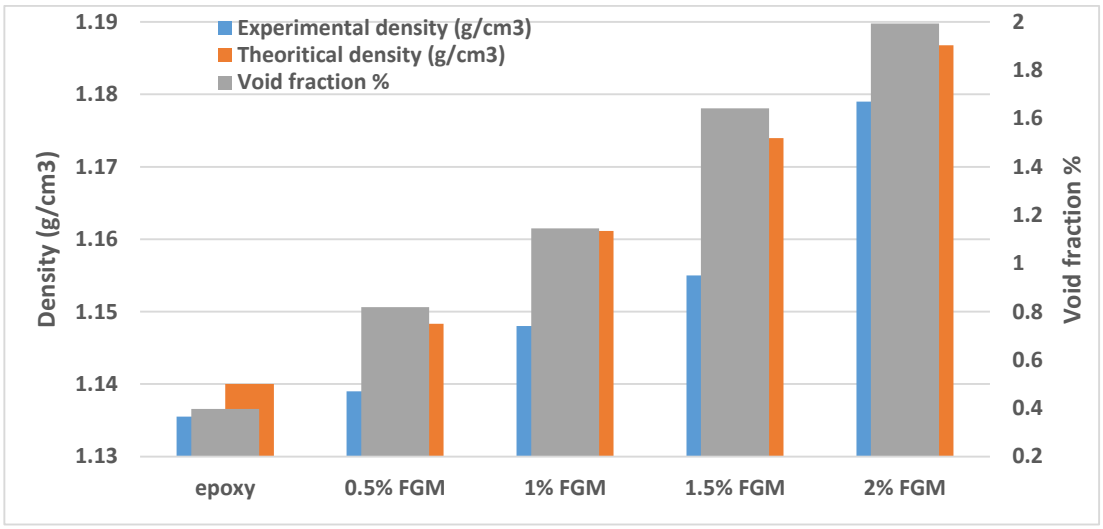

Figure (4.4): The theoretical, experimental densities and the corresponding content of void of the neat epoxy, FGM's (Al_2O_3) and equivalent alumina nanocomposite with constant centrifugation speed of 1200 r.p.m and centrifugation time of 6 min

Figure (4.5) shows that when the centrifugal speed increases, the density increases slightly. The reason for this is due to the centrifugal mechanism, where the centrifugal force separates the materials of higher density towards the periphery and the material of lower density is towards the center, and since the mass of dissolved air bubbles is less flows towards the surface and is released out faster than in the case of mechanical methods, so the material is free of bubbles draws.

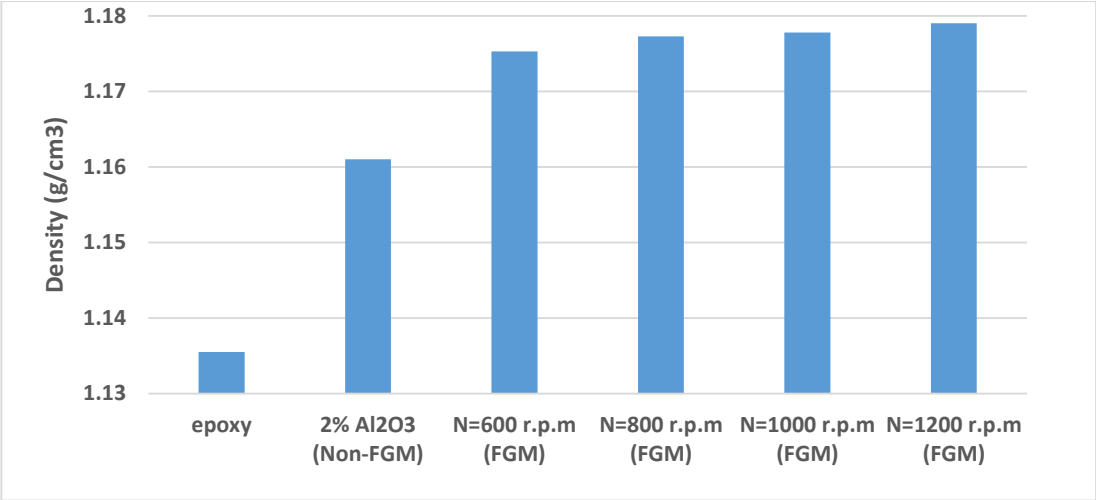

Figure (4.5): The experimental densities of neat epoxy, homogenous nanocomposite and FGM at different centrifugation speeds

Figure (4.6) shows that the density increases with centrifugation time because the bubbles have sufficient time to come out and release to the outside.

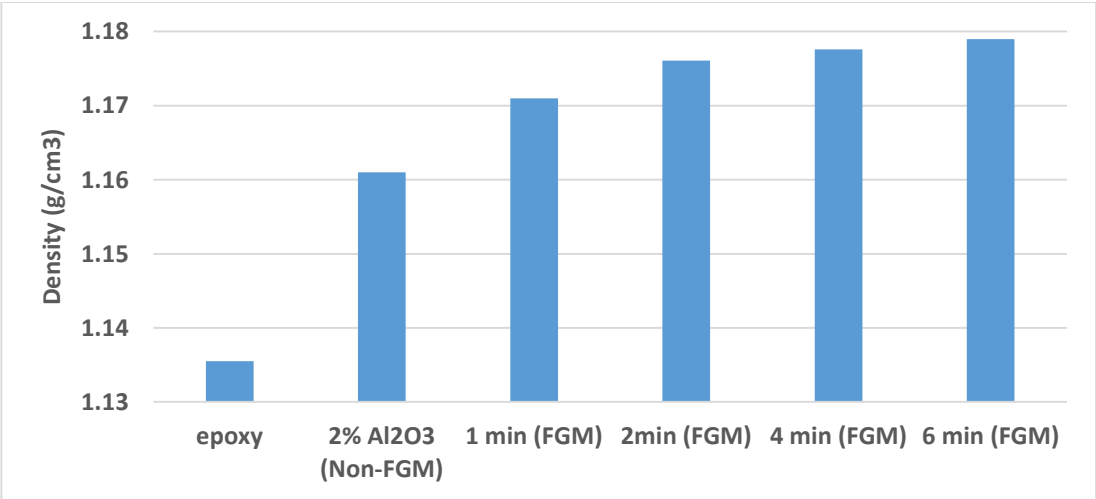

Figure (4.6): The experimental densities of neat epoxy, homogenous nanocomposite and FGM at different centrifugation times

4.5 Flexural Results

4.5.1 Homogenous nanocomposites

Figure (4.7) shows the results of the flexural strength of the pure epoxy and different concentration of alumina particles. The flexural stress shows a straight increasing with the filler contented until 2 %V_f after that can be seen stability in ultimate stress value of nano alumina composite because of alumina nano-particles display a constructive outcome on the flexural stress.

As shown in Figure (4.7), adding 2% V_f of alumina nano particles to the neat epoxy increased the amount of the flexural ultimate stress by 22.68%. An increase in the flexural stress for the samples with 2% V_f of alumina nano-particles were due to both a reduction in the crosslinking degree of the matrix and the physically better interaction between the polymer matrix and the filler [116].

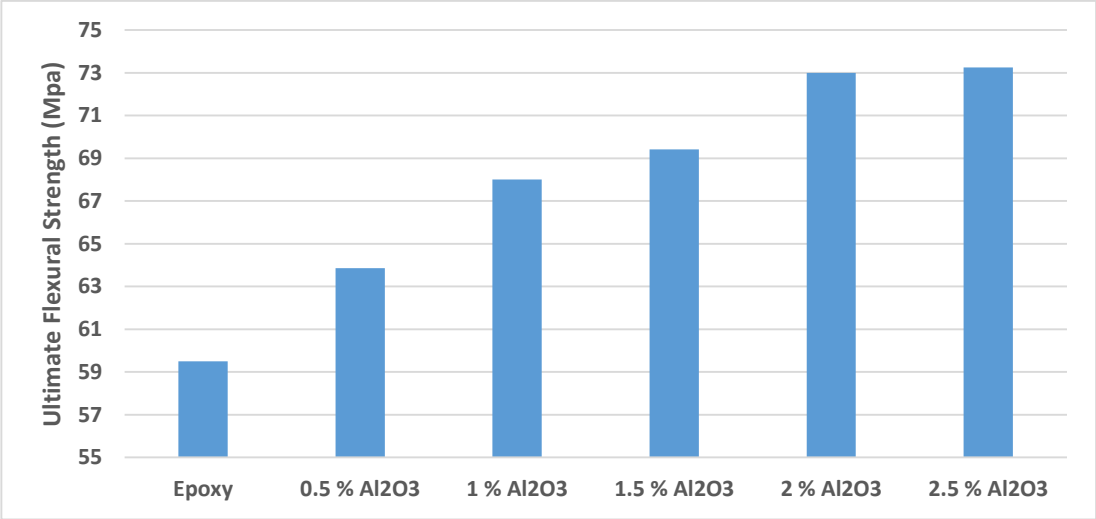

Figure (4.7): Effect of different alumina volume fraction on ultimate flexural strength of homogenous nanoparticles

Also, the results indicate that Al_2O_3 nano-particles are effective to enhance the Young's modulus as shown in Figure (4.8), while the elongation at break was decrease compared to epoxy resin as in Figure (4.9). At 2% V_f of nano particles, an increment of 52.74% in elastic modulus and the elongation at break decreased to 85.5% were recorded over that of neat

epoxy. Rigid alumina particles restrict the deformation of local matrix under applied load causing enhancement in the stiffness of composites. Due to the interface between the particles and matrix (imperfect bonding), stress concentration and void content-effects may reduce the bending strength at break.

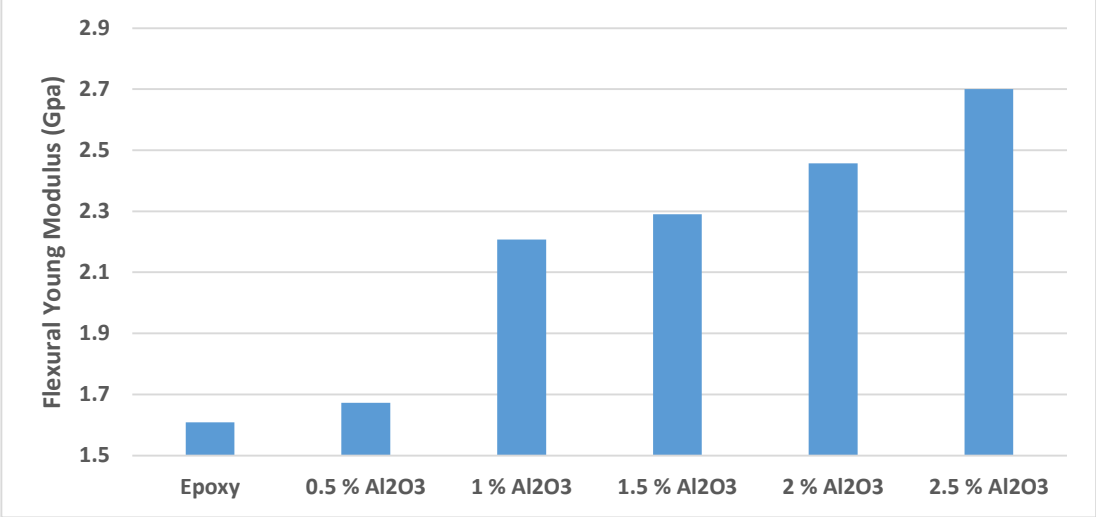

Figure (4.8): Effect of different alumina volume fraction on Young's modulus of homogenous nanoparticles

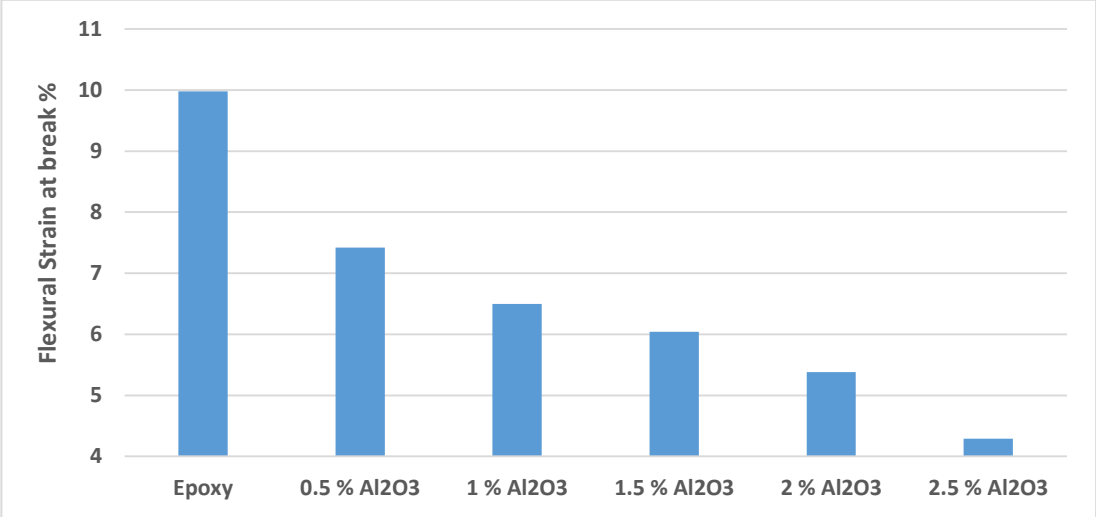

Figure (4.9): Effect of different alumina volume fraction on strain at break of non-FGM

4.5.2 FGM at different volume fractions

Figure (4.10) shows the comparison of Young's modulus between neat epoxy, homogenous alumina nano-composite and FGMs at different volume fraction and constant speed (N=1200 r.p.m) and constant time (t=6 min) for nano-alumina side and epoxy side. The results indicated an incensement in the flexural modulus with increasing volume fraction of the functionally graded polymer composite above those for the samples of the neat epoxy if loaded from both the side of neat epoxy and nano-alumina side. It was observed that the Young's modulus for the non-graded composites were higher than pure epoxy, due to the presence of particles. The results also show that the enhancement about (59.27%) in the flexural modulus for the samples if loaded from the alumina rich side at 2%V_f, while the enhancement about (81.11%) in the flexural modulus was noted for the samples of epoxy if loaded from the epoxy rich side at 2% V_f nano-Al_2O_3.

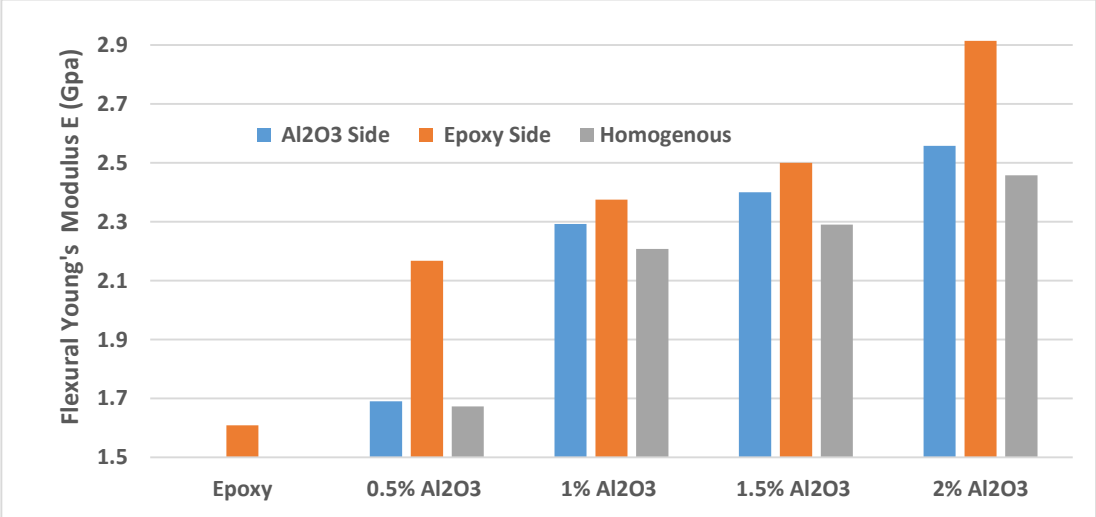

Figure (4.10): The flexural Young's Modulus for FGMs and non-FGM at different volume fractions

Figure (4.11) shows the comparison of flexural strength between neat epoxy, homogenous nano- alumina composite and FGMs at different volume fraction and constant speed (N=1200 r.p.m) and constant time (T=6 min) for

epoxy side and nano-alumina side. The results indicate a (122.4%) decreasing in the flexural strength of the functionally graded polymer composite over those for the samples of the neat epoxy if loaded from the neat epoxy side and it was observed that the flexural strength for non-graded composites were higher than the pure epoxy, due to presence of alumina particles. While, an improvement about of (43.69%) in the flexural strength were noticed over those for the samples of the neat epoxy if loaded from the nano-alumina rich side.

In addition, presence of higher void content in homogeneous composites causes stress concentration that results in ultimate failure of material.

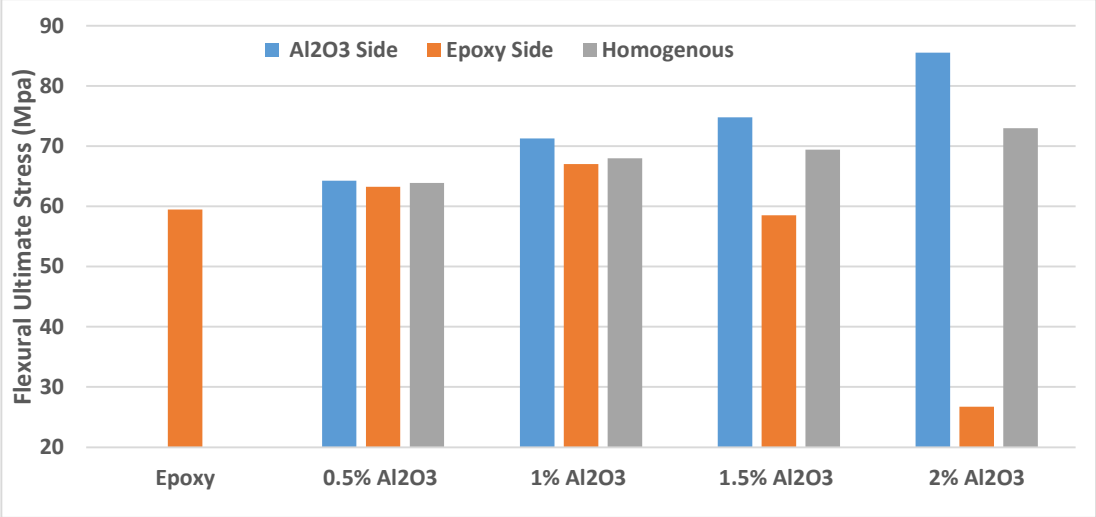

Figure (4.11): The ultimate stress for FGMs and non-FGM at difference volume fraction and constant rotational speed (N=1200 r.p.m) and constant time of rotation (t=6 min) for nano-alumina side and epoxy side

From Figure (4.12), the results indicate that the elongation at strain decrease with increasing volume fraction for homogenous nanocomposite and FGMs at a constant rotational speed (N=1200 r.p.m) and constant time of rotation (t=6 min) for both sides (nano alumina and epoxy) rich side due to brittle nature of nano- alumina. The maximum strain at the break at 2%V_f

of nano-Al_2O_3 was decreased by (78.984%) when they were loaded from the epoxy side while reducing about (62.8%) when loaded from nano alumina rich side and the decrement about (85.5%) for homogenous nanocomposite.

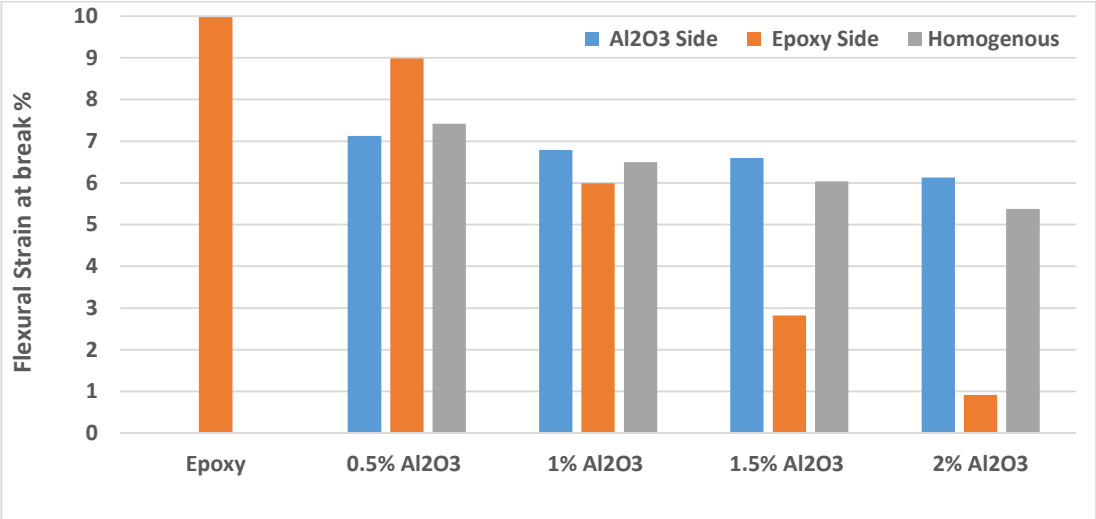

Figure (4.12): The strain at break FGMs and non-FGM at difference volume fraction and constant rotational speed (N=1200 r.p.m) and constant time of rotation (t=6 min) for alumina side and epoxy side

4.5.3 Results for FGM at different centrifugation speeds

Figure (4.13) shows the comparison of flexural modulus of FGM's at constant volume fraction (2% V_f nano-Al_2O_3) and constant time of rotation (t=6 min) in the case of nano alumina side and epoxy side with homogenous nano composite and neat epoxy. The results indicate an increasing in flexural modulus of FGPC with increasing rotational speed over that of the neat epoxy samples when loaded from both neat epoxy side and nano alumina rich side, it was observed that Young's modulus for non-graded composites was higher than pure epoxy, due to present of alumina nanoparticles. The improvement about 52.82 % in flexural modulus was observed at 2%V_f nano-Al_2O_3 when loaded from nano- alumina rich side over that of net epoxy.

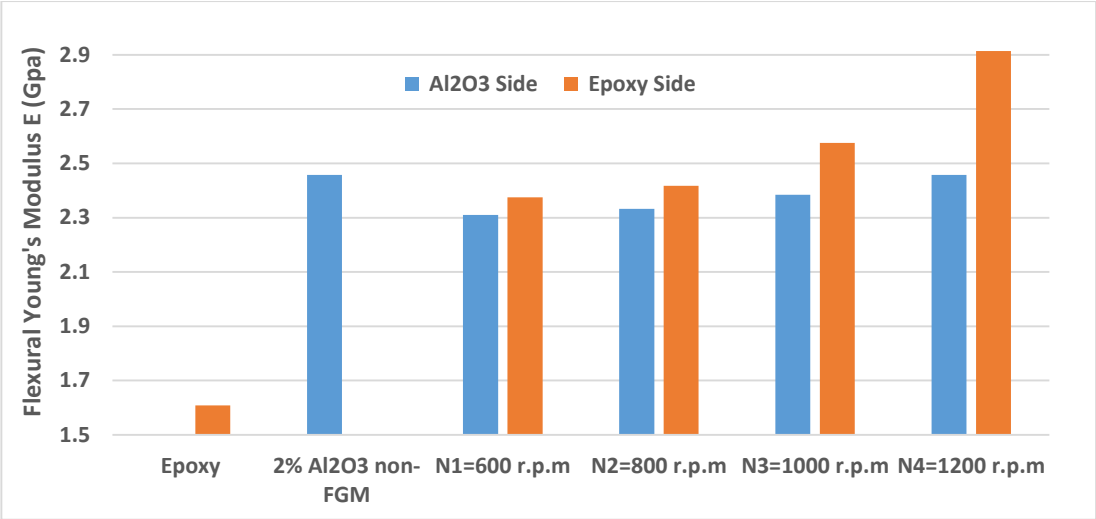

Figure (4.13): Flexural Young's modulus for FGMs and non-FGM at various centrifugal casting speeds in the case of nano-alumina side and epoxy side

In flexural test, the layers at which load is applied are experience to compressive stress while layers at the opposite side will be under tensile stress. In other words, in three-point bending layers below the neutral axis will experience tensile stresses while layers above the neutral axis towards the loading side will experience compressive stresses. The ultimate strength increases with increasing rotational speed of the mould when loaded from nano-alumina side as shown in Figure (4.14), while the strain at break decreases with increasing rotational speed in case of nano-alumina and epoxy rich side as shown in Figure (4.15).

Generally, when the brittleness of material increases, the resistance to compressive stress increase and resistance to tensile stress decrease. The flexural test in case of epoxy rich side, where the epoxy side subjected to compression load while the other side which rich in alumina nano-particles subjected to tension load which acceleration the failure. As well as the increase in centrifugal casting velocity leads to orientation the alumina nano-particles towards the outer surface and the brittleness of the material increases and when subjected to tensile stress, it quickly fails. As well as

with increasing centrifugal speed the agglomerations and impurities are oriented towards the outer surface and thus failure occurs. In the case of the nano-alumina side, the side subjected to the compression stress is the nano-alumina side and thus bear the high compression and the exposed side. The tension is on the side of the epoxy, so the bending results are better.as well as the compressive stresses developed on the specimen surface while applying load perpendicular to the specimen axis tends to block the movement of molecular chain and defects (e.g., cracks, flaws, etc.), thus enhancing the material strength under the loaded area by the virtue of work hardening, and thereby improving the magnitude of flexural strength. Its future improves with increase in the content of alumina nano-particles, this may be due to increasing the rotational speed of the mold the higher particles concentration towards outer pile that receives maximum stress during test. In other words, better reinforcement of nano-particles towards periphery enhances flexural strength in FGMs than the homogeneous nano-composites.

The propagation of crack that initiated in the layer under tensile stresses will become easier than that of in the layer under compressive stresses. Thus, the stiffer and stronger layers in the tensile stress region in the three-point bending test contribute more in enhancing the flexural properties of the FGPC. Thus, for 3-PB test outer most layer i.e., the layer opposite to the surface of applied load plays an important role in the increment of flexural properties of FGPCs. Layered FGPC having stronger and stiffer outer layer will have better flexural property.

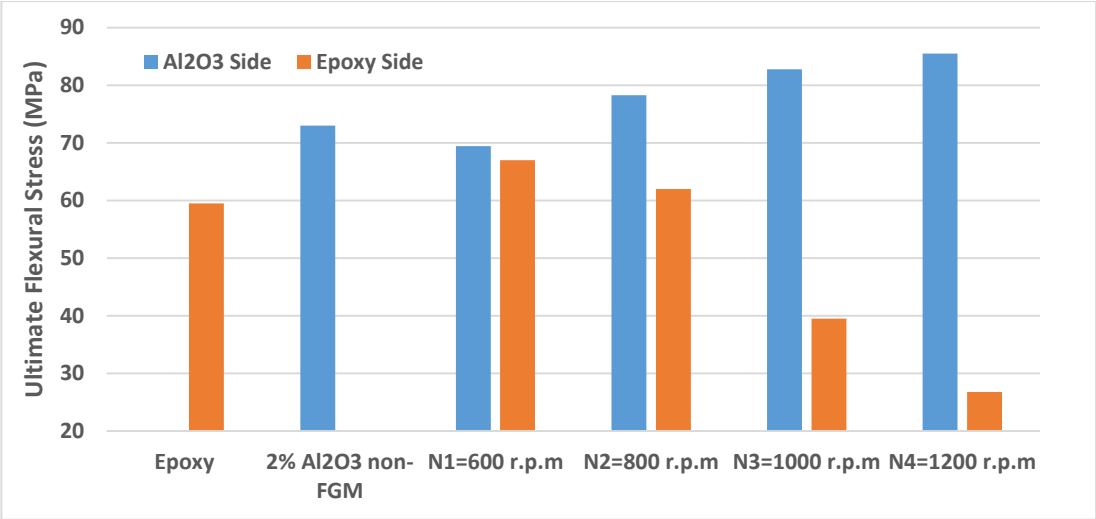

Figure (4.14): Ultimate flexural stress with various centrifugal casting velocities for FGMs and non-FGM

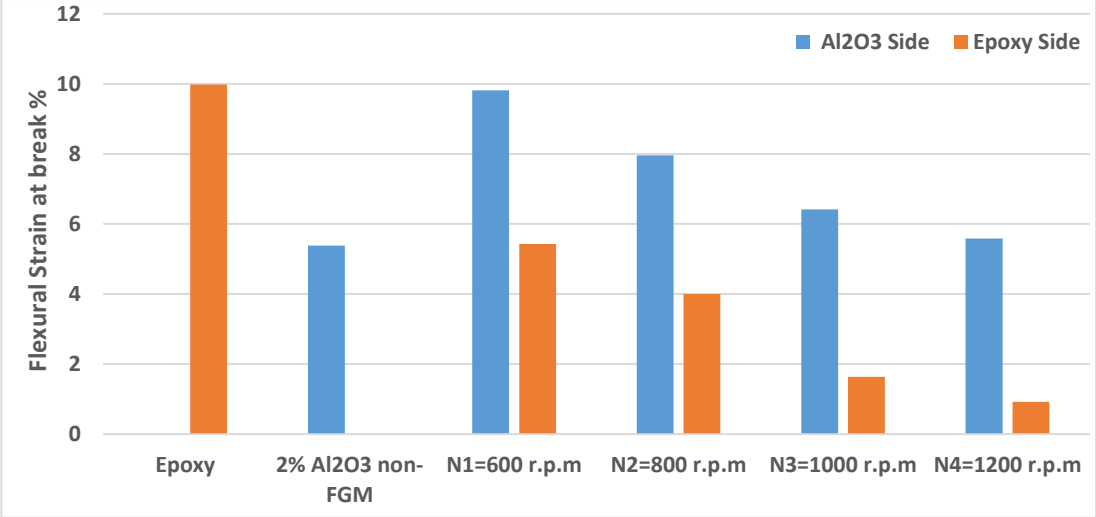

Figure (4.15): Flexural strain at the break with various centrifugal casting velocities for FGM's and non-FGM

4.5.4 Results for FGM at different centrifugation times

The comparison of Young's Modulus for epoxy, homogenous nano-composite and FGM's at a different rotation times and constant rotational speed N=1200 r.p.m and constant volume fraction 2%V_f Al_2O_3 in the case of nano- alumina rich side and epoxy rich side are shown in Figure (4.16). The results indicated that as rotational time increased, the flexural modulus of the FGM increased as compared to the samples of pure epoxy if loaded from

both the pure epoxy and nano- alumina sides. The existence of nano alumina particles causes by rising in the flexural modulus of the ungraded composites compared to neat epoxy.

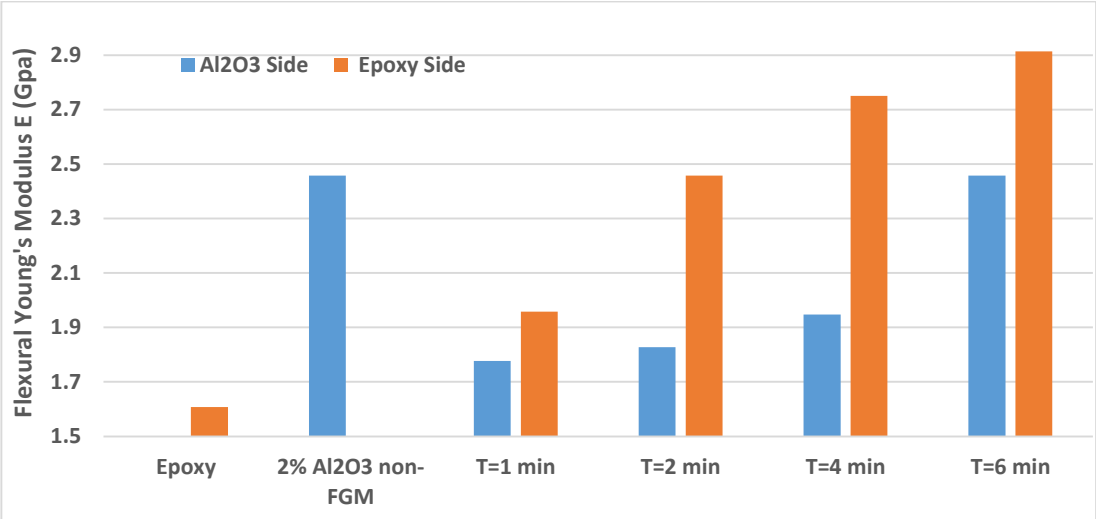

Figure (4.16): Flexural Young's Modulus for FGM's and non-FGM for both nano-alumina and epoxy rich sides with different centrifugation times

Figures (4.17 and 4.18) show comparison of flexural strength and strain at break respectively for neat epoxy, homogenous nano-composite and FGM's with different times of rotation and constant rotational speed N=1200 r.p.m and constant volume fraction 2%V_f Al_2O_3 in the case of nano-alumina side and epoxy side. The results indicate that the flexural strength increase with increasing the time of rotation if loaded from nano-alumina rich side and decreasing with increasing the time of rotation if loaded from epoxy rich side, while the strain at break decrease with increasing time of rotation if loaded from both nano-alumina and epoxy side.

Under flexural loading situation, the nano fillers apparently aid in bearing the load acting on the nano-composite, whereas it acts as stress raiser under tensile loading. The compressive stress applied to the specimen during flexural loading tends to suppress the cracks and flaws that are perpendicular to the applied load, contrary to the crack opening mechanism occurring in a tensile loading situation. The applied compressive stresses on the specimen

surface block the movement of the molecular chain and defects (e.g., cracks, flaws, etc.). Consequently, material strength improves by the virtue of work hardening and it future improves with the increase in the content of alumina nano filler. The presence of higher alumina nano-filler concentration around the periphery in the case of FGMs (due to the centrifugal action while fabrication) will lead to greater resistance to the compressive force. Such effects originating from the unique internal structure are thought to be able to handle the higher flexural strength.

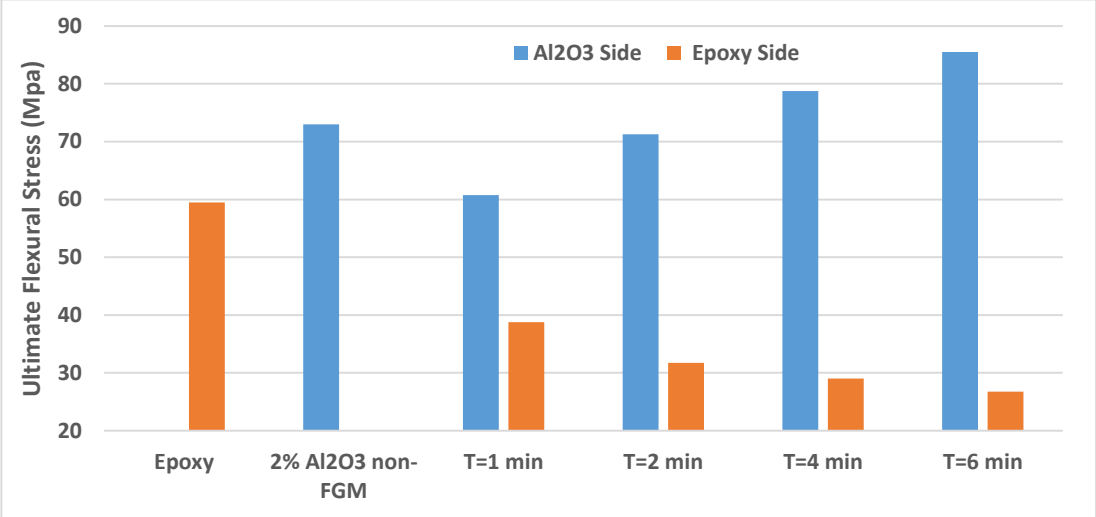

Figure (4.17): Flexural strength for FGM's and non-FGM for both nano-alumina and epoxy side with different centrifugation times

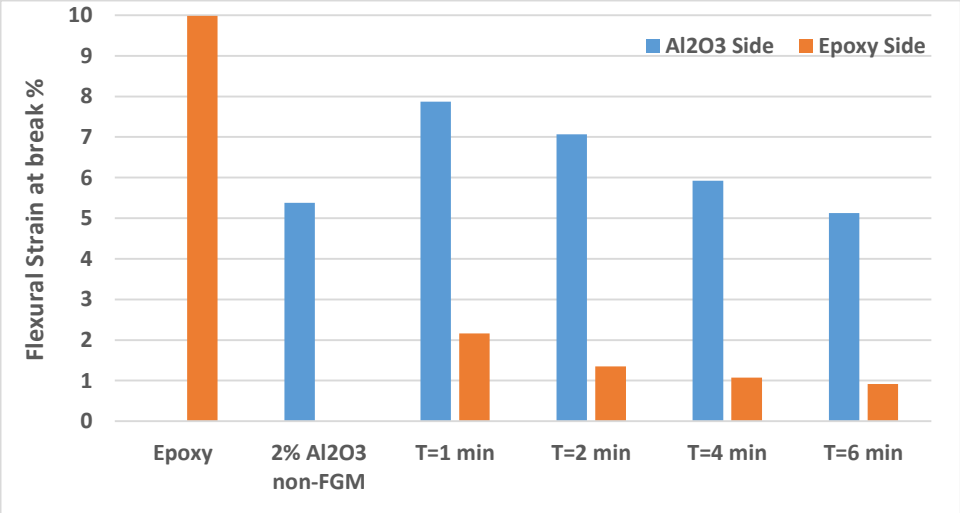

Figure (4.18): Flexural strain at break for FGM's and non-FGM for nano-alumina and epoxy side with different centrifugation times

4.6 Impact Results

After obtaining the absorbed energy values from the Charpy test device, they were divided into impacted sections to allow for a more reliable comparison. When a small number of nano-alumina particles were added, the impact energy increased but decreased at high concentrations. The maximum impact strength for homogenous samples was found at the particles content 1.5%V_f of nano Al_2O_3 which increased by 95.09% over neat epoxy, as shown in Figure (4.19). The brittle nature of particles reasons for decreases in the material's impact strength. The same behavior was obtained in reference [22 and 92].

According to reports, physicochemical interactions between nano particles and the matrix play a significant role in the formation of composites. Composites also have better mechanical properties as a result of alumina nano particles with a high modulus which absorbing higher mechanical stresses, an interfacial surface is formed, which increases values of mechanical properties where the nano-alumina particles act as strong stress concentrators, reducing crack propagation by increasing crack deflections (creating multiple crack propagation directions) [88].

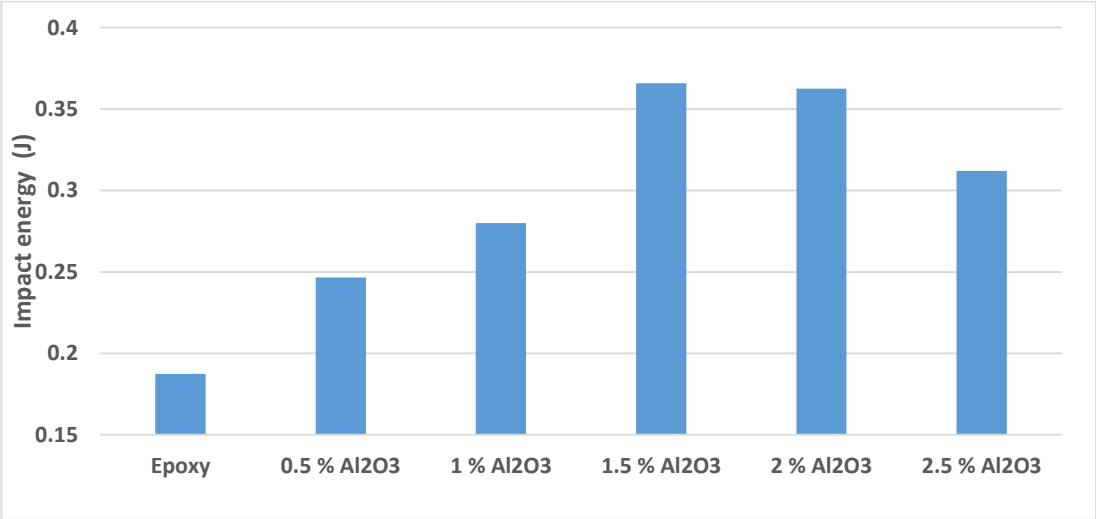

Figure (4.19): The impact strength of non-FGM material

According to Figure (4.20), the impact strength of functionally graded composites is greater when loaded from the nano alumina rich side (the maximum value at 1% V_f was 133.33 % greater than the epoxy side) because the impact load causes a more excellent elongation to break in pure epoxy on the opposite side. In contrast, the composites loading side improves the resistance to impact, which is consistent with reference [117]. These two phenomena may be partially responsible for the increased impact strengths of these samples [118].

It is noticed that FGMC have higher impact strength in comparison with homogenous composite at different concentrations of nanoparticles because of the changes in microstructural levels and the overall FGM accomplish the multi structural position from their property gradation, which result in constant change properties from one surface to another, thus removing any interface problems.

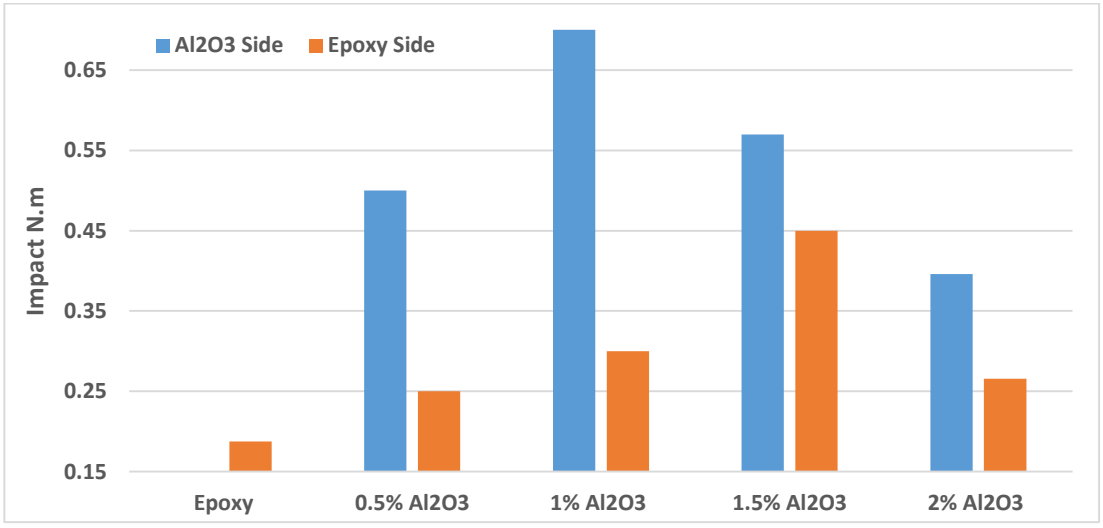

Figure (4.20): Impact strength of FGMs alumina particles at different volume fractions with constant rotational speed of 1200 r.p.m and 6 min centrifugation time

Figures (4.21) and (4.22) depict the comparison impact strengths of neat epoxy, homogenous and FGMPS with different times of rotation and

different rotational speed of FGMPS on the nano- alumina and epoxy sides, respectively. The results indicate that the impact strength of the both homogenous nano-composites, as well as FGM, is higher than the pure epoxy, but the increment level is higher in FGM when loaded from the nano-Al_2O_3 side.

From these figures noticed that the impact strengths of FGM increase with increasing rotational speed and time of rotation when loaded from the Al_2O_3 side, where the maximum value of impact strength at the time of rotation is 4 min by 168% higher than neat epoxy and decreases after that as shown in Figure (4.21), while the maximum value of impact strength at 1000 r.p.m rotational speed by 133% higher than neat epoxy and decrease after that as shown in Figure (4.22), This indicates that proper mixing occurred during centrifugation, and nano-filler particle agglomeration occurred at 1000 r.p.m rotational speed and time of rotation (4min), which reduces the tendency of nano-fillers to effect as stress concentrations through the epoxy matrix, where FGMs had fewer crack initiation sites. At 1000 r.p.m rotational speed and time of rotational speed (4min), the graded materials show excellent interfacial adhesion, finally increasing the impact strength. Overall, FGMs show higher impact strength than homogeneous composite because the agglomeration of nano-fillers is significantly reduced during the manufacturing of centrifugal casting. Improvements in impact performance imply a reduction in the embrittling effect under high-strain conditions—a finding that accords with research [99].

Figures (4.21) and (4.22), also show that the strength of impact of FGMs decreases as speed and time of rotation increasing respectively when a sudden load applied from the epoxy side. This may be explained because nano-alumina effectively absorbed the transferred stress and prevented matrix failure inhomogeneity due to uniform distribution of nano particles. In comparison, in the case of graded materials, failure occurs at the interior of the composite due to a lack of strengthening caused by the alumina-nano

particle moving towards the periphery during fabrication. This reduces the composite's transverse strength. Additionally, the lack of particle and matrix adhesion across the outer pile due to a lack of resin likely reduces the composite's shear strength. As a result, the ability of the composite to absorb impact energy decreases, and failure occurs, which agrees with research [119].

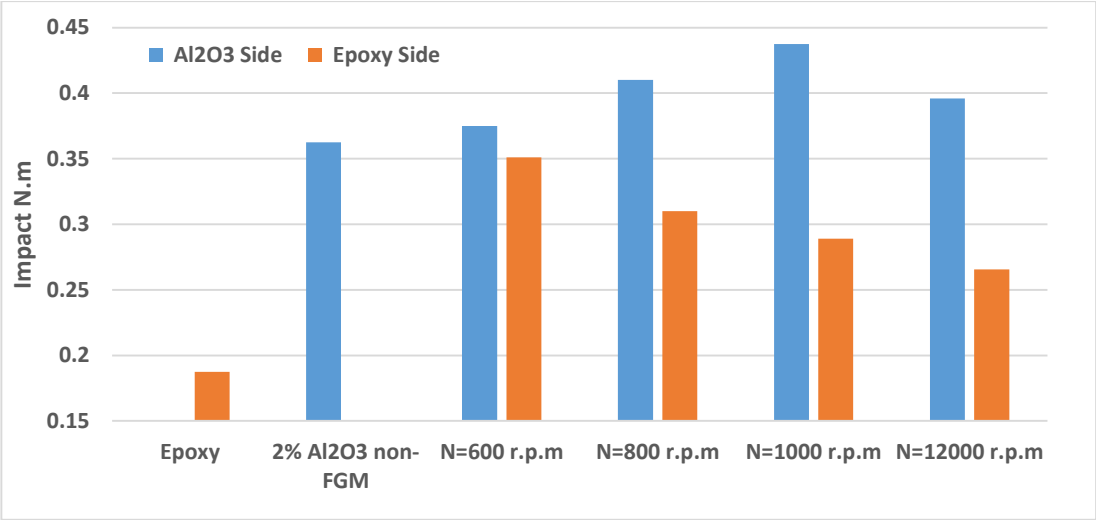

Figure (4.21): Impact strength for FGM's and non-FGM in the case of nano-alumina and epoxy rich at constant rotational time of 6 min r.p.m

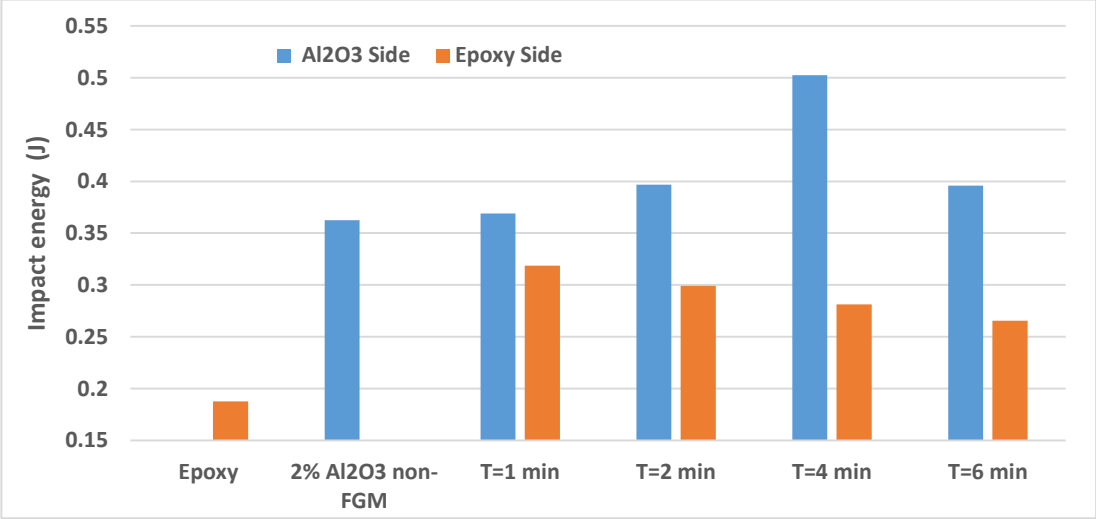

Figure (4.22): Impact strength for FGM's and non-FGM with different centrifugation times and constant rotational speed of 1200 r.p.m

4.7 Hardness Results

Figure (4.23) depicts the Shore-D hardness of pure epoxy and nano-composites of Al_2O_3/epoxy with various volume fractions. This Figure demonstrates that introducing nano fillers into the epoxy significantly improved the composites' toughness. It can be seen that the addition of 2% Al_2O_3 nano powders increases the material's hardness by more than 7%. Adding additional powder gradually improves the material's hardness. This may result from the strong bonding formed between Al_2O_3 and epoxy.

Therefore, this increase in hardness may have contributed to improvement in wear resistance of nanocomposites. Due to Al_2O_3's ceramic nature, its surface hardness is significantly greater. Consequently, the addition of nano-Al_2O_3 to the epoxy enhances its hardness.

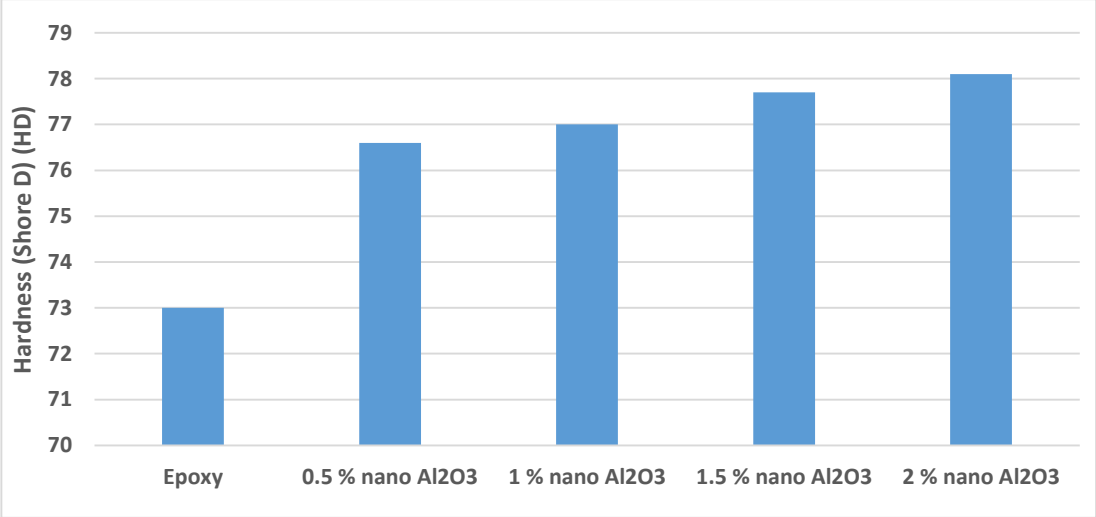

Figure (4.23): Shore D surface hardness as a function of volume fraction of alumina nanoparticles

Figure (4.24) depicts the hardness of pure epoxy, FGM with varying volume fractions for both sides of samples. The hardness of FGM increase with increasing volume fractions from both side but the nano- alumina rich side hardness was greater than that of the pure epoxy side, due to brittle nature of nano-alumina, its surface hardness is significantly greater.

Consequently, the addition of nano-Al_2O_3 to the epoxy enhances its hardness.

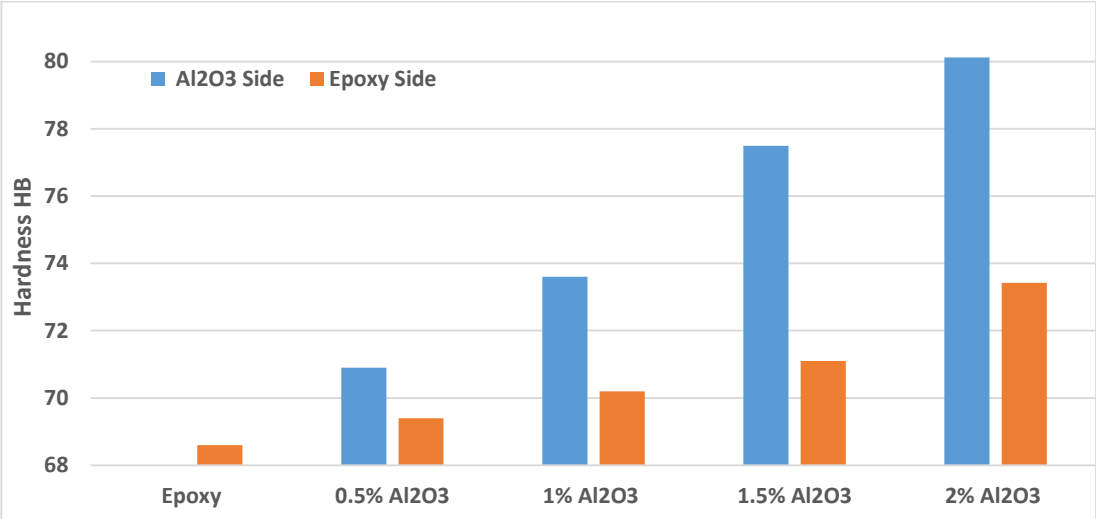

Figure (4.24): Shore D surface hardness of neat epoxy and FGM at different volume fractions with constant rotational speed of 1200 r.p.m

The best contact between epoxy resin and nanoparticles, which speeds up active hardness transfer, is responsible for the increased hardness of composites. So, the hardness of the composite depends on the intermolecular bonds between the epoxy matrix and the nanoparticles. The composite's increased hardness shows that the Al_2O_3 nano- particles are evenly distributed in the epoxy matrix.

The composite's increased hardness can be attributed to the addition of stiff inorganic nanoparticles, which impeded the passage of molecular chains and made them more rigid and brittle [120].

Accordingly, the addition of nano-alumina and the way it is distributed throughout the graded sample directly effect on the hardness and other mechanical properties. In addition, centrifugal casting process variables, such as rotational speed, centrifugal casting time and volume fraction play an essential role in the distribution of alumina nano-particles through the thickness. Figure (4.25) shows the hardness comparison of homogeneous,

FGNC and pure epoxy at different centrifugal speeds. The results indicate that the hardness of the FGM from alumina rich side is improved compared to the pure epoxy and homogeneous nano-composite samples.

The hardness resistance of the epoxy-rich side and the alumina-rich side was examined. The results showed that the hardness resistance of the alumina-rich side increased with the increase of the centrifugal speed and the maximum value of the hardness at a rotational speed (1200 r.p.m.) where high spinning speeds (that is, centrifugal forces) operate. High velocities push the alumina nano-particles towards the outer surface of the FGM sample, while low rotation speeds help to agglomerate the nano-alumina inside the inner surface. At the same time, the hardness decreases on the epoxy-rich side with increasing rotation speed due to the decrease in the concentration of alumina particles.

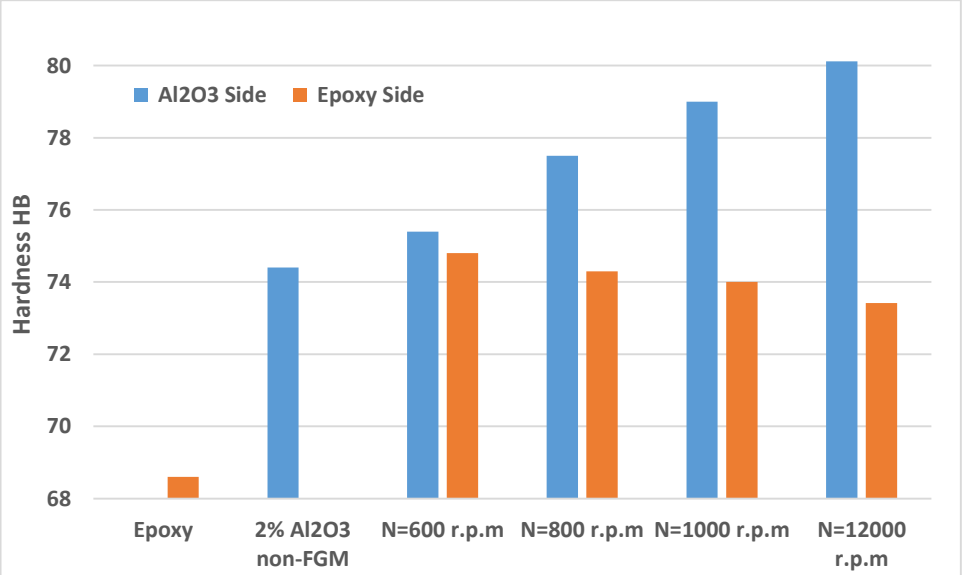

Figure (4.25): Hardness strength of FGM and non-FGM at different rotational speeds with constant rotational time of 6 min

Figure (4.26) depicts the hardness of pure, non-graded, and graded nano-composites with varying rotation times of centrifugation for both sides of samples. The hardness of the model at the time of rotation (6 minutes) from the nano- alumina rich side was greater than that of the pure epoxy side

(168 % than the pure epoxy specimen) to resistance that hardness, which is the resistance of the surface to indentation. Thus, the composites' hardness ratings were high because the nano-fillers were more rigid and brittle than the matrix material. And the filler particles' addition raised the composite's hardness by enhancing the stiffness of the matrix or the adhesion to filler particles. In general, adding nano alumina as a graded or non-graded structure increases the hardness of laminates relative to pure epoxy.

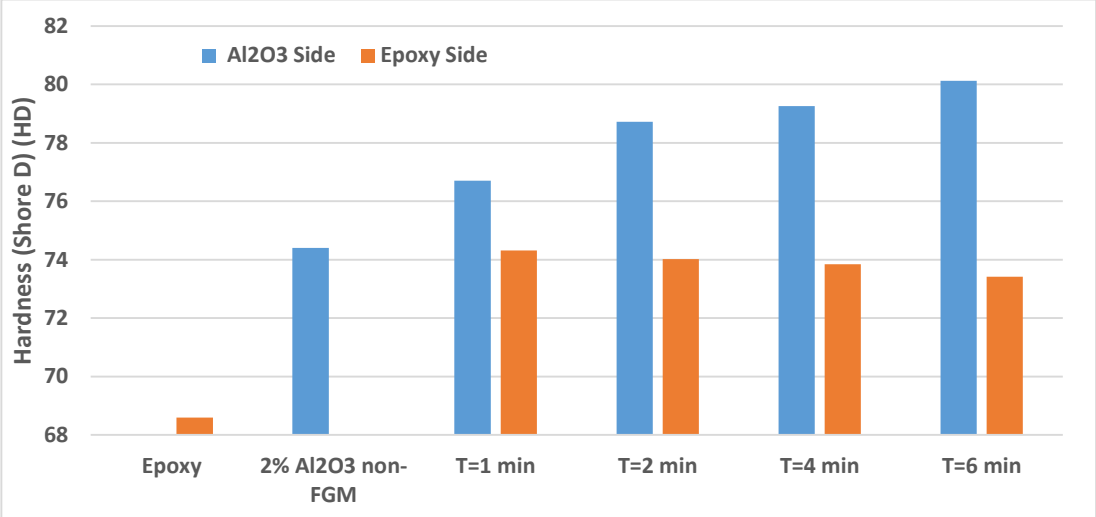

Figure (4.26): Shore D surface hardness of FGM and non-FGM at different centrifugation times with constant rotational speed of 1200 r.p.m

The hardness test is considered an excellent test for the gradation of material properties through the thickness. Therefore, ensure the correct distribution of nanoparticles through the thickness of FGM samples at the highest and lowest centrifugal speed with constant volume fraction (2% V_f Al_2O_3) and constant time (T = 6 min). The hardness of the samples was measured from the alumina-rich side to the epoxy-rich side (divided by five layers L1, L2, L3, L4 and L5). The hardness of each layer was measured at the lowest and highest speed, as shown in Figures (4.27) and (4.28) respectively. For five different regions and calculating the average values of all FGM as shown in table (4.1), where the values of the percentage results

are the amount of difference between the mean values of the FGM samples and the equivalent homogeneous material, and there is a good agreement in the results.

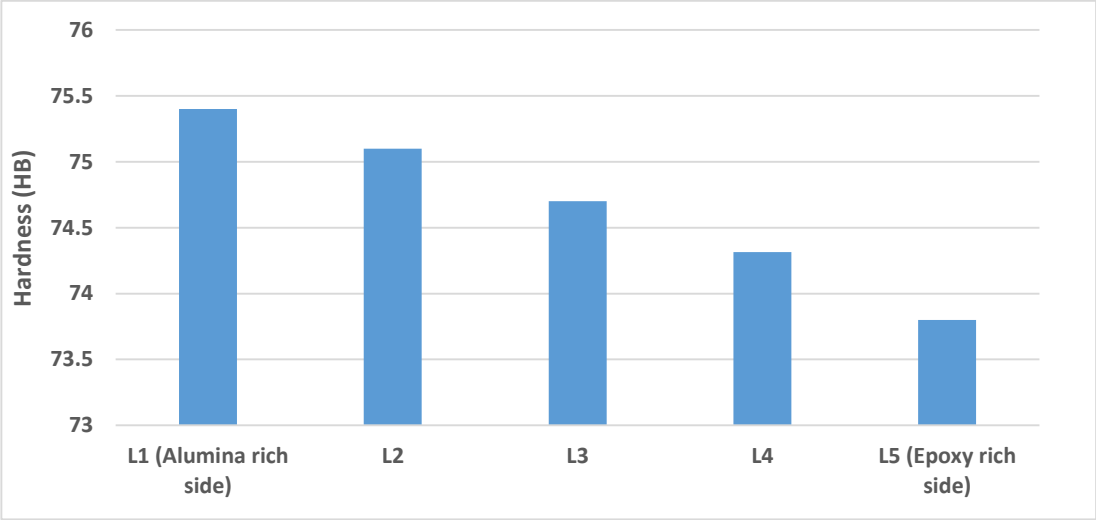

Figure (4.27): The hardness of the functionally graded material for five different regions at minimum centrifugal force (N=600 r.p.m, t=6 min)

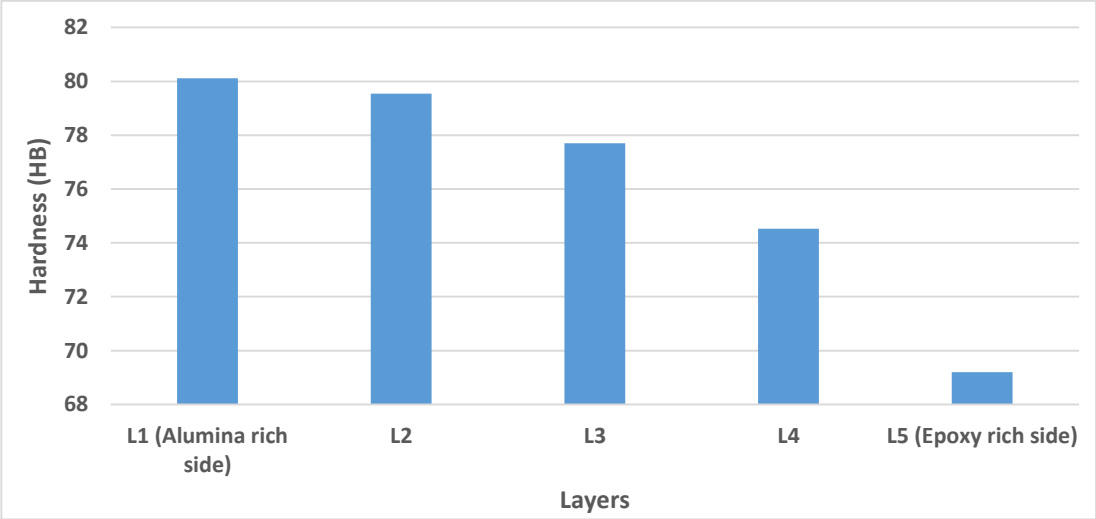

Figure (4.28): The hardness of the functionally graded material for five different regions at the highest centrifugal force (N=1200 r.p.m, t=6 min)

Table (4.1): Hardness of the FGM for five different regions at the highest and lowest centrifugal force.

Regions	**Hardness Shore D (Hv)**	
	FGM (600 r.p.m) t=6 min. V_f=2%	**FGM (1200 r.p.m), t=6 min. V_f=2%**
L1(Alumina rich side)	75.4	80.12
L2	75.1	79.55
L3	74.7	77.7
L4	74.314	74.53
L5(Epoxy rich side)	73.8	69.2
Average	74.6628	76.22
% Difference (with homogenous nanocomposite)	+4.6036	+2.446

4.8 Pin on Disk results

4.8.1 Effect of Volume Fraction on Specific Wear Rate and Coeff. Friction for Homogenous Nano-composite

Figure (4.29) summarizes the effect of volume fraction of Al_2O_3–nano-particles on coefficient of friction for homogeneous nano-composites at the wearing conditions of (velocity: 125.6 mm/s, load: 30 N, time: 20 min, and sliding distance: 150 m) for all samples. The friction coefficient of nano-composite decrease with increased the volume fraction.

Hence, it was proposed that during the sliding process many of the hard particles were embedded in the soft polymeric transfer films on the counter surface and grooved the sample surface. In this way, the particle acted as spacers. This in turn can cause a reduction in the adhesion between the contacting surfaces. Therefore, the coefficient of friction of nano-Al_2O_3 filled epoxy was always less than that of neat epoxy. Moreover, as the nanoparticles were free to move, they tend to be dispersed uniformly over

the transfer films during the wear process, which would result in a more uniform contact stress between the contact surfaces and in turn minimizes the stress concentration. The addition of nanoparticles into epoxy changed the contact conditions for Al_2O_3 filled epoxy versus counter surface and effectively reduced the friction force.

The ability of nano-Al_2O_3 to improve the tribological behavior is increased with decreasing particle size of nano-Al_2O_3. In the present work, the wear-resistant epoxy nano-composite which was filled with Al_2O_3 particles transferred well to the counter face and its transfer film was thin, uniform and adhered strongly to the counter surface. Thus, the improvement in the tribological behavior of nano-Al_2O_3 filled epoxy composite is related to the improved characteristics of the transfer film. Besides improving the wear resistance, the nanoparticles also reduced the frictional coefficient of epoxy as shown in Figure (4.29). Evidently, the composites with Al_2O_3 nanoparticles have lowered the frictional coefficients of neat epoxy.

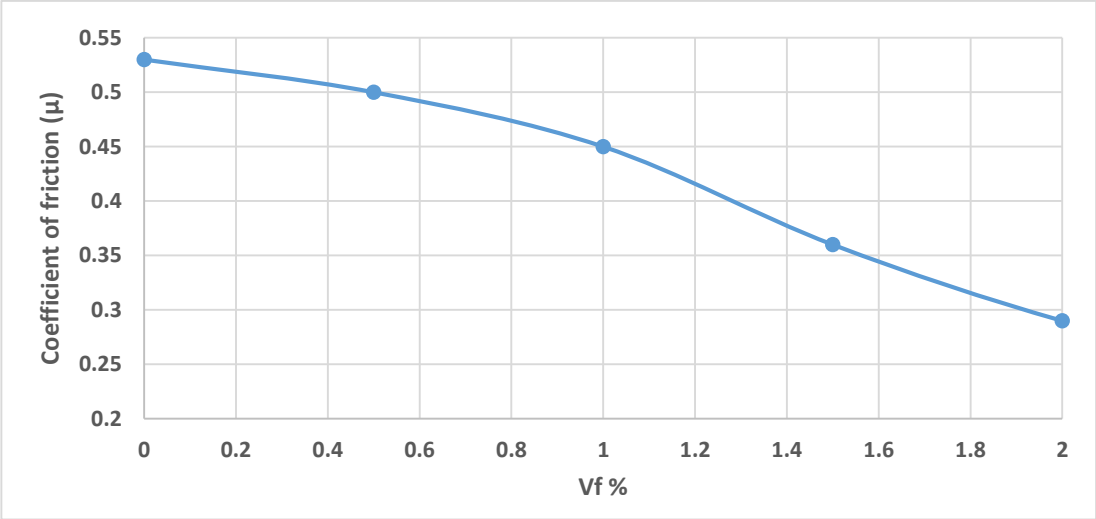

Figure (4.29): Variation of average friction coefficient with different Al_2O_3 volume fractions for non-FGM

Figure (4.30) shows how the concentration of alumina nanoparticles in epoxy effects on the specific wear rates. Because of how the nano-

composites work mechanically, adding more nanoparticles made the individual wear rate go down. This means that as the concentration of nanoparticles went up, the strength of the epoxy compounds also went up. Therefore, the alumina nanoparticles prevented the composite surfaces from degrading during the slip test and increased their wear resistance.

This is probably because epoxy can be easily removed on slippery surfaces (contact area). Still, the ceramic nanoparticles reduce the adhesion between the sliding surfaces. So, the better tribological behavior of the epoxy composite with nanometer-sized particles is linked to the better properties of the transfer film. The results match with [88, 96].

Thus, the specific wear rate (W_s) of the neat epoxy depends on the account of various particles in the wear debris. During wear process, no transfer film was formed on the counter surface leading to higher the specific wear rate (W_s) for neat epoxy as shown in Figure (4.30).

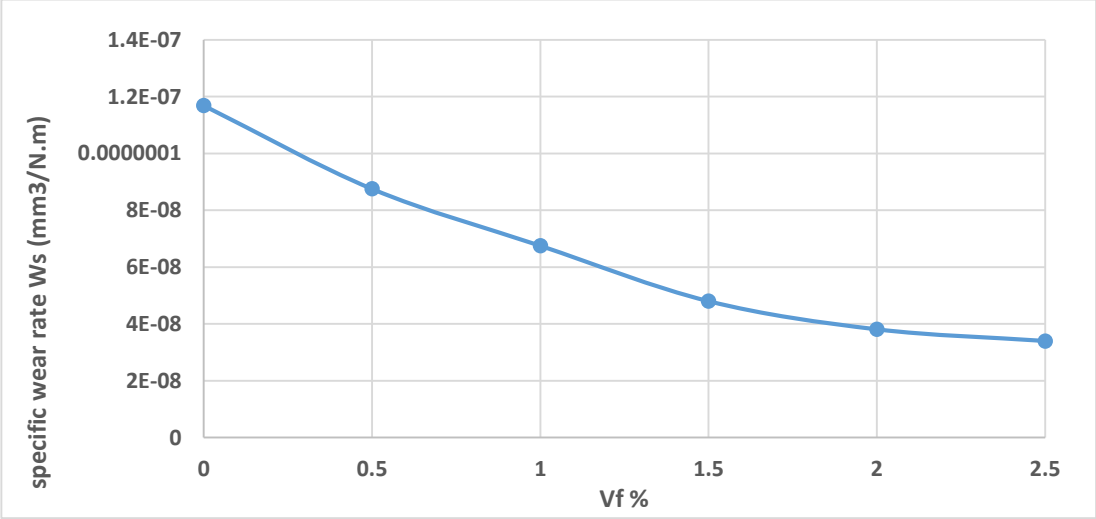

Figure (4.30): Changes in wear rate with volume fractions for the non-FGM

4.8.2 Influence of the different volume fractions on the wear rate and Coefficient of friction of FGM

Figure (4.31) represents the variance in the specific wear rate with varying volume fractions (0, 0.5, 1, 1.5 and 2% V_f) of epoxy-based homogeneous nano-composites and the corresponding FGM under a centrifugal rotation speed of 1200 r.p.m. and time centrifugation for rotation 6 min; FGM and homogenous nano-composites show lower wear rate compared to neat epoxy. Both the 2% V_f homogeneous and FGM nano-composite show a significant reduction in specific wear rate as shown in Figure (4.31), indicating enhanced interaction inside and outside the nanoparticles agglomerates, the resistance to periodic frictional stress is greatly increased. Detachment of nanoparticles and small amount of the surrounding matrix plays the leading role in material removal due to wear. The detached nanoparticles might also act as solid lubricants. These account for the low wear rates and frictional coefficients of the composites.

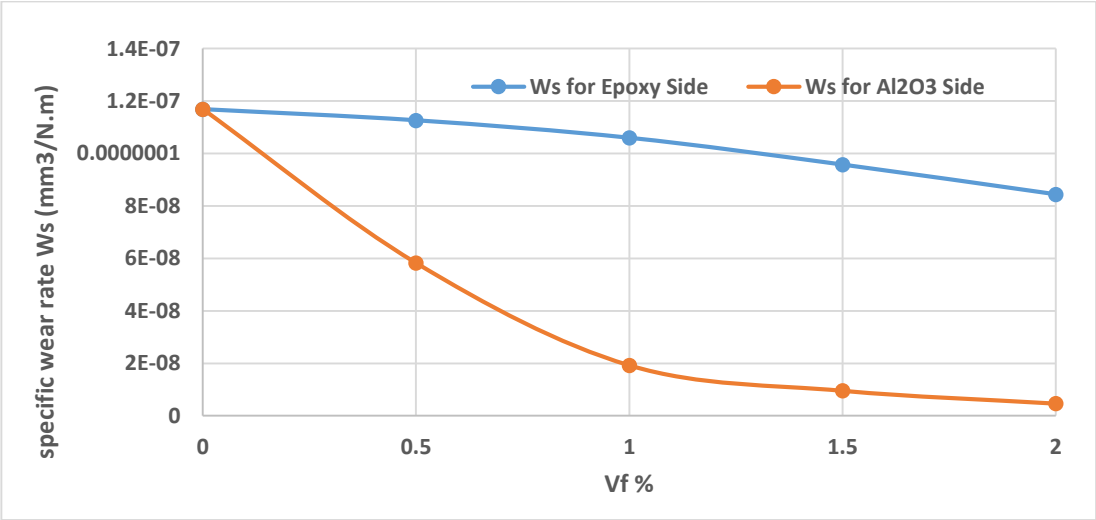

Figure (4.31): Specific wear rate variation with volume fraction for the FGM with constant rotational speed of 1200 r.p.m and 6 min centrifugation time

Figure (4.32) depicts the coefficient of friction behavior with different volume fraction. Across the whole range of volume fractions used in the experiment and on both sides of samples, the average coefficient of friction is determined to be highest for neat epoxy. Simultaneously, the individual wear rate is most significant for the similar composite; functionally graded materials with 2% V_f have a low average coefficient of friction.

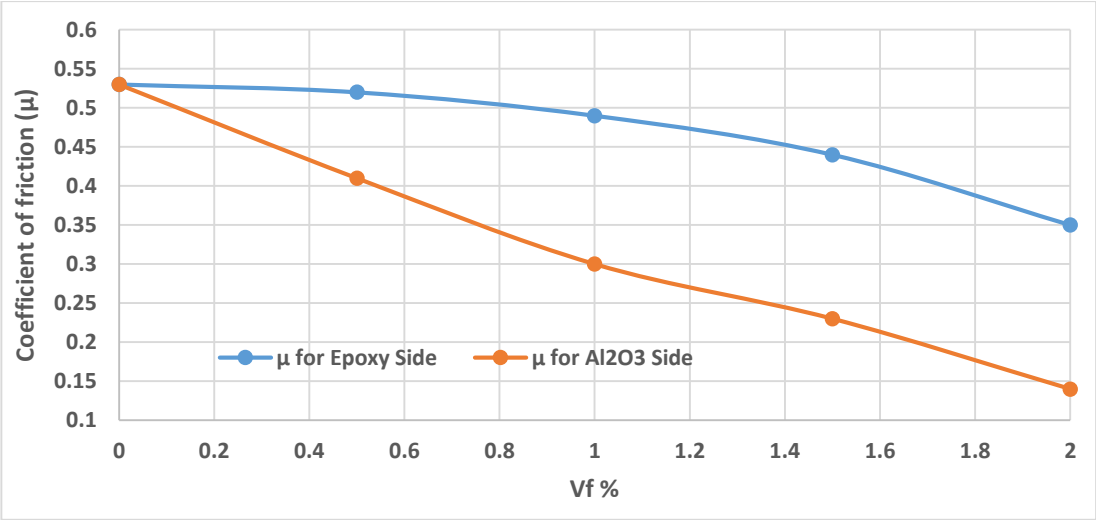

Figure (4.32): Coefficient of friction variation with volume fraction for the FGM and neat epoxy with constant rotational speed of 1200 r.p.m and 6 min centrifugation time.

4.8.3 Effect of centrifugation rotational speed on the specific wear rate and friction coefficient

The specific wear rate of pure epoxy resin and graded nano-Al_2O_3 filled epoxy polymer composites as a function of centrifugation rotational speeds (0, 600, 800, 1000, and 1200 r.p.m.) for a 6-minute centrifugation time and a 2%volume fraction is displayed in the Figure (4.33). When the centrifuge's rotation speed goes up, the specific wear rate of the epoxy rich side goes up also, while the wear rate of the nano-alumina rich side starts to decrease. Figure (4.33) shows that the reinforced samples on the Al_2O_3-rich

side lose less weight as the rotation speed increases. This indicates that the particles stop the matrix epoxy resin from wearing down.

The higher hardness of Al_2O_3 nanoparticle is supposed to be main reason for the enhancement of the wear resistance. This behavior is consistent with the (Shore-D) results.

It is already known that majority nano-fillers are more effective in reducing the wear of different polymers. In the case of neat epoxy, wear debris consists of shear deformed polymer matrix containing broken pulverized parts of matrix and wear powder of the metallic counter surface. The particles can either be lost from the contact zone or remains there for a fixed time as a transfer layer. In such cases, their polymer component can cushion the counter surface asperities and reduce the effective toughness, but the pulverized matrix particles and wear powder of the metallic counter surface can act as a third body abrasive leading to enhanced roughening of the counter surface.

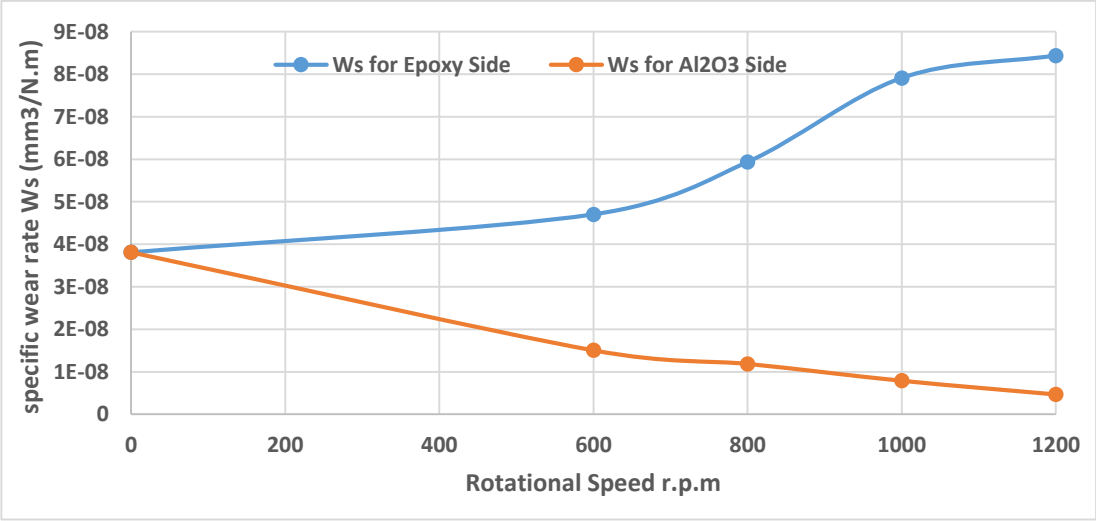

Figure (4.33): Specific wear rate variation with centrifugation rotational speed for FGM and neat epoxy with constant centrifugation time of 6 min

The variation in coefficient of friction with centrifugation rotating speed for the FGM for both alumina-rich and epoxy-rich sides was depicted

in Figure (4.34). The particle-filled epoxy exhibits rotational speed dependence. The results show that the coefficient of friction decrease when the rotating speed increases for the nano-alumina rich side while the coefficient of friction increase as rotational speed increase for the epoxy-rich side. This reliance can be attributed firstly to the presence of nano-Al_2O_3 in the matrix and secondly to the exposure of the particles to the surface, which causes their fragmentation and consequently a change in the surface properties.

Moreover, when polymer samples slide against their steel counterparts for a long time, enough heat is made to cause the nano-composites to melt in one spot. So, thin films of the studied polymer compounds were transferred to their steel counterparts to act as a third body between the contact bodies and lower the friction coefficient of the compounds. Nanoparticles made the transferred layer more even, which decreased the friction coefficient [120].

The results show that the lowest friction coefficient was recorded for the alumina rich side with a rotational speed of 1200 r.p.m with the value of (0.14) with a 51.7% decrease compared with homogenous nanocomposite (0.29). At 1200 r.p.m, the friction coefficient of epoxy rich side was more than that of the homogenous nanocomposite by approximately 20.6%.

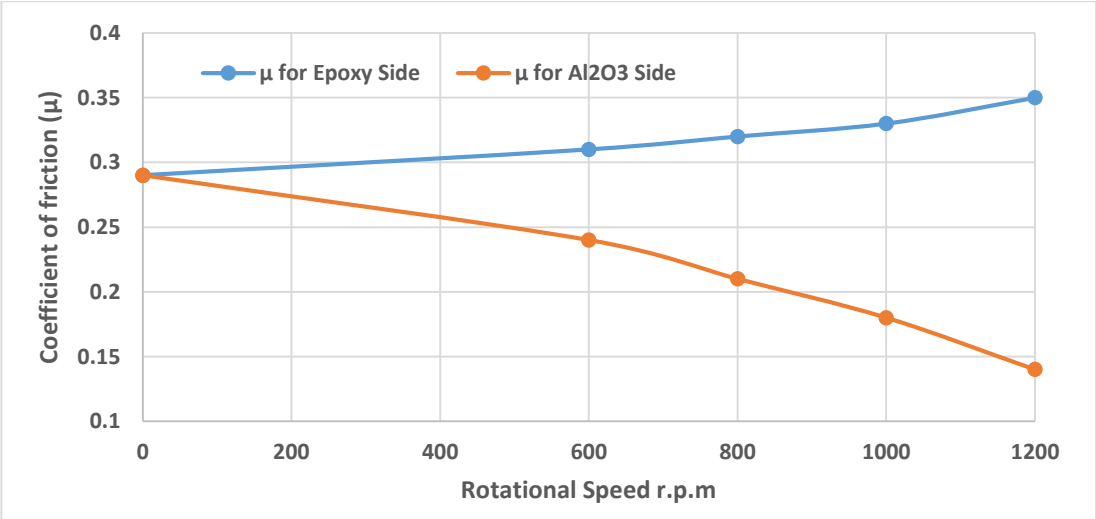

Figure (4.34): Coefficient of friction variation with centrifugation rotational speed for FGM and neat epoxy with constant centrifugation time of 6 min

4.8.4 Influence of centrifugation time on specific wear rate and coefficient of friction behavior of nano-alumina graded:

The wear rates versus centrifugation time (0, 1, 2, 4 and 6 min) at constant centrifugation speed (1200 r.p.m) for particulate volume fraction (2%) filled alumina nano-composites were shown in Figure (4.35). The results show that the specific wear rate decrease with increasing the time of rotation for the nano-alumina rich side while the specific wear rate increase as time of rotation increase for the epoxy-rich side.

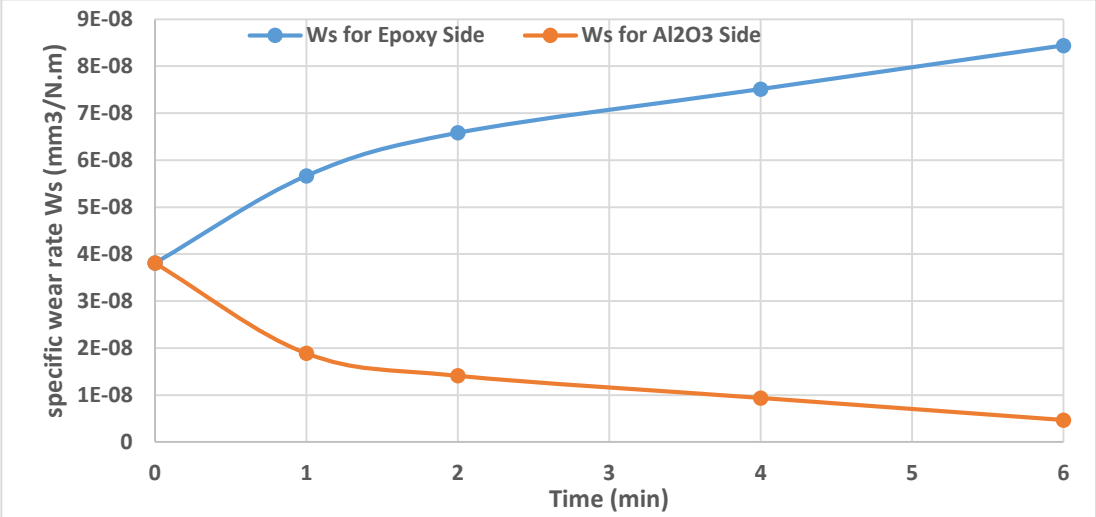

Figure (4.35): Changes in specific wear rate with centrifugation time for the FGM and neat epoxy with constant centrifugation speed of 1200 r.p.m

Figure (4.36) depicts the coefficient of friction with centrifugation time for both alumina-rich and epoxy-rich sides. As illustrated in this Figure, the friction coefficient of the functionally graded epoxy-side composites for various centrifugation times increased significantly while the coefficient of friction for alumina side decrease with increasing time of rotation throughout the early stages of the run-in phase. Moreover, the graded composites demonstrated greater reinforcing particle segregation than the homogeneous nano-composites. It appears to be an efficient reinforcement for enhancing the composite's wear resistance.

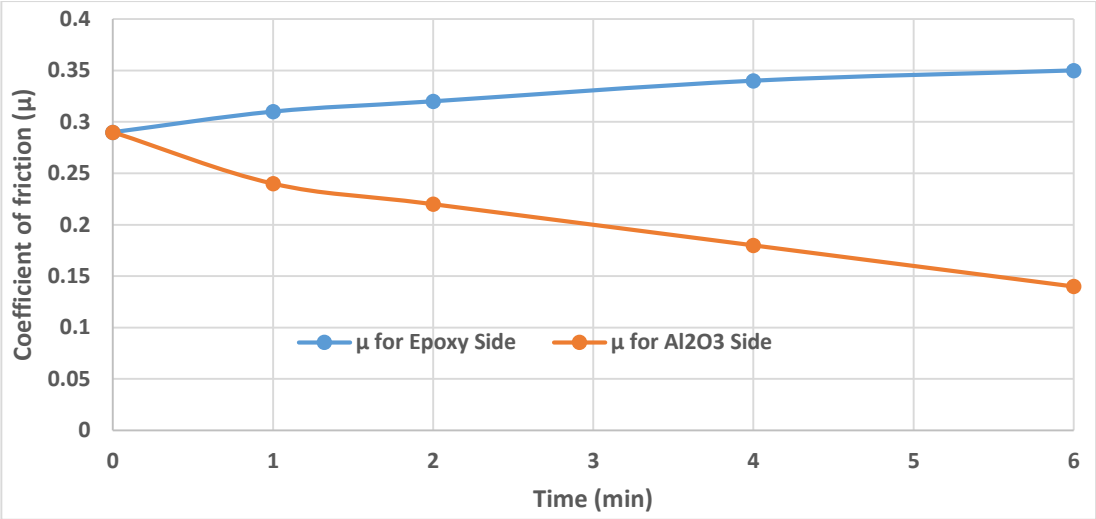

Figure (4.36): Variation of the friction coefficient with centrifugation time for FGM and neat epoxy with constant centrifugation speed of 1200 r.p.m

4.9 Dispersion and Morphology Analysis

The impact behaviour of epoxy nano-composite can be explained in terms of the morphology observed by SEM. The fracture surface morphologies and dispersions of alumina nanoparticles with different magnification are shown in Figures (4.37) to (4.40). The improvement of the impact behaviour of FGM can be explained by a close look at the fracture surfaces of the damaged specimens.

Figure (4.37) (A-D) shows a sample FGM with 0.5% V_f of nano - Al_2O_3 with rotational speed N=1200 r.p.m which centrifuged for 6 min and loaded from epoxy side. Generally, for all cases in Figures (4.36 to 4.39) (A), fractograph consist from three zone: the upper zone clearly shows the highly dense of alumina nano- particles in the sample where the particles heading towards the centrifugal force, the middle zone which represented transition region while the bottom part of this fractograph shows the epoxy resin with few alumina nano-particles are also observed. As rotational speed increases the alumina nano-particles are directed toward out surface of sample.

Figure (4.37) (B) shows a magnification of the upper zone, which presents a homogeneous appearance without any phase separation. However,

this phenomenon can be considered good compatibility between the alumina nano particles and the epoxy matrix. This morphology, in addition, presents a rough and coarse surface that has a large number of propagated cracks, crack deflection and shear deformation. Figure (4.37) (C-D) shows the transition region's magnification, which illustrates the nano-alumina distribution in the epoxy matrix. However, the dispersion of alumina nano particles of FGM samples was observed and showed that the diffusion was insufficient. Compared with other models, a non-uniform distribution and agglomerates at the content of this nano filler were regarded as the main reasons for the drop in properties.

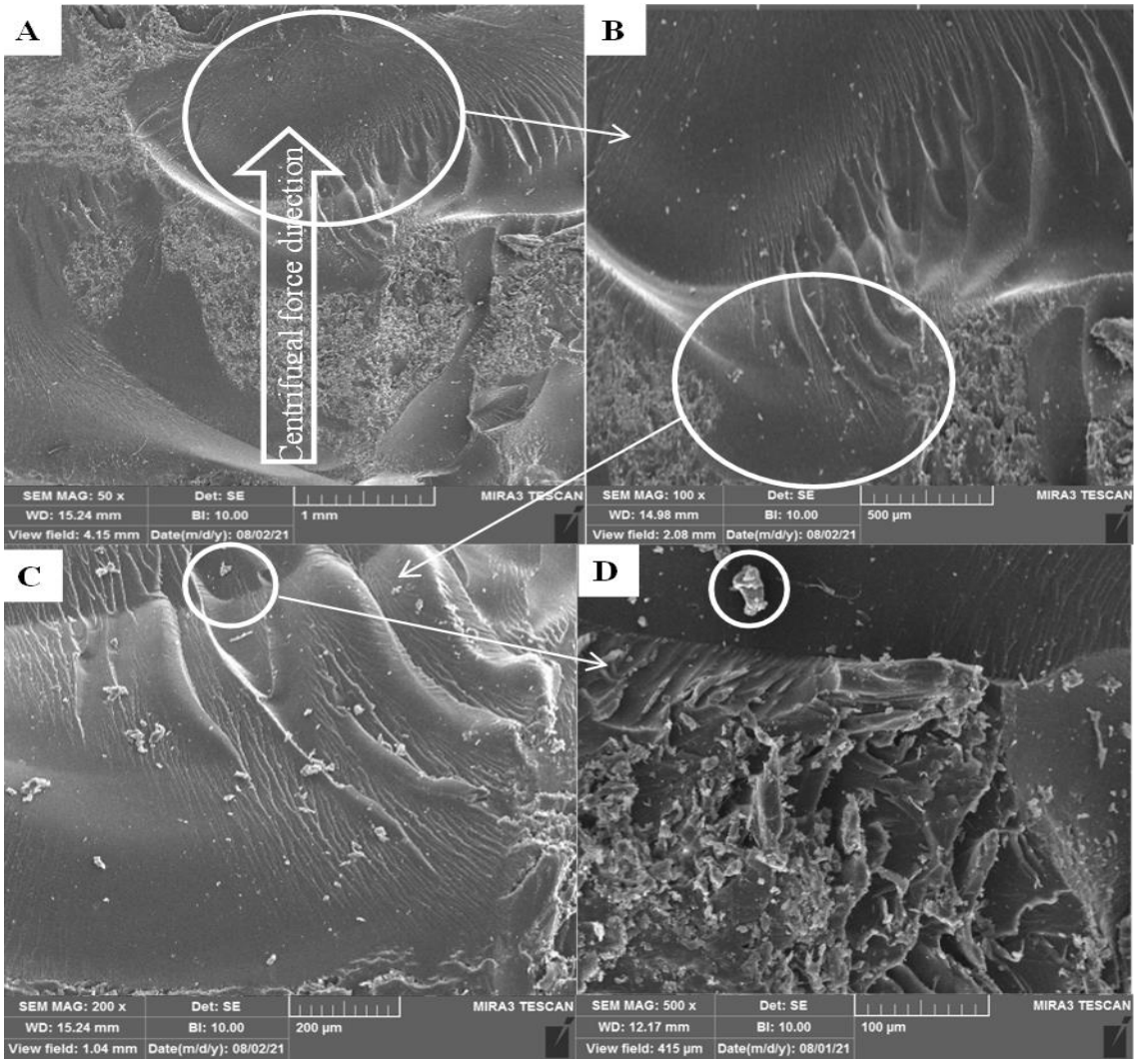

Figure (4.37): SEM images of the FGM impact fracture surface of 0.5% nano Al_2O_3 with rotational speed (N=1200 r.p.m) and time of rotation (t= 6 min.) with different magnifications.

The fracture surface of impact test for 2%V_f nano Al_2O_3 FGM with rotational speed N=1200 r.p.m and time of rotation (T= 6 min), which loaded from the epoxy side, was shown in Figure (4.38) (A-D). The graded sample was shown in Figure (4.38) (A) while Figure (4.38) (B) shows a magnification of the upper zone containing many reinforcing nano-particles; due to the increase in the rotational speed N=1200 r.p.m and the time of rotational (t=6min), the alumina nano-particles are trending to the outer surface of the FGM sample as shown in Figure (4.38) (B). On the other hand, from Figure (4.38) (A-B), the FGM sample shows a finer fracture surface. In this case, the failure initiates from the outer region of the sample, which is highly filled with Al_2O_3 nano-particles. The shear deformation can absorb fracture energy when cracks initiate and interrupt crack propagation.

The dispersion of nano-fillers into the matrix is significant, where the non-uniform dispersion and fabrication defect (void) shown in Figure (4.38) (C-D) result in an earlier failure of the matrix and prevent it from achieving the desired properties. The dispersion technique was ineffective for higher content of alumina nano-particles.

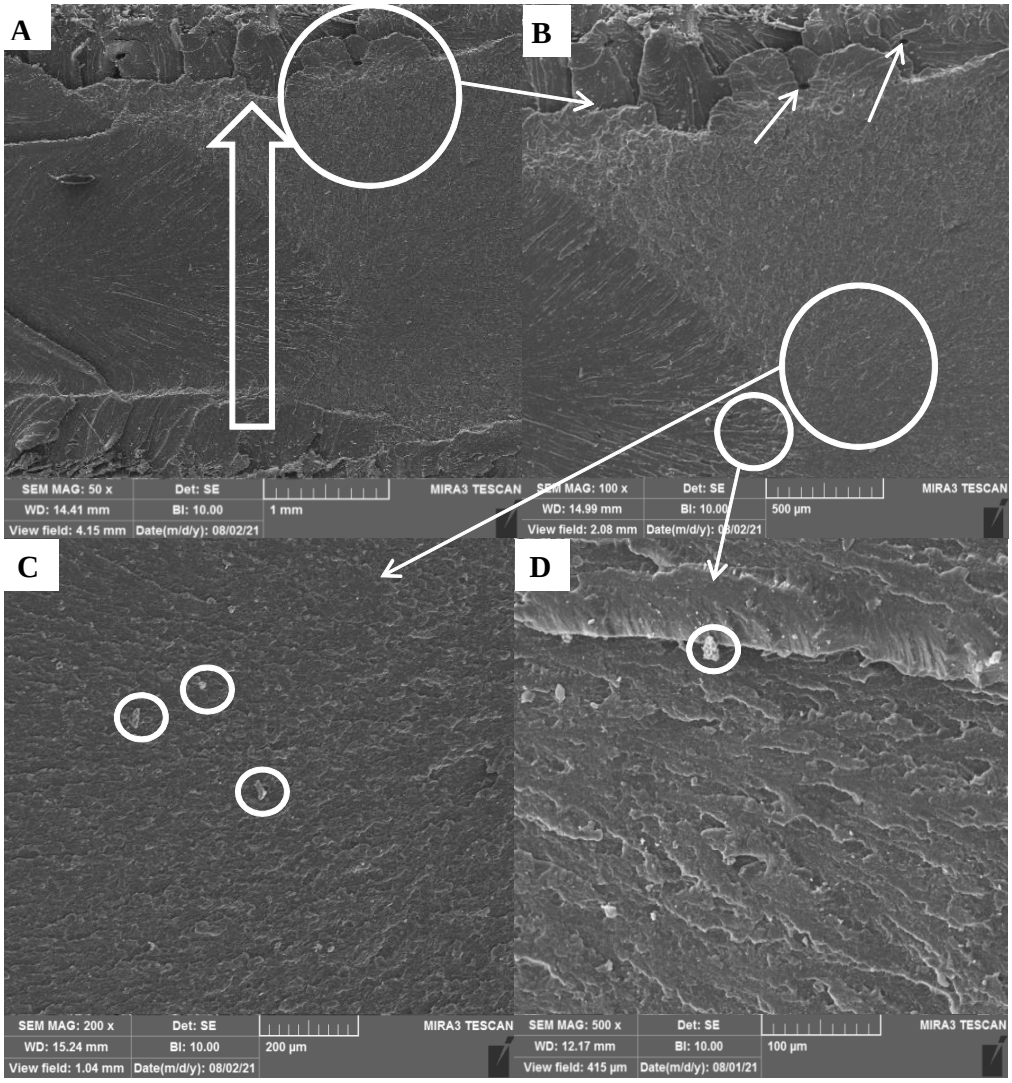

Figure (4.38): SEM images of the FGM impact fracture surface of 2% V_f of nano- Al_2O_3 with rotational speed N=1200 r.p.m and time t= 6 min with different magnifications

The micrograph of the fracture surface of FGM with 2%V_f of nano-Al_2O_3, rotational speed N=600 and time of rotation, t=6min is shown in the image of Figure (4.39) (A-D). The nano-Al_2O_3 distribution along the thickness of the FGM sample is illustrated in Figure (4.39) (A). Because of low rational speed N= 600 r.m.p, the alumina nano-particles don't reach the outer surface of the sample as shown in Figure (4.39) (A), where Figure (4.40) (B) represented magnification of upper zone.

Figure (4.39) (C-D) depicts a dispersion of Al_2O_3 nanoparticles in an epoxy matrix with low aggregation. Phase separation occurs, and nanoparticles of Al_2O_3 are dispersed in the epoxy matrix. The high impact

strength of the epoxy/Al_2O_3 nano-composite results from the dispersion of Al_2O_3 nanoparticles that act as crack stoppers. Al_2O_3 nanoparticles were used as a toughening agent, and nano-sized Al_2O_3 particles were dispersed in the epoxy matrix. As a result, a new morphology for the Al_2O_3 phase was achieved in the epoxy-rich matrix. Nanoparticles of Al_2O_3 with a higher aspect ratio and interface area between the epoxy and Al_2O_3 phases resulted in improved mechanical properties.

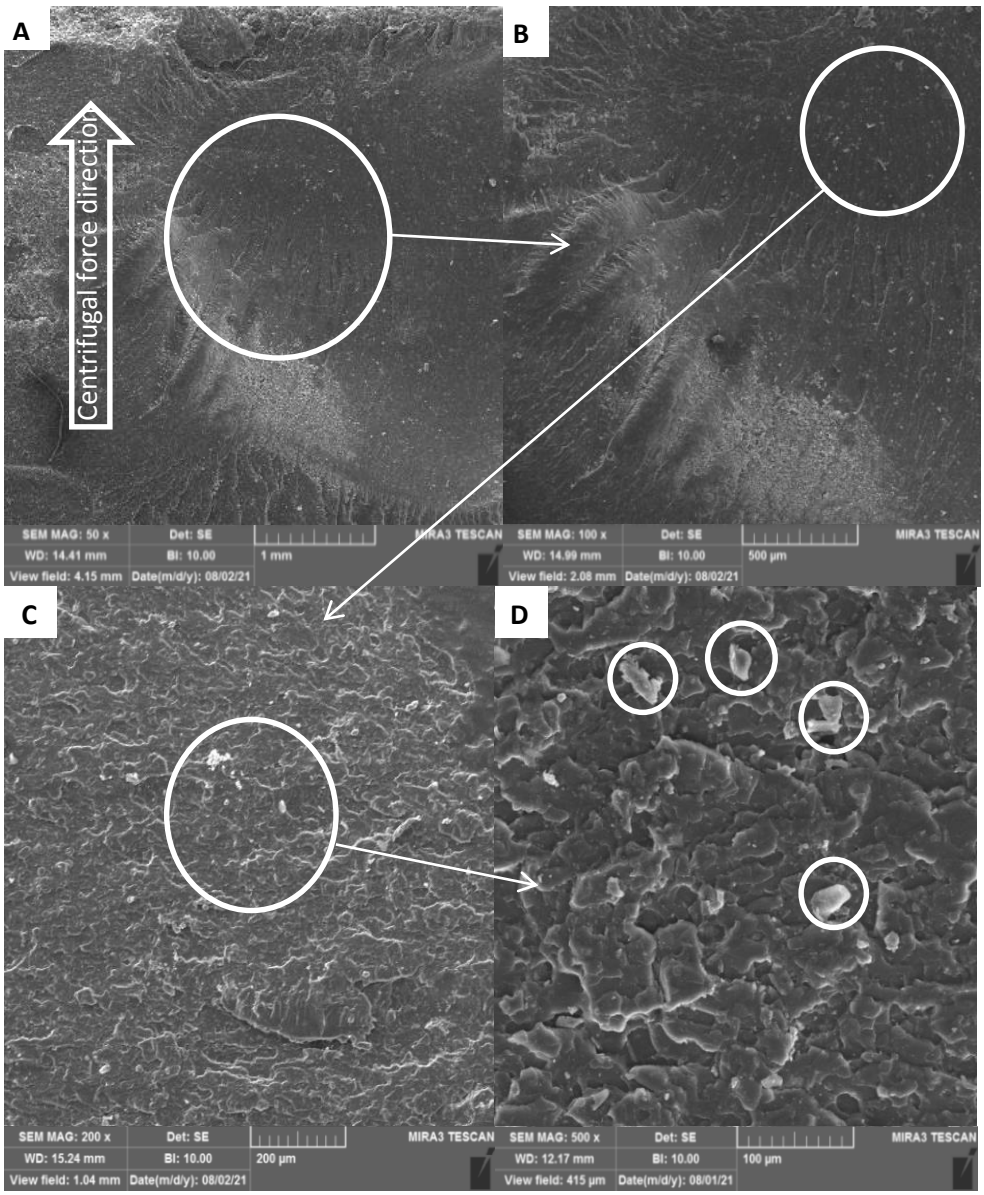

Figure (4.39): SEM images of the FGM impact fracture surface of 2% V_f Al_2O_3 with rotational speed N=600 r.p.m and time of rotation t= 6 min with different magnifications

Figure (4.40) (A-D) shows the fracture surface of an impact specimen for FGM at 2%V_f nano Al_2O_3 with rotational speed N=1200 and time of rotational T=1min loaded from the epoxy rich side. Figure (4.40) (A-B) does not show any noticeable gradient through thickness due to the short time of rotation, so the distribution of alumina nano-fillers in the matrix of epoxy was homogeneous.

Figure (4.40) (C-D) shows that good dispersion of Al_2O_3-nanofillers with little aggregation has occurred. Fascinatingly, finely dispersed and homogeneous particles provide a greater surface area and increased interfacial interaction. This homogeneous dispersion modifier can be used as crack stoppers and reinforcements to improve mechanical properties such as impact strength. Consistent with the SEM analysis of the epoxy/nano Al_2O_3 samples, a homogeneous mixture of alumina nano fillers in the matrix is demonstrated.

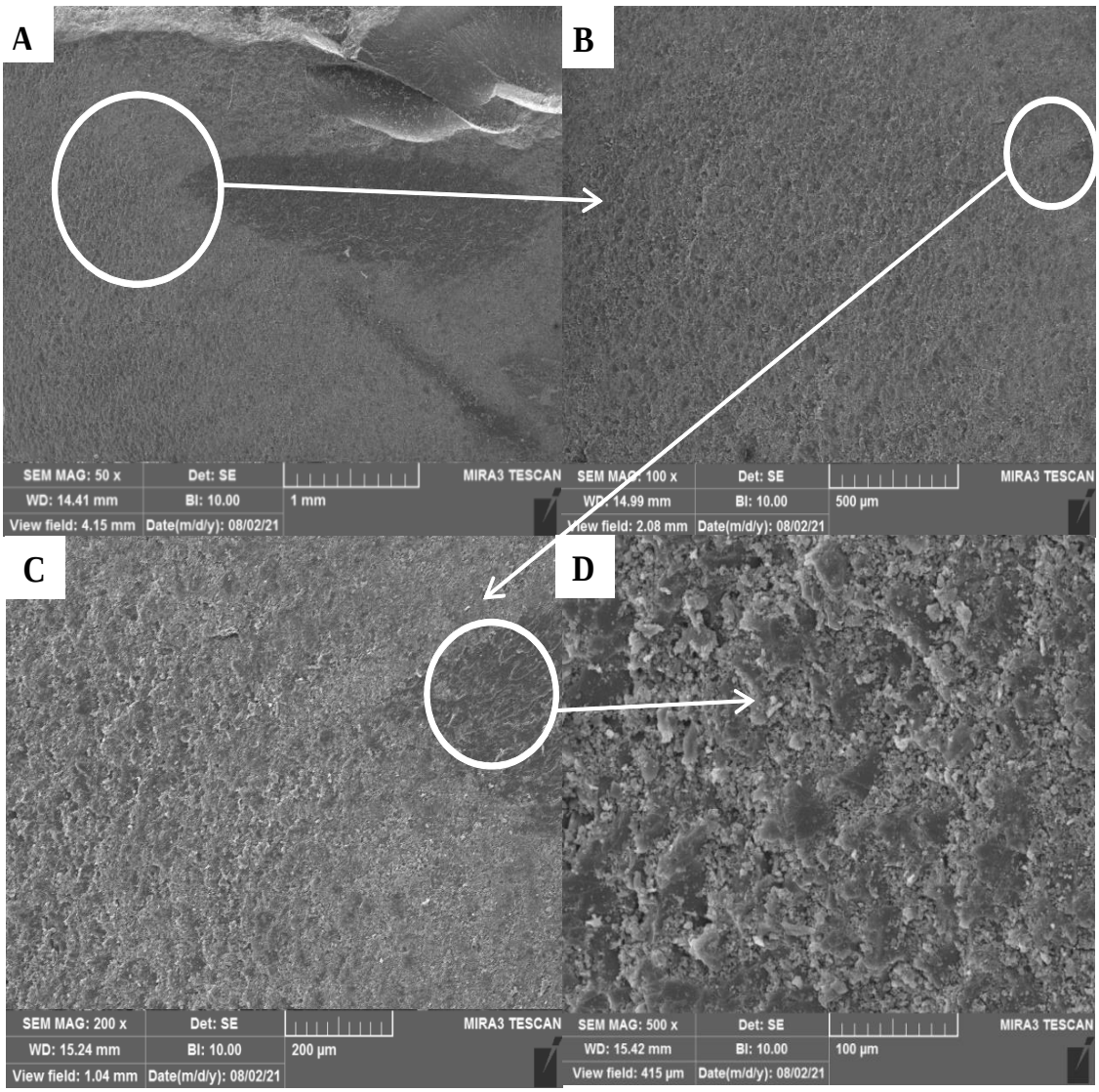

Figure (4.40): SEM images of the FGM impact fracture surface of 2%V_f of nano-Al_2O_3 with rotational speed N=1200 r.p.m and time of rotation (t= 1 min.) with different magnifications

CHAPTER FIVE
CONCLUSIONS AND RECOMMENDATIONS

5.1 Introduction

A synthesis procedure was followed for producing continuous graded and non-graded nanocomposites with two phases (Epoxy and Nano alumina) employing the centrifugal casting technique. A gradation was attained in the thickness direction of rectangular specimen based on varying the concentration of nanoparticles. Mechanical and wear tests were conducted to investigate the properties of the pure epoxy, graded, and non-graded nanocomposites reinforced by alumina nanoparticles.

The most important conclusions obtained from this study are mentioned in this chapter, and some recommendations are suggested, which may be useful for future research work.

5.2 Conclusions

Concerning the obtained results and their discussion, the subsequent conclusions can be mainly drawn from this study:

1. The mechanical and wear properties for all types of FGM and non FGM nanocomposite enhanced compared to those for the pure epoxy.
2. The non-graded nanocomposites' modulus of elasticity and flexural strength increased with increasing nanoparticles volume fraction; the Young's modulus maximum value was increased up to 2% V_f for alumina nanoparticles, but ultimate strength remained increasing.
3. The centrifugation rotational speed and centrifugation time significantly influence the mechanical and surface properties of FGMs.
4. The alumina nano particles reinforcement with continuous gradation shape can be an excellent attracting method for developing the mechanical behavior of FGM over those of the homogenous nanocomposite and neat epoxy. Mechanical properties are strongly

affected via the direction of an applied load of FGM. The results indicated that the samples loaded from the nano alumina side had higher flexural strength and impact strength than those loaded from the pure epoxy side. While the Young's modulus for samples loaded from the nano-alumina side was less than from the epoxy side for FGM.

5. The hardness varied in each layer of the fabricated FGM according to the content percentage of harder nanoparticles. The average of each FGM sample gave a good agreement with the non FGM.

   In addition the alumina nano particles enhance the hardness for non FGM and FGM in comparison to the pure epoxy, with a maximum increment in the hardness of around (16.8%) for the specimen (N = 1200 r.p.m, t = 6 min, and 2%V_f) FGM loaded from alumina rich side.
6. By examining the fracture surfaces of impact samples by SEM, it was shown that the alumina nanoparticles (at 1200 r.p.m) have fine dispersion into the epoxy matrix more than at (600 r.p.m) and the gradation of alumina nanoparticles through the thickness was evident in the epoxy matrix.
7. The hardness and wear analysis of FGM at various centrifugation speeds and various rotational times show better resistance than homogeneous nanocomposites.
8. The results indicated that the specific wear rate for samples loaded from the nano-alumina side was less than from the epoxy side for FGM. As well as the results show the increase in volume fraction of Al_2O_3 nano-particulates enhance the ware resistance reveals that 2 % V_f of non-FGM and FGMs nanocomposites which improve surface properties.
9. The gradation method led to a lower friction coefficient of around (51.7 %) for the FGM loaded from the alumina rich side (N = 1200 r.p.m, t = 6min and V_f = 2%) compared with the pure epoxy specimen.

5.3 Recommendations for Future Work

Depending on the investigation conducted in this thesis, the following recommendations for further studies can be proposed:

1. Study the mechanical fatigue behavior of FGMs used in this work at room and different temperatures (below and above the room temperature).
2. Study the factors affecting on friction and wear, creep, and creep-fatigue interaction properties of the FGMs used in this work.
3. Study the buckling and vibration behavior of the prepared FGMs in this thesis.
4. Preparing functionally graded polymer materials using other methods, like hand lay-up, 3D printer, etc.
5. Investigating the influence of varying the nanoparticles on the mechanical and wear behavior.

REFERENCES

1. Bharti, I., Gupta, N., and Gupta, K. M. (2013). Novel Applications of Functionally Graded Nano, Optoelectronic and Thermoelectric Materials. In International Journal of Materials, Mechanics and Manufacturing (pp. 221–224).
2. Mortensen, A., and Suresh, S. (1995). Functionally graded metals and metal-ceramic composites: Part 1 Processing. In International Materials Reviews (Vol. 40, Issue 6, pp. 239–265). https://doi.org/10.1179/imr.1995.40.6.239
3. Nabaa S. R. (2018). A Review for Functionally Gradient Materials Processes and Useful Application. Journal of the University of Babylon for Engineering Sciences (Vol. 26, Issue 9).
4. Sola, A., Bellucci, D., and Cannillo, V. (2016). Functionally graded materials for orthopedic applications – an update on design and manufacturing. In Biotechnology Advances (Vol. 34, Issue 5, pp. 504–531). Elsevier B.V.
5. Sai B.V., H. (2018). A Review on Functionally Gradient Materials (FGMs) and Their Applications. In International Journal of Current Engineering and Technology (Vol. 8, Issue 01). https://doi.org/10.14741/ijcet.v8i01.10894.
6. Srividhya, S., Basant, K., Gupta, R. K., Rajagopal, A., and Reddy, J. N. (2018). Influence of the homogenization scheme on the bending response of functionally graded plates. In Acta Mechanica (Vol. 229, Issue 10, pp. 4071–4089). Springer Science and Business Media LLC. https://doi.org/10.1007/s00707-018-2223-2
7. Naeem, M. N., Kanwal, S., Shah, A. G., Arshad, S. H., and Mahmood, T. (2012). Vibration Characteristics of Ring-Stiffened Functionally Graded Circular Cylindrical Shells. In ISRN Mechanical Engineering (Vol. 2012, pp. 1–13). Hindawi Limited.

8. Megahed, A. A., and Megahed, M. (2017). Fabrication and characterization of functionally graded nanoclay/glass fiber/epoxy hybrid nanocomposite laminates. In Iranian Polymer Journal (Vol. 26, Issue 9, pp. 673–680). Springer Science and Business Media LLC. https://doi.org/10.1007/s13726-017-0552-
9. Vijay, K. B., and Dharminder S. (2013). Research work on composite epoxy matrix and Ep polyester reinforced material. International Journal of Engineering Research and Technology (IJERT) (Vol. 2, Issue 1).
10. Miyamoto Y, Kaysser, Rabin BH, Kawasaki A, and Ford RG. Functionally Graded Materials Design, Processing and Applications. Kluwer Academic Publishers; 1999.
11. El-Galy, I. M., Ahmed, M. H., and Bassiouny, B. I. (2017). Characterization of functionally graded Al-SiC p metal matrix composites manufactured by centrifugal casting. In Alexandria Engineering Journal (Vol. 56, Issue 4, pp. 371–381). https://doi.org/10.1016/j.aej.2017.03.009
12. Gangwar, T., and Schillinger, D. (2019). Microimaging-informed continuum micromechanics accurately predicts macroscopic stiffness and strength properties of hierarchical plant culm materials. In Mechanics of Materials (Vol. 130, pp. 39–57). Elsevier B.V. https://doi.org/10.1016/j.mechmat.2019.01.009
13. Birman, V. (2014). Functionally Graded Materials and Structures. In Encyclopedia of Thermal Stresses (pp. 1858–1865). Springer Netherlands. https://doi.org/10.1007/978-94-007-2739-7_573
14. Ichikawa, K. (Ed.). (2001). Functionally Graded Materials in the 21st Century. Springer US. https://doi.org/10.1007/978-1-4615-4373-2
15. Saleh, B., Jiang, J., Fathi, R., Al-hababi, T., Xu, Q., Wang, L., Song, D., and Ma, A. (2020). 30 Years of functionally graded materials: An overview of manufacturing methods, Applications and Future

Challenges. In Composites Part B: Engineering (Vol. 201, p. 108376). https://doi.org/10.1016/j.compositesb.2020.108376

16. Siddesh Kumar, N. M., Shashank, T. N., Khan, N., Mahendra Babu, K. J., and Ajit Prasad, S. L. (2021). Modal and Harmonic Analysis of Spur Gear using FEA. In Journal of Failure Analysis and Prevention (Vol. 21, Issue 5, pp. 1855–1865). Springer Science and Business Media LLC. https://doi.org/10.1007/s11668-021-01243-2
17. Singh, A. K., and Siddhartha. (2017). A novel technique for in-situ manufacturing of functionally graded materials based polymer composite spur gears. In Polymer Composites (Vol. 40, Issue 2, pp. 523–535). Wiley. https://doi.org/10.1002/pc.24682
18. Ebhota, W. S., Karun, A. S., and Inambao, F. L. (2016). Centrifugal casting technique baseline knowledge, applications, and processing parameters: overview. In International Journal of Materials Research (Vol. 107, Issue 10, pp. 960–969). Walter de Gruyter GmbH. https://doi.org/10.3139/146.111423
19. K.M. Gupta," Engineering Materials", Research, Applications and Advances, © Taylor and Francis Group, LLC, 2015.
20. R.V. Kurahatti, A. O. Surendranathan, A.V. Ramesh Kumar, V. Auradi ،C. S. Wadageri and S. A. Kori," Mechanical and Tribological Behaviour of Epoxy Reinforced with Nano-Al_2O_3 particles", Applied Mechanics and Materials Vols 592-594, pp 1320-1324 Trans Tech Publications,doi:10.4028/www.scientific.net/AMM.592-594.1320 ©2014.
21. C.S Gill and J.S Sidhu,"Dry Sliding Wear Behavior of Epoxy Based Composites Filled with WS2 and B4C ", International Journal of Material Sciences and Technology. ISSN 2249-3077 Volume 6, Number 1, pp. 21-32, © 2016
22. V Siddhartha1, A Patnaik1., and A D Bhatt," Friction and wear analysis of a cement kiln dust reinforced epoxy-based functionally

graded materials", Proc. IMechE Vol. 224 Part J: J. Engineering Tribology, DOI: 10.1243/13506501JET798, 2010.

23. Akhil S. Karun, "Fabrication and Characterization of Functionally Graded Metal and Polymer Composites by Sequential and Centrifugal Casting Techniques", PhD. thesis, the Cochin University of Science and Technology (CUSAT), 2017.
24. Rasheedat Modupe Mahamood Esther Titilayo Akinlabi, "Functionally Graded Materials", Metallurgy and Materials Engineering, ISBN 978-3-319-53756-6 (eBook), DOI 10.1007/978-3-319-53756-6 © Springer International Publishing AG 2017.
25. Noor Bayan Muslim Saad," Functionally Graded Polymer Composite for Automotive Application", MSc thesis, Babylon University, 2018.
26. Hon, D., Shiraishi, W., "Cellulose Chemistry", 2nd ed. Marcel Dekker, New York (2001).
27. Wang, S.S. "Fracture mechanics for delamination problems in composite materials". J. Compos. Mater. 17(3), 210–223 (1983).
28. Mahamood, R. M., and Akinlabi, E. T. (2017). Types of Functionally Graded Materials and Their Areas of Application. In Functionally Graded Materials (pp. 9–21). Springer International Publishing. https://doi.org/10.1007/978-3-319-53756-6_2
29. Shanmugavel, P., Bhaskar, GB, Chandrasekaran, M., Mani P.S., Srinivasan, S.P." An overview of fracture analysis in functionally graded materials", Eur. J. Sci. Res. 68(3), 412–439, (2012).
30. Mahamood, R.M., Akinlabi, E.T., Shukla M., Pityana, S. "Functionally graded material: an overview". In: Proceedings of the World Congress on Engineering WCE 2012, vol. 3, pp. 1593–1597 (2012).
31. Jha, D.K., Kant, T., Singh, R.K.: "A critical review of recent research on functionally graded plates". Compos. Struct. 96, 833–849, 2013.

32. Mia, X., Sun, D.," Graded/gradient porous biomaterials", Materials 3, 26–47. doi:10. 3390/ma3010026, 2010.
33. G.E. Knoppers, J.W. Gunnink, J. Van Den Hout, and W. P. V. Vliet, "The Rreality of Functionally Graded Material Products", presented at the International Solid Freeform Fabrication Symposium, University of Texas at Austin, Texas, 2004.
34. Patricia Popoola, Gabriel Farotade, Olawale Fatoba and Olawale Popoola, " Laser Engineering Net Shaping Method in the Area of Development of Functionally Graded Materials (FGMs) for Aero Engine Applications - A Review", © Licensee InTech, 2016.
35. J. Saifulnizan, "Application of Functionally Graded Materials for Severe Plastic Deformation and Smart Materials: Experimental Study and Finite Element Analysis," PhD thesis, Department of Engineering Physics, Electronics and Mechanics, Graduate School of Engineering, Nagoya Institute of Technology, 2012.
36. Zhang, N., Khan, T., Guo, H., Shi, S., Zhong, W., and Zhang, W. (2019). Functionally Graded Materials: An Overview of Stability, Buckling, and Free Vibration Analysis. In Advances in Materials Science and Engineering (Vol. 2019, pp. 1–18).
37. Panjan, P., Drnovšek, A., Gselman, P., Čekada, M., and Panjan, M. (2020). Review of Growth Defects in Thin Films Prepared by PVD Techniques. In Coatings (Vol. 10, Issue 5, p. 447).
38. Jayakumar E.," Processing and Characterization of Functionally Graded Metal and Polymer Composites", Ph.D. Thesis, Cochin University of Science and Technology (CUSAT), 2016.
39. J. Sobczak, J., and B. Drenchev, L. (Eds.). (2012). Metal Based Functionally Graded Materials. BENTHAM SCIENCE PUBLISHERS. https://doi.org/10.2174/97816080503831090101
40. P L Jain," Principles of Foundry Technology", Fifth Edition, Copyright © by Tata McGraw-Hill Education Private Limited, 2009.

41. Williams S. Ebhota, Akhil S. Karun, and Inambao, F. L. (2016). "Principles and Baseline Knowledge of Functionally Graded Aluminium Matrix Materials (FGAMMs)", Fabrication Techniques and Applications. In International Journal of Engineering Research in Africa (Vol. 26, pp. 47-67). Trans Tech Publications.
42. Krishnan, B. P., and Rohatgi, P. K. "Modification of Al–Si alloy melts containing graphite particle dispersions". Metals Technology, 11(1), 41-44.2013.
43. Mikell P. Groover,"Fundamentals Of Modern Manufacturing", Materials, Processes, and Systems Fourth Edition, Copyright © John Wiley and Sons, Inc2010.
44. Beeley, P. R. "Foundry Technology", Newnes-Butterworths، London, 1972.
45. Vukota Boljanovic, "Metal-shaping Processes", Casting and Molding; Particulate Processing; Deformation Processes; and Metal Removal, Copyright © by Industrial Press Inc., New York. Printed in the United States of America. 2010.
46. Edward Petrie, "Epoxy Adhesive Formulations," 1st Edition, McGraw Hill Professional, 2005.
47. Cavezza, F., Boehm, M., Terryn, H., and Hauffman, T. (2020). A Review on Adhesively Bonded Aluminium Joints in the Automotive Industry. In Metals (Vol. 10, Issue 6, p. 730). MDPI AG. https://doi.org/10.3390/met10060730
48. James G. Bralla," Handbook of Manufacturing Processes", Copyright© by Industrial Press Inc., New York, 2007.
49. Kannabiran Vasudevan, and Dinesh Kumar (2016). Mechanical and fatigue characterization of carbon fiber reinforced containing rubber micro particles and silica nanoparticles (Unpublished thesis). Texas State University, San Marcos, Texas.

50. Kannan, P., and Sudhakara, P. (2011). Liquid Crystalline Thermoset Epoxy Resins. High Performance Polymers and Engineering Plastics (pp. 387–422). https://doi.org/10.1002/9781118171950.ch11

51. Panda, H. (2019). Epoxy Resins Technology Handbook (Manufacturing Process, Synthesis, Epoxy Resin Adhesives and Epoxy Coatings. 2nd Revised Edition, Publisher: Asia Pacific Business Press Inc.

52. Ashcroftm W. R. (1993). Curing agents for epoxy resins. Chapter 2, Springer Science and Business Media LLC.

53. Parameswaranpillai, J., Hameed, N., Kurian, T., and Yu, Y. (Eds.). (2016). Nanocomposite Materials. CRC Press.

54. Jeevanandam, J., Barhoum, A., Chan, Y. S., Dufresne, A., and Danquah, M. K. (2018). Review on nanoparticles and nanostructured materials: history, sources, toxicity and regulations. Beilstein Journal of Nanotechnology (Vol. 9, pp. 1050–1074).

55. Vollath, D. (2013). Nanomaterials: An introduction to synthesis, properties and applications. Wiley-VCH Verlag GmbH and Co. KGaA, Boschstr. 12, 69469 Weinheim, Germany.

56. Arvind Kumar Thakur (2016). Elastic and thermal analysis of clay/polymer nanocomposite material. MSc thesis, Department of Mechanical Engineering National Institute of Technology Rourkela.

57. Siddhartha, Patnaik, A., and Bhatt, A. D. (2011). Mechanical and dry sliding wear characterization of epoxy–TiO_2 particulate filled functionally graded composites materials using Taguchi design of experiment. In Materials and Design (Vol. 32, Issue 2, pp. 615–627). https://doi.org/10.1016/j.matdes.2010.08.011.

58. Ghulam, N. A., Abbas, M. N., and Sachit, D. E. (2019). Preparation of synthetic alumina from aluminium foils waste and investigation of its performance in the removal of RG-19 dye from its aqueous

solution. Indian Chemical Engineer (Vol. 62, Issue 3, pp. 301–313). https://doi.org/10.1080/00194506.2019.1677512

59. Khodadadi Darban, A., Kianinia, Y., and Taheri-Nassaj, E. (2013). Synthesis of nano- alumina powder from impure kaolin and its application for arsenite removal from aqueous solutions. In Journal of Environmental Health Science and Engineering (Vol. 11, Issue 1). Springer Science and Business Media LLC. https://doi.org/10.1186/2052-336x-11-19

60. Saud, A. N., Majdi, H. Sh., and Saud, S. N. (2019). Synthesis of nano-alumina powder via recrystallization of ammonium alum. In Cerâmica (Vol. 65, Issue 374, pp. 236–239). FapUNIFESP (SciELO). https://doi.org/10.1590/0366-69132019653742636

61. Brinson, H. F., and Brinson, L. C. (2015). Polymer Engineering Science and Viscoelasticity. Springer US. https://doi.org/10.1007/978-1-4899-7485-3.

62. William D. Callister, Jr. and David G. Rethwisch (2008). Fundamentals of Materials Science and Engineering: An Integrated Approach. Third edition, Copyright, John Wiley and Sons, Inc. All rights reserved.

63. Donald R. Askeland and Pradeep P. Fulay (2010). Essentials of Materials Science and Engineering. Second Edition, Cengage Learning.

64. Hart, Nicolas and Nimphius, Sophia and Rantalainen, Timo and Ireland, Alex and Siafarikas, Aris and Newton, Robert. (2017). Mechanical Basis of Bone Strength: Influence of bone material, bone structure and muscle action. J Musculoskelet Neuronal Interact 2017; 17(3):114-139

65. Debdatta Ratna (2009). Handbook of Thermoset Resins. Smithers Rapra Technology.

66. Domagała, I., Przystupa, K., Firlej, M., Pieniak, D., Gil, L., Borucka, A., Naworol, I., Biedziak, B., and Levkiv, M. (2021). Analysis of the Statistical Comparability of the Hardness and Wear of Polymeric Materials for Orthodontic Applications. In Materials (Vol. 14, Issue 11, p. 2925). MDPI AG. https://doi.org/10.3390/ma14112925

67. Sudharshan Phani, P., and Oliver, W. C. (2019). A critical assessment of the effect of indentation spacing on the measurement of hardness and modulus using instrumented indentation testing. In Materials and Design (Vol. 164, p. 107563). Elsevier BV.

68. Grum, J. (2006). Book Review: Handbook of Polymer Testing Short-Term Mechanical Tests. International Journal of Materials and Product Technology (Vol. 27, Issue 3/4, p. 293).

69. Kenneth Holmberg,Allan Matthews," Coatings Tribology: Properties, Mechanisms, Techniques and Applications in Surface Engineering", Copyright © Elsevier BV, 2009.

70. Raymond G. Bayer," Mechanical Wear Fundamentals and Testing", Copyright by Marcel Dekker, Inc. All Rights Reserved, 2004.

71. J.R. Davis," Surface Engineering for Corrosion and Wear Resistance", Copyright © by ASM International, 2001.

72. J. Zhang, P. P. L. Regtien, "Illumination methods for optical wear detection", Measurement Science Review, Vol. 7, Section 3, No. 3, 2007.

73. Ola A. Kadhum Al-Shammary," Enhancing the Tribological and Mechanical Properties of Polyphenylene Sulfide Reinforced with TiO_2 nanoparticles", MSc thesis, University of Babylon, 2013.

74. A.I. Sviridenok, A.F. Klimovich, and V.N Kestelman," Electrophysical Phenomena in The Tribology of Polymers", Copyright © OPA (Overseas Publishers Association) NV Published by license under the Gordon and Breach Science Publishers imprint.

75. Sabah Khan," Analysis of Tribological Applications of Functionally

Graded Materials in Mobility Engineering" International Journal of Scientific and Engineering Research, Volume 6, Issue 3, March-2015 1150.

76. E. Richard Booser," Tribology Data Handbook", Copyright © CRC Press, LLC, 1997.
77. Halling. J.," Introduction to Tribology", First Published by Wykeham Publications (London) Ltd, 1976.
78. Jamal Takadoum " Materials and Surface Engineering in Tribology", First published in Great Britain and the United States by ISTE Ltd and John Wiley and Sons, Inc,2008.
79. Ming Qiu, Long Chen, Yingchun Li Jiafei Yan, "Bearing Tribology Principles and Applications", © National Defense Industry Press, Beijing and Springer-Verlag Berlin Heidelberg 2017.
80. Robert J. K. Wood," Multifunctional Materials for Tribological Applications", © by Taylor and Francis Group, LLC, 2015.
81. Carlos P. Bergmann and Juliane Vicenzi," Protection against Erosive Wear Using Thermal Sprayed Cermet", © Springer-Verlag Berlin Heidelberg, 2011.
82. George E. Totten, "Handbook of Hydraulic Fluid Technology", Second Edition, Taylor and Frank's group, 2012.
83. R. Chattopadhyay," Surface Wear Analysis, Treatment, and Prevention", Copyright © by ASM International®2001.
84. Kenneth G. Budinski," Friction, Wear, And Erosion Atlas", © by Taylor and Francis, Group, LLC, 2014.
85. Bharat Bhushan, " MODERN TRIBOLOGY HANDBOOK," Volume One Principles of Tribology The MECHANICS and MATERIALS SCIENCE Series Series Editor, 2001
86. Macro-Wear Theory. (2017). In Principles of Tribology (pp. 314–336). John Wiley and Sons Singapore Pte. Ltd. https://doi.org/10.1002/9781119214908.ch13

87. Ahmed Abdelbary, "Wear of Polymers and Composites", Elsevier, 2014.

88. Downl Anderson, J.C. "Wear of commercially available plastic materials", Tribology International, 198210

89. Ian Hutchings, Philip Shipway," Tribology", Friction and Wear of Engineering Materials, Second Edition ©Published by Elsevier Ltd. All rights reserved, 2017.

90. Klaus Friedrich," Friction and Wear of Polymer Composites", ©elsevier science BV 1996. Pdf 338

91. James C. Gerdeen, Ronald A. L. Rorrer, "Engineering Design with Polymers and Composites" Second Edition, © by Taylor and Francis Group, LLC, 2012.

92. Hussein, Seenaa and Ali, Nadia. (2015). Effect of Al_2O_3 and SiO_2 Nanopartical on Wear, Hardness and Impact behavior of Epoxy composites. Chemistry and Materials Research (Vol.7, Issue 4).

93. Malia M. Farhan and Baraa C. maizh. (2016). Some Mechanical Properties of Epoxy Composites and Epoxy Polysulfide Blend Composites Reinforced with Nano Alumina Particles. International Journal of Advance Research, IJOAR .org (Vol. 4, Issue 6).

94. Yousri, O. M., Abdellatif, M. H., and Bassioni, G. (2017). Effect of Al_2O_3 Nanoparticles on the Mechanical and Physical Properties of Epoxy Composite. In Arabian Journal for Science and Engineering (Vol. 43, Issue 3, pp. 1511–1517). Springer Science and Business Media LLC. https://doi.org/10.1007/s13369-017-2955-7

95. Mishra, S. K., Kumar Shukla, D., and Kumar Patel, R. (2018). Flexural Properties of Functionally Graded Epoxy-Alumina Polymer Nanocomposite. In Materials Today: Proceedings (Vol. 5, Issue 2, pp. 8431–8435). https://doi.org/10.1016/j.matpr.2017.11.538

96. Bazrgari, D., Moztarzadeh, F., Sabbagh-Alvani, A. A., Rasoulianboroujeni, M., Tahriri, M., and Tayebi, L. (2018).

Mechanical properties and tribological performance of epoxy/Al_2O_3 nanocomposite. Ceramics International (Vol. 44, Issue 1, pp. 1220–1224). https://doi.org/10.1016/j.ceramint.2017.10.068

97. Raju B.R, Shreyas Shenoy, Somanna K K, Supreeth Shetty, and Vasuki K (2018). Investigation on Mechanical and Tribological Characterization of Nano Particulate Filled Fiber Reinforced Hybrid Composites for Automobile Applications. International Journal of Creative Research Thoughts (Volume 6, Issue 2).
98. Mishra, S. K., Shukla, D. K., and Patel, R. K. (2020). Effect of particle morphology on flexural properties of functionally graded epoxy-alumina polymer nanocomposite. Materials Research Express (Vol. 6, Issue 12). https://doi.org/10.1088/2053-1591/ab70e2
99. Fouly, A., and Alkalla, M. G. (2020). Effect of low nanosized alumina loading fraction on the physicomechanical and tribological behavior of epoxy. In Tribology International (Vol. 152, p. 106550). https://doi.org/10.1016/j.triboint.2020.10655
100. Shareef, M., Al-Khazraji, A., and Amin, S. (2021). Flexural Properties of Functionally Graded Polymer Alumina Nanoparticles. In Engineering and Technology Journal (Vol. 39, Issue 5A, pp. 821–835). University of Technology. https://doi.org/10.30684/etj.v39i5a.1949
101. Siddhartha, Singh, A. K., and Yadav, S. (2015). Exploring the Possibility of Utilization of Red Mud Epoxy Based Functionally Graded Materials as Wear-Resistant Materials Using Taguchi Design of Experiment. In Advances in Polymer Technology (Vol. 36, Issue 1, pp. 5–22). Wiley. https://doi.org/10.1002/adv.21567
102. Singh, A. K., Siddhartha, and Hussain, S. (2015). Wear Peculiarity of TiO_2 Filled Polyester-Based Homogeneous Composites and their Functionally Graded Materials Using Taguchi Methodology and

ANN. In Materials Today: Proceedings (Vol. 2, Issues 4–5, pp. 2718–2727). Elsevier BV. https://doi.org/10.1016/j.matpr.2015.07.239

103. Singh, A. K., Siddhartha, Yadav, S., and Singh, P. K. (2016). Repercussion of manufacturing techniques on mechanical and wear peculiarity of ZnO particulate-filled polyester composites. In Polymer Composites (Vol. 39, Issue 3, pp. 654–667). Wiley. https://doi.org/10.1002/pc.23982
104. Stabik, J., and Chomiak, M. (2016). Graded epoxy-hard coal composites: Analysis of filler particle distribution in the epoxy matrix. In Journal of Composite Materials (Vol. 50, Issue 26, pp. 3663–3677). SAGE Publications. https://doi.org/10.1177/0021998315623626
105. Singh, A. K., and Vashishtha, S. (2016). Mechanical and Tribological Peculiarity of Nano-TiO_2 -Augmented, Polyester-Based Homogeneous Nanocomposites and Their Functionally Graded Materials. In Advances in Polymer Technology (Vol. 37, Issue 3, pp. 679–696). Wiley. https://doi.org/10.1002/adv.21710
106. Prasad, L., Singh, G., and Pokhriyal, M. (2018). A Comparative Study on Physical and Mechanical Behaviour of Functionally Graded Composite Materials reinforced with Natural Fillers. In Materials Today: Proceedings (Vol. 5, Issue 9, pp. 16990–16994). Elsevier BV. https://doi.org/10.1016/j.matpr.2018.04.103
107. Singh, A. K., and Siddhartha. (2018). Noise Emission Form Functionally Graded Materials based Polypropylene Spur Gears - A Tribological Investigation. In Materials Today: Proceedings (Vol. 5, Issue 2, pp. 8199–8205). Elsevier BV. https://doi.org/10.1016/j.matpr.2017.11.509
108. Gangil, B., Kukshal, V., Sharma, A., Patnaik, A., and Kumar, S. (2019). Development of hybrid fiber reinforced functionally graded polymer composites for mechanical and wear analysis. In AIP

Conference Proceedings. PROCEEDINGS OF THE 3RD INTERNATIONAL CONFERENCE ON AUTOMOTIVE INNOVATION GREEN ENERGY VEHICLE: AIGEV 2018. Author(s). https://doi.org/10.1063/1.5085630

109. Prasad, L., Singh, G., Yadav, A., Kumar, V., and Kumar, A. (2019). Properties of functionally gradient composites reinforced with waste natural fillers. In Acta Periodica Technologica (Issue 50, pp. 250–259). National Library of Serbia. https://doi.org/10.2298/apt1950250p
110. Farahnakian, M., Elhami Joosheghan, S., and Moradi, M. (2020). Dual filler functionally graded polymermaterials – manufacturing process and characteristics. In Materials and Manufacturing Processes (Vol. 36, Issue 3, pp. 301–307). Informa UK Limited. https://doi.org/10.1080/10426914.2020.1832690
111. Abdelaziz, M. A. (2012). Synthesis of nanocomposites with nano-TiO_2 particles and their applications as dental materials. MSc thesis, Cape Peninsula University of Technology, Cape Town, South Africa.
112. Le Pevelen, D. D. (2010). Small Molecule X-Ray Crystallography, Theory and Workflow. In Encyclopedia of Spectroscopy and Spectrometry (pp. 2559–2576). Elsevier. https://doi.org/10.1016/b978-0-12-374413-5.00359-6
113. Lian, Q., Yang, C., and Cao, J. Experimental Study on the Transition between Static and Kinetic Frictions of Steel/Shale Pairs. In P. Wang (Ed.), Shock and Vibration, 2021, 2021, 1–12. https://doi.org/10.1155/2021/2764803
114. Naguib, H. M., Ahmed, M. A., and Abo-Shanab, Z. L. (2018). Silane coupling agent for enhanced epoxy-iron oxide nanocomposite. Journal of Materials Research and Technology (Vol. 7, Issue 1, pp. 21–28). https://doi.org/10.1016/j.jmrt.2017.03.002

115. Mahmood, I. Study the mechanical properties of epoxy resin reinforced with silica (quartz) and alumina particles, The Iraqi Journal for Mechanical and Material Engineering, 2011, 11, 486-506.
116. Albooyeh A, Bayat M, Rafieian P, Dadrasi A, Khatibi MM. (2020) Silica aerogel/epoxy nanocomposites: Mechanical, vibrational, and morphological properties. J Appl Polym Sci; 137(43): 49338. http://dx.doi.org/10.1002/app.49338
117. Karthikeyan P, Babu B, Siva K, Chellamuthu, S. Experimental investigation on mechanical behavior of carbon nanotubes -alumina hybrid epoxy nanocomposites. Digest Journal of Nanomaterials and Biostructures 2016; 11(2): 625 – 632.
118. Singh S, Srivastava VK, Prakash R. (2014). Influences of carbon nanofillers on mechanical performance of epoxy resin polymer. Appl Nanosci; 5(3): 305–13. http://dx.doi.org/10.1007/s13204-014-0319-0
119. Ali A, Zainab R. (2019) Hardness and Impact Strength of Functionally Graded Nanocomposites. Indian Journal of Natural Sciences; 9(52): 16683-16688.
120. B. Gangil, A. Patnaik, A. Kumar and M. Kumar, (2012). Investigations on mechanical and sliding wear behaviour of short fibre-reinforced vinylester-based homogenous and their functionally graded composites. Proceedings of the Institution of Mechanical Engineers, Part L: Journal of Materials: Design and Applications 226, 300–315. doi: 10.1177/1464420712450956

الخلاصة:

لتجنب مشاكل الطور البيني مثل تركيز الاجهادات وضعف الالتصاق بين التقوية والارضية وغيرها من الانعكاسات غير المرغوبة التي تسببها المادة المركبة لذلك تم استخدام المادة المتدرجة وظيفيا وهي مادة مركبة متقدمة تمتلك خصائص متغيرة باستمرار خلال الموقع.

تتألف هذه الدراسة من ثلاثة أجزاء. الجزء الأول يتضمن تصنيع جهاز طرد مركزي بطريقة جديدة تختلف عن اجهزة الطرد المركزي الموجودة في الابحاث السابقة من حيث شكل العينة واتجاه التدرج باستخدام قوالب اكريليك ذات اشكال ومقاسات مختلفة حسب الاختبار المطلوب للمادة. يتضمن الجزء الثاني تصنيع عينات متدرجة وظيفيا باستخدام جهاز الطرد المركزي المصنع وعند ظروف مختلفة. حيث تم دراسة تأثير ثلاثة عوامل في عملية السباكة بالطرد المركزي: يشمل العامل الأول دراسة تأثير الكسور الحجمية المختلفة من الألومينا ($0.5,1,1.5.2\%V_f$)، اما العامل الثاني يتضمن دراسة تأثير سرع الطرد المركزي المختلفة (600، 800، 1000 و1200 دورة في الدقيقة) اما العامل الثالث هو دراسة تأثير اختلاف زمن الطرد مركزي (1، 2، 4 و6 دقائق). وكذلك التصنيع ماده غير متدرجه للمقارنة بين النتائج. اما الجزء الثالث من هذا العمل يتضمن دراسة الخصائص الهيكلية والفيزيائية والميكانيكية والترايبولوجية للمقارنة بين الخصائص للعينات المتدرجة وغير المتدرجة.

شملت الخصائص الميكانيكية مقاومة الانحناء (الانحناء ثلاثي النقاط)، الصدمة والصلادة. اما الخصائص الترايبولوجيه تشمل دراسة معدل البلى ومعامل الاحتكاك. حيث تم تسليط الحمل لجميع أنواع المادة المتدرجة وظيفيا ومن كلا الجانبين (جهة المادة المركبة وجهه الإيبوكسي النقي) .

تظهر نتائج تحليل الحجم الحبيبي أن اقصى حجم لجسيمات الالومينا النانوية هو 520.1 نانومتر. اما نتائج XRD توضح أن جسيمات الألومينا النانوية تحتوي فقط على طور الفا.

اظهر هذا العمل أن دمج جزيئات الالومينا النانوية يحسن من المقاومة الميكانيكية و مقاومة البلى الانزلاقي للمركبات المتدرجة حيث اظهرت النتائج ان أقصى مقاومة

للانحناء ومعامل انحناء للمادة النانوية المتدرجة وظيفيًا تحسنت بنسبة (43.69٪) و (52.82٪) على التوالي عند تحميلها من جانب الألومينا النانوية ، بينما عند تحميل المادة النانوية المتدرجة وظيفيًا من الجانب الغني بالإيبوكسي كان الانخفاض في مقاومة الانحناء بمقدار (122.42٪) بينما تحسن معامل الانحناء كان بنسبة (81.215٪) مقارنة مع الايبوكسي النقي عند تركيز $2\%V_f$ (Al_2O_3) وسرعة الدوران = (N = 1200دورة في الدقيقة ووقت الطرد المركزي (t = 6 min).

كما أظهرت النتائج أن قوة الصدمة للعينات المحملة من جهة المادة المركبة كانت أعلى من قوة الصدمة للعينات المحملة من جهة الإيبوكسي لجميع أنواع العينات المتدرجة وظيفيًا؛ بشكل عام كانت اقصى فرق لقوة الصدمة عندما تحميل المواد المتدرجة وظيفيًا من الجهة الغنية ب الألومينا النانوية حيث كانت اقصى قيمه حوالي 168 ٪ مقارنة ب الإيبوكسي النقي عند وقت الدوران (4 دقائق) وسرعة طرد المركزي (1200 دورة في الدقيقة) وكسر حجمي ($2\%V_f$).

تم قياس صلادة العينات من الجانب الغني بالألومينا إلى الجانب الغني بالإيبوكسي (حيث تم تقسيم العينة الى خمس مناطق) حيث أظهرت النتائج اختلاف الصلادة في كل منطقة، مما يضمن التوزيع الصحيح للجسيمات النانوية خلال السمك مما يدل على أن اختبار الصلادة يعتبر اختبارًا ممتازًا لتدرج خصائص المواد من خلال السمك. وكذلك أظهرت النتائج ان أقصى زيادة في الصلادة حوالي (16.8٪) للعينة N = 1200 (دورة في الدقيقة)، t = 6 دقائق، و$2\%V_f$ للمادة المركبة النانوية عند تحميلها من الجهة الغنية بالألومينا.

اظهرت النتائج كذلك ان المادة المركبة المتدرجة وظيفيا تمتلك مقاومة بلى انزلاقي عالية مقارنة بالمادة المركبة المتجانسة، حيث تمتلك معامل احتكاك منخفض حوالي (51.7٪) عند تحميل العينات من الجانب الغني بالألومينا N = 1200 (دورة في الدقيقة)، t = 6 دقائق و$2\%V_f$) مقارنة بعينة الايبوكسي النقية.

تمت دراسة أسطح الكسر لعينات الصدمة باستخدام الفحص المجهري الإلكتروني (SEM) عند أقصى وأدنى ظروف للطرد المركزي وكذلك عند اعلى واقل تركيز لجزيئات الالومينا النانوية للتحقق من تشتت الجزيئات النانوية.

جمهورية العراق
وزارة التعليم العالي والبحث العلمي
جامعة بابل
كلية هندسة المواد
قسم هندسة البوليمر والصناعات البتروكيماوية

تحضير وتوصيف المواد المركبة البوليميرية المتدرجة وظيفياً

أطروحة مقدمة إلى

كلية هندسة المواد / جامعة بابل وهي جزء من متطلبات نيل درجة

الدكتوراه فلسفة في هندسة المواد / البوليمر

من قبل

أضواء محمد عبد المجيد

بإشراف

أ.د. احمد فاضل حمزة

2022